Aus dem
Walther-Straub-Institut für Pharmakologie und Toxikologie
Institut der Ludwig-Maximilians-Universität München

Dissertation

zum Erwerb des Doctor of Philosophy (Ph.D.)

an der Medizinischen Fakultät der

Ludwig-Maximilians-Universität München

Expression and function of Transient Receptor Potential channels in murine lung interstitial macrophages, alveolar epithelial cells and fibroblasts

vorgelegt von:

Suhasini Rajan

aus:

Chembur / Indien

Jahr:

2024

Mit Genehmigung der Medizinischen Fakultät der
Ludwig-Maximilians-Universität München

Erstes Gutachten von:	Prof. Dr. Alexander Dietrich
Zweites Gutachten von:	Prof. Dr. Annette Nicke
Drittes Gutachten von:	Prof. Dr. Christian Wahl-Schott
Viertes Gutachtes:	Prof. Dr. Markus Diefenbacher

Dekan: **Prof. Dr. med. Thomas Gudermann**

Datum der Verteidigung:

05.12.2024

Affidavit

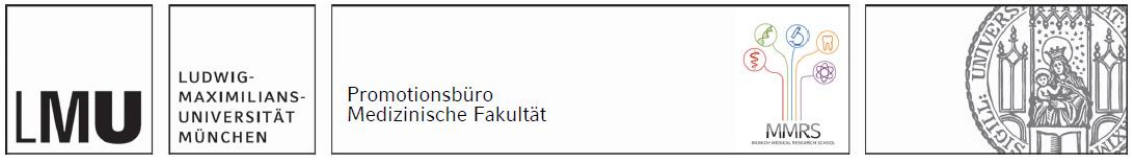

Affidavit

Rajan, Suhasini
Surname, first name

Nussbaumstr. 26
Street

80336, Munich, Germany
Zip code, town, country

I hereby declare, that the submitted thesis entitled:

Expression and function of Transient Receptor Potential channels in murine lung interstitial macrophages, alveolar epithelial cells and fibroblasts

is my own work. I have only used the sources indicated and have not made unauthorised use of services of a third party. Where the work of others has been quoted or reproduced, the source is always given.

I further declare that the dissertation presented here has not been submitted in the same or similar form to any other institution for the purpose of obtaining an academic degree.

Ingolstadt, 15.05.2025
place, date

Suhasini Rajan
Signature doctoral candidate

Confirmation of congruency

LMU LUDWIG-MAXIMILIANS-UNIVERSITÄT MÜNCHEN

Promotionsbüro
Medizinische Fakultät

MMRS

Confirmation of congruency between printed and electronic version of the doctoral thesis

Rajan, Suhasini
Surname, first name

Nussbaumstr. 26
Street

80336, Munich, Germany
Zip code, town, country

I hereby declare, that the submitted thesis entitled:

Expression and function of Transient Receptor Potential channels in murine lung interstitial macrophages, alveolar epithelial cells and fibroblasts

is congruent with the printed version both in content and format.

Ingolstadt, 15.05.2025
place, date

Suhasini Rajan
Signature doctoral candidate

Table of content

Affidavit **3**

Confirmation of congruency **4**

Table of content **5**

List of abbreviations **6**

List of publications **8**

Contribution to the publications **9**
1.1 Contribution to paper I 9
1.2 Contribution to paper II 9
1.3 Contribution to paper III 10

2. Introductory summary **11**
2.1 TRP channels 12
2.1.1 TRPM channels and TRPM2 13
2.1.2 TRPV channels - TRPV4 and TRPV2 14
2.1.3 TRPA1 15
2.2 The respiratory system 16
2.2.1 Alveolar epithelial cells 16
2.2.2 Fibroblasts 17
2.3 Lung immunity 17
2.3.1 Resident macrophages and their functions 18
2.3.2 Alveolar macrophages 18
2.3.3 Interstitial macrophages 19
2.2 Aim of the thesis 20

3. Paper I **21**

4. Paper II. **38**

5. Paper III **54**

References **66**

Acknowledgements **73**

List of abbreviations

AT1	Alveolar Type 1
AT2	Alveolar Type 2
IMs	Interstitial macrophages
AMs	Alveolar macrophages
DC	Dendritic cell
ARD	Ankyrin repeat domain
ROS	Reactive oxygen species
COPD	Chronic Obstructive Pulmonary
ALI	Acute Lung Injury
EMT	Epithelial to mesenchymal transition
ECM	Extracellular matrix
TNF	Tumor necrosis factor
IL	Interleukin
LPS	Lipopolysaccharide
IFN	Interferon
GM-CSF	Granulocyte-Macrophage colony stimulating factor
TRP	Transient Receptor Potential
TRPV	Vanilloid Transient Receptor Potential
TRPM	Melastatin Transient Receptor Potential
TRPA	Ankyrin Transient Receptor Potential
TRPC	Canonical Transient Receptor Potential
CaM	Calmodulin-binding domain
c-terminal	Carboxy-terminal
PBD	Phosphoinositide Binding Domain
TMD	Transmembrane domain
DAG	Diacylglycerol

ADPR	Adenosine diphosphate ribose
TGF	Tumor necrosis factor
CD11b	Integrin alpha M
CD11c	Integrin alpha X
Cx3cr1	CX3C motif chemokine receptor 1
Mertk	Mer tyrosine kinase
MHCII	Major Histocompatibility Complex 2
IR-induced	Ischemia-Reperfusion- induced

List of publications

Research papers included in this dissertation

Research Paper I [1]

Rajan, S., Shalygin, A., Gudermann, T., Chubanov, V., Dietrich, A. (2024) TRPM2 channels are essential for regulation of cytokine production in lung interstitial macrophages. *Journal of Cellular Physiology* (In press).

Research Paper II [2]

Weber, J., **Rajan, S**., Schremmer, C., Chao, Y.-K., Krasteva-Christ, G., Kannler, M., Dietrich, A. (2020). TRPV4 channels are essential for alveolar epithelial barrier function as protection from lung edema. *JCI Insight*, *5*(20). https://doi.org/10.1172/jci.insight.134464

Research Paper III [3]

Geiger, F., Zeitlmayr, S., Staab-Weijnitz, C. A., **Rajan, S**., Breit, A., Gudermann, T., & Dietrich, A. (2023). An Inhibitory Function of TRPA1 Channels in TGF-β1–driven Fibroblast-to-Myofibroblast Differentiation. *American Journal of Respiratory Cell and Molecular Biology*, *68*(3), 314–325. https://doi.org/10.1165/rcmb.2022-0159oc

Review articles not included in this dissertation

Rajan S, Schremmer C, Weber J, Alt P, Geiger F, Dietrich A. Ca2+ Signaling by TRPV4 Channels in Respiratory Function and Disease. Cells**.** 2021; 10: 822. https://doi.org/10.3390/cells10040822

Müller I, Alt P, **Rajan S**, Schaller L, Geiger F, Dietrich A. Transient Receptor Potential (TRP) Channels in Airway Toxicity and Disease: An Update. Cells. 2022; 11: 2907. https://doi.org/10.3390/cells11182907

1. Contribution to the publications

1.1 Contribution to paper I

This study aimed to develop a new method for isolating interstitial macrophages (IMs) from murine lungs and elucidate the role of transient receptor potential (TRP) channels, particularly TRPM2 (melastatin), in regulating inflammatory responses and reactive oxygen species (ROS) production in lung IMs. As the first author of paper I, I was instrumental in conceptualizing the research question, devising the experimental framework, and pioneering a novel technique for isolating lung IMs due to their historically challenging isolation process. This involved the innovative approach of co-culturing IMs with stromal cells followed by immune-magnetic separation targeting CD11b-positive IMs.

Subsequently, I rigorously validated this methodology by assessing the expression of IM-specific surface markers, including CD11b and Cx3cr1, alongside common macrophage markers like Mertk and CD64, employing both quantitative real-time polymerase chain reaction (q-RT-PCR) and flow cytometry utilizing fluorescence-conjugated antibodies with appropriate isotype controls to ensure specificity. Upon successful establishment of the isolation protocol, I investigated the expression profiles of TRP channels in IMs, corroborating findings through analysis of publicly available transcriptomic datasets. Notably, IMs exhibited expression of TRP channels across canonical, melastatin, and vanilloid families. Subsequent polarization of IMs to a pro-inflammatory M1 state, induced by lipopolysaccharide and interferon-gamma, led to significant upregulation of TRPM2, a member of the melastatin family, which became a focal point of investigation. Notably, TRPM2-deficient IMs demonstrated heightened secretion of pro-inflammatory cytokines TNFα, IL-6, and IL-1α, as determined by enzyme-linked immunosorbent assay (ELISA). Moreover, elevated reactive oxygen species (ROS) production, as assessed through direct measurement of H2DCFDA fluorescence and indirect assessment of glutathione levels in oxidized and reduced states were detected in TRPM2-/- IMs compared to control cells.

Further exploration by coauthors involved recording TRPM2 activity via whole-cell patch clamp analysis, with intracellular application of adenosine diphosphate ribose (ADPr), and quantifying membrane voltage in current clamp mode, revealing TRPM2-mediated membrane depolarization and subsequent inhibition of NADPH oxidase (NOX)-derived ROS release.

Delving deeper into the signaling cascade, my examination of NOX isoforms unveiled significant upregulation of NOX2 in M1-polarized IMs, with subsequent inhibition using GSK2795039 confirming NOX2-mediated ROS generation during M1 polarization.

These collective findings underscore the pivotal role of TRPM2 in modulating cytokine secretion and ROS release in M1-activated IMs within the pulmonary microenvironment. Finally, comprehensive data analysis was conducted utilizing R programming software for flow cytometry and RNA-seq datasets, with statistical analyses performed using GraphPad Prism.

1.2 Contribution to paper II

This study aimed to elucidate the role of TRPV4 (vanilloid) channels in alveolar epithelial cells, particularly in regulating edema formation, epithelial barrier integrity, and repair processes in the

lung. As a second co-author of the paper, my primary contributions involved isolating ATII cells for the electrophysiological recording of TRPV4 channel activity, and performing and analyzing immunohistochemical experiments with paraffin-embedded lungs. During the first revision, a reviewer requested a quantification of TRPV4 channel activity by its activator GSK using the patch clamp technique. I isolated the cells for patch experiments by a collaborator. Another reviewer advised reevaluation of the first set of paraffin-embedded lung sections, which had been treated with paraformaldehyde (PFA) for fixation. This necessitated analyzing both the previously analyzed sections and new additional tissue samples for each time point. The preparation process involved perfusing and inflating lungs with 2.5% (m/v) glutaraldehyde in PBS, followed by paraffin embedding, sectioning, mounting on glass slides, and staining with Masson Goldner trichrome dye.

Mean chord lengths (MCL) were then analyzed by another coauthor in tissue sections using design-based stereology, utilizing an Olympus BX51 light microscope equipped with the new Computer Assisted Stereological Toolbox (newCAST, Visiopharm) at the Helmholtz Institute. This setup allowed for comparison between mice with functional TRPV4 channels (wildtype, WT) and those without (TRPV4-/-, KO) across three age groups: Young (4-6 weeks of age), middle-aged (28-30 weeks of age), and old (47-52 weeks of age), in both sexes. The results revealed elevated mean chord length values in old TRPV4-/- mice compared to same-aged WT mice, supported by representative images, confirming the development of emphysema-like changes due to ongoing growth and repair processes. These findings were consistent with previously gathered data indicating altered lung function in adult TRPV4-/- mice.

1.3 Contribution to paper III

The process of fibroblast to myofibroblast differentiation is widely acknowledged as a significant contributor to the pathogenesis of pulmonary fibrosis. Building upon previous findings showing TGF-β1-induced myofibroblast differentiation and upregulation of TRPC6 expression in murine lung fibroblasts [4], we investigated the role of TRPA1 (ankyrin) in TGF-β1-induced myofibroblast differentiation in primary human lung fibroblasts (HLF) from healthy donors.

To comprehensively understand the impact of TGF-β1 treatment on primary HLF, samples from three healthy donors were subjected to RNA sequencing (RNAseq). My contribution was an in-depth analysis of the acquired transcriptome data using DESeq2 and the R software. The analysis revealed a distinct pattern indicating TGF-β1-mediated downregulation of the transient receptor potential A1 (TRPA1) gene in HLFs. The results containing differentially expressed genes were depicted in a volcano plot with upregulated genes including fibrotic marker genes such as ACTA2, COL1A1, FN1, and SERPINE1. Additionally, gene ontology (GO) analysis identified significantly upregulated biological processes such as extracellular matrix organization, collagen metabolic process, and connective tissue development following TGF-β1 treatment. The normalized counts of TRPC, TRPM, TRPV, and TRPA1 genes in HLF post-treatment showed distinct patterns between TGF-β1 and solvent conditions.

2. Introductory summary

The three manuscripts collectively shed light on the critical roles of transient receptor potential (TRP) channels in lung physiology and pathology. Paper I focuses on interstitial macrophages (IMs) critical for innate immunity, which harbors in the lungs along with alveolar macrophages (AMs) IMs are less understood due to low counts and remote location. They exhibit varied transcriptional profiles distinct from AMs and contribute to lung homeostasis. We have developed a novel method for isolating lung interstitial macrophages (IMs) after co-culture with stromal cells, yielding significantly higher cell counts compared to fluorescence-activated cell sorting (FACS) and allowing a more comprehensive characterization of IMs. The isolation technique was validated by testing specific surface markers such as CD11b and Cx3cr1 distinguishing them from alveolar macrophages (AMs). Transient receptor potential (TRP) channels, known regulators of intracellular Ca^{2+} concentrations, are expressed in various tissue-resident macrophages and are involved in the immune response. We investigated TRP mRNA levels in isolated IMs to reveal that TRP channels of vanilloid, canonical, and melastatin families were expressed and our findings were further corroborated with transcriptomic analysis of the publicly available RNA sequencing dataset (GSE94135). Of all the TRP channels, upregulation of TRPM2 mRNA was observed in IMs polarized to M1 state with lipopolysaccharide (LPS) and interferon-gamma (IFNγ). We showed that TRPM2 activation modulates cytokine production in IMs, as TRPM2-deficient IMs exhibit elevated levels of inflammatory cytokines TNFα, IL-1α, and IL-6, alongside increased ROS production, indicating a regulatory role for TRPM2 in cytokine secretion and oxidative stress modulation. In addition, TRPM2 activation induced membrane depolarization and attenuated NOX2-mediated ROS production, suggesting a mechanism for modulating cytokine release and maintaining redox balance in IMs. These findings highlight TRPM2 as a potential therapeutic target for immune modulation in lung inflammation and infection. Paper II shows an *ex vivo* model mimicking ischemia/reperfusion-induced edema (IRE) in mouse lungs. TRPV4-deficient lungs exhibited exacerbated IRE compared to wild-type controls, suggesting a protective role of TRPV4 in maintaining the alveolar epithelial barrier. Immunohistochemistry and mRNA profiling revealed TRPV4 expression in bronchial and alveolar epithelial cells, with TRPV4 deficiency leading to reduced expression of aquaporin-5 (AQP-5) in alveolar type I (ATI) cells. Additionally, impaired cell migration and barrier function were observed in TRPV4-deficient ATI cells, along with reduced surfactant protein C expression in alveolar type II (ATII) cells, indicating the critical involvement of TRPV4 in alveolar epithelial function and prevention of edema formation. Finally, Paper III explores the potential of TRPA1 activation in mitigating TGF-β-induced fibroblast-to-myofibroblast transition, suggesting a protective role against pulmonary fibrosis. TRPA1, a Ca^{2+}-permeable cation channel found in human lung fibroblasts (HLFs), exhibits reduced expression after TGF-β exposure. Its downregulation correlates with increased markers of fibrosis, while TRPA1 activation with AITC attenuates TGF-β-induced fibroblast-to-myofibroblast transition, suggesting a potential protective role against pulmonary fibrosis. Together, these papers underscore the diverse functions of TRP channels in lung health and disease, offering insights into potential therapeutic strategies for respiratory diseases.

2.1 TRP channels

The research on transient receptor potential (TRP) channels has gained significant recognition in the scientific community, notably with David Julius receiving the Nobel Prize in 2021 for their contributions. Although TRP channels were first discovered in *Drosophila melanogaster* [5], it was only 20 years later that they were categorized as ion channels majorly associated with photo-transduction [2, 3] and thereafter extensive research has been conducted in mammalian TRP channels, where they serve diverse biological function (reviewed in 4). Since its inception, the classification of TRP channels has evolved in many ways. The recent classification consists of 28 mammalian TRP channels divided into six subfamilies as shown in Figure 1 (left): TRPC (canonical), TRPM (melastatin), TRPV (vanilloid), TRPA (ankyrin), TRPML (mucolipin), and TRPP (polycystin) (reviewed in [8]).

Structurally, TRP channels consist of six transmembrane domains (TMD), with the pore-forming domain, which is cation permeable, in between the fifth and the sixth segments. Key structural features include ankyrin repeat domains (ARD) in the intracellular N-terminus and a conserved TRP box domain in the C-terminus, which is essential for channel gating. TRP channels can form homo- or heterotetrameric complexes and are found either in the plasma membrane or intracellularly in lysosomal, endosomal membranes [9]. TRP channels are molecular sensors that can be activated by various stimuli such as temperature, reactive oxygen species (ROS), diacylglycerol (DAG), to name a few (reviewed in [8]). Majority of TRP channels are present in sensory neurons mediating thermal sensation [10]. Prime function of most TRP channels is facilitating influx of calcium ions (Ca^{2+}), that are crucial second messengers [11]. Intracellular calcium $[Ca^{2+}]_i$ serves as a regulator of numerous cellular functions, spanning from cell proliferation and growth to apoptosis and muscle contraction [6, 7].

TRP channels are expressed in all major organs of the body (Figure 1, right) and have been linked to various conditions like inflammatory bowel disease, chronic obstructive pulmonary disease, and recently in COVID-19 (reviewed in [14]). While TRP channels are found in all major organs, this thesis predominantly focuses on their role in lung-specific cell types, highlighting their significance in lung immunity (e.g., TRPM2, TRPV2), ischemia-reperfusion injury (TRPV4), and pulmonary fibrosis (TRPA1).

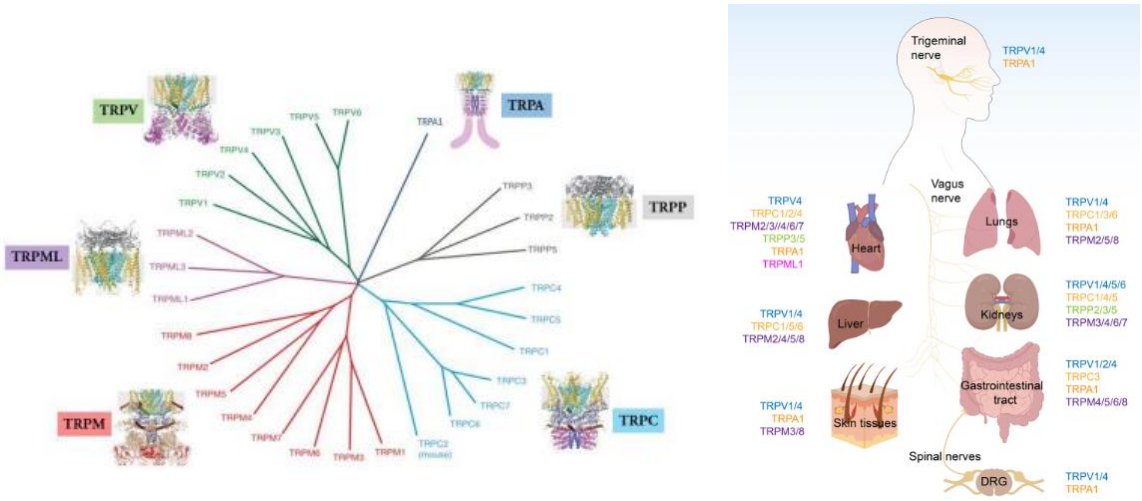

Figure 1: TRP channel superfamily (left). Protein structure of the transient receptor potential (TRP) channels in the phylogenetic tree in mammals including six sub-families of TRPC (canonical), TRPM (melastatin), TRPV (vanilloid), TRPA (ankyrin), TRPML (mucolipin), and TRPP (polycystin) (modified from [15], [16], master thesis of Annaya Kadekar). **TRP channel expression in the body (right).** Expression of various TRP channels in different organs of the body, namely lungs, kidney, gastrointestinal tract, heart, liver, skin, and the nervous system [14].

2.1.1 TRPM channels and TRPM2

Members of the TRPM (Transient receptor potential melastatin) family stand out due to their extensive cytosolic domain, with each subunit consisting of 732 to 1611 amino acids, making them the most sizable in the TRP superfamily. These channels possess a unique N-terminal TRPM homology region (MHR) domain, the usual TMD that includes six transmembrane helices, alongside a TRP helix, and a C-terminal coiled-coil domain. The C-terminal domain (CTD) varies among the different members [17]. The TRPM sub-family consists of eight members (TRPM1-8), of which TRPM7 is ubiquitously expressed in the human body. While they share certain structural characteristics, the TRPM subfamily members display less homogeneity than those in other subfamilies. Based on the spectrum of ion permeability TRPMs can be further categorized into (1) channels of increased permeability to Ca^{2+}, Zn^{2+} and Mg^{2+} like M1, M3, M6, and M7, (2) channels that conduct non-selective cations like M2, and M8, (3) channels that are permeable to monovalent cations like M4 and M5 [18].

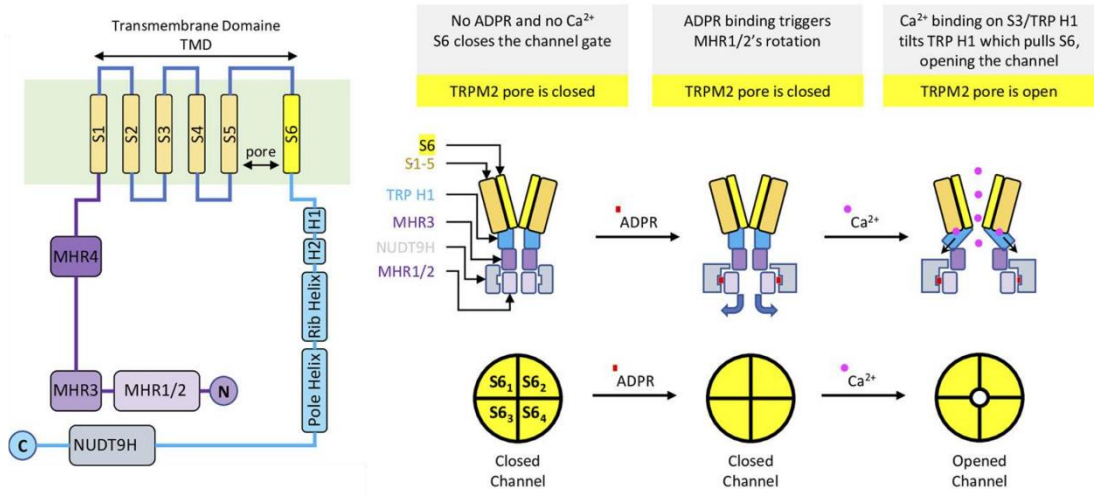

Figure 2: TRPM2 (melastatin) channel structure (left). Structure of TRPM2 channel with six transmembrane domains (TMD) and a pore between segments S5 and S6. The N-terminus has TRPM homology regions (MHR1-4), while the C-terminus harbors a NUDT9-H (Nudix hydrolase 9) domain. **Gating dynamics of TRPM2 channel opening (right).** The conformational changes of TRPM2 channel in its closed to open states in the absence or presence of adenosine diphosphate ribose (ADPR) and Ca^{2+}. Binding of ADPR causes rotation of MHR and concomitant Ca^{2+} binding opens the channel resulting in cation influx (modified from [19]).

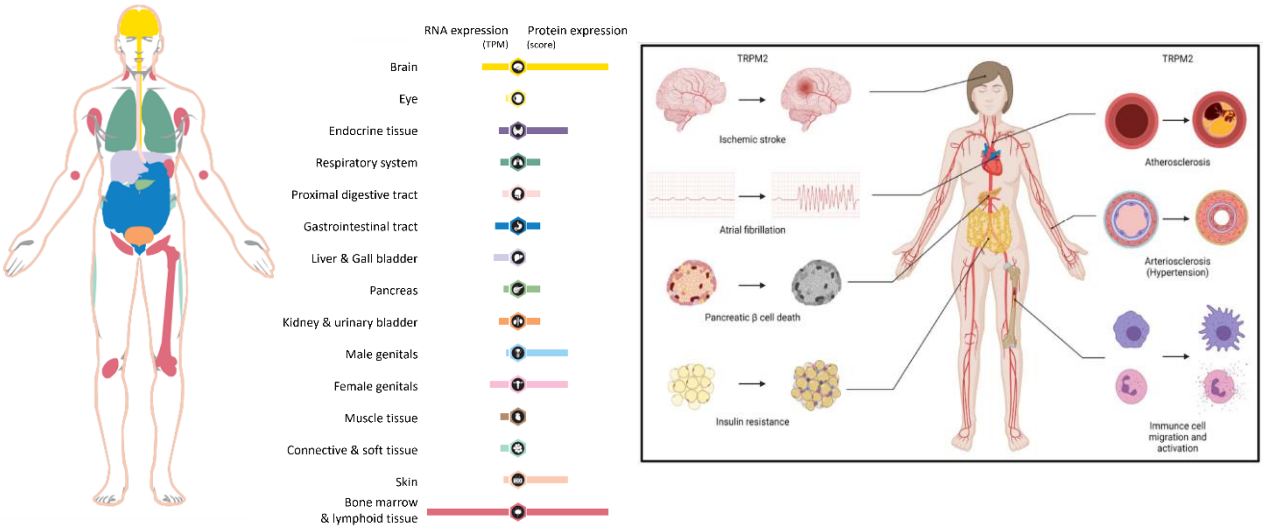

Figure 3: Expression of TRPM2 in various organs of the body (left). The distribution of TRPM2 expression, both RNA and protein, in various organs of the entire body is created on https://www.proteinatlas.org. **Effects of TRPM2 activation (right).** The picture shows the detrimental effects of oxidative stress-induced TRPM2 activation in the brain, heart, pancreas, and immune cell response [20].

TRPM2, the second member of the melastatin sub-family, exhibits a similar channel architecture to the rest of the TRP superfamily. Unlike other TRP channels, TRPM2 is equipped with a unique NUDT9-H domain at the C-terminal end. Adenosine diphosphate ribose (ADPR) is a well-known activator of TRPM2 inducing cation influx. ADPR has a high binding affinity to the NUDT9-H domain (Figure 2, right) and induces channel opening in the presence of Ca^{2+} (Figure 2, left) [19]. Along with TRPM6 and M7, TRPM2 was previously named a “chanzyme” owing to its enzymatic function of cleavage of ADPR [21]. But recent studies on the influence of enzymatic activity on channel gating proved otherwise changing the status of TRPM2 from a “chanzyme” to a mere ligand-gated channel [13, 14].TRPM2 is expressed in almost all major organs of the body (Figure 3, left). A major physiological function of TRPM2 is the regulation of insulin secretion from the pancreatic β-cells [24]. On the other hand, when the β-cells are subjected to oxidative stress, TRPM2-mediated Ca^{2+} release from lysosome causes apoptosis [25]. TRPM2 mRNA is the most abundantly expressed TRP channel in the brain tissue [26]. Genetic studies have linked TRPM2 mutations to bipolar disorder and other neurological disorders [27]. Activation of the oxidative sensor TRPM2 leads to various pathologies in the body (Figure 3, right, reviewed in [20]). Laborious and elaborate research on TRPM2 suggests that channel inhibitors could be effective in treating CNS disorders by moderating aberrant TRPM2 activation.

2.1.2 TRPV channels – TRPV4 and TRPV2

The TRPV (Transient Receptor Potential Vanilloid) subfamily, initially identified in 1997 as capsaicin receptors, displays unique characteristics, including multiple ankyrin-repeat domains (ARD) at the N-terminus, a phosphoinositide binding domain (PBD), a C-terminal calmodulin-binding domain (CaM), and a PDZ-like motif [16, 17]. Expanding from the discovery of TRPV1, currently,

the TRPV subfamily comprises six members, with TRPV1-4, which are non-selective cation channels, and TRPV5 and 6, which exhibit high selectivity for Ca^{2+} ions [28]. It exhibits polymodal activation to stimuli such as hypo-osmolarity, fluctuations in temperature, and mechanical stress [29]. TRPV4 demonstrates ubiquitous expression throughout the body, including various cells within the respiratory system like fibroblasts and epithelial cells [8]. In the vascular tissue, smooth muscle cells and endothelial cells express TRPV4 [30], where its activation is detrimental to the maintenance of the alveolar and endothelial barrier functions inducing heightened endothelial permeability in the lungs [31]. In addition, TRPV4 regulates the muscular tone of pulmonary arterial smooth muscle cells, which is mediated by α-adrenoceptor activation [32]. While the endothelial role of TRPV4 is well-established, its functions within lung epithelial cells remain less understood. Cumulative research on TRPV4 in the lungs deems this ion channel as a potential drug target for various respiratory illnesses [33]. Recent studies on the activation of TRPV4 have revealed the binding sites of a popular agonist - GSK1016790A, at the cytosolic cavity in the TMD 1-4 [34], thereby shedding more light on the potential application of TRPV4 as a drug target.

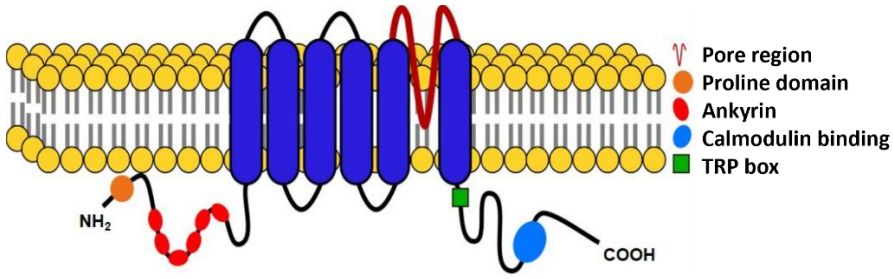

Figure 4: Structure of TRPV4 channel. Like all representatives of the TRPV family, TRPV4 also has 6 transmembrane domains with a pore region between the 5th and 6th domains. Channels of this family harbor between 3 and 6 ankyrin domains in the N-terminus. The proline domain causes this region to bind to PIP2 in the cell membrane. The calmodulin binding site causes a conformational change of the channel by binding Ca^{2+} (Modified from [29]).

TRPV2 is the second member of the vanilloid family, which is found in fibroblasts, smooth muscle cells, T-cells, and at the highest levels in macrophages of the lungs [35]. TRPV2 plays a pivotal role in immune cell response discussed in 2.3.3.

2.1.3 TRPA1

TRPA1, the solitary member of the ankyrin family of TRP channels, derives its name from its numerous ARD at the N-terminus. TRPA1 is a non-selective cation channel highly permeable to calcium ions and is widely expressed throughout the body, with its cDNA initially cloned from human lung fibroblasts [36]. A distinctive feature of TRPA1 is the absence of its murine counterpart in the pulmonary fibroblasts (Unpublished RNA-seq data from primary lung murine fibroblasts from our group). TRPA1 is extensively researched for its role in sensory neurons, responding to various sensations including pain, itch, and inflammatory stimuli Mechanistically, TRPA1 exhibits complex gating mechanisms influenced by extracellular calcium levels and temperature [37]. TRPA1 is associated with the nociceptor system of the lungs, where it activates bronchopulmonary c-fibers [38].

2.2 The respiratory system

The respiratory system consists of the upper respiratory tract which includes the nasal and oral cavities, and the pharynx. The lower respiratory tract encompasses the larynx, trachea, bronchi, bronchioles, and alveoli, facilitating oxygen (O2) supply to the body. The lungs mediate the exchange of oxygen (O2) and carbon dioxide (CO2) between the air and the bloodstream. Inhaled air, carrying foreign particles, initially traverses the upper airways, comprising the trachea and primary and secondary bronchi. The cellular composition of larger bronchi and alveoli is depicted in Figure 4. Mucus, secreted by goblet cells, traps airborne particles. The coordinated action of cilia on ciliated cells, along with the cough reflex, facilitates the expulsion of most particles from the lungs [39]. The basal cells in the trachea act as progenitor cells. They transition into a highly proliferative state during ongoing turnover and following epithelial injury and can differentiate into ciliated, goblet, and club cells [40]. Club cells produce surfactant proteins A and D, which possess antimicrobial properties and regulate immune responses. Following epithelial injury, they also serve as precursors for alveolar epithelial cells type 2 (ATII), which further differentiate into alveolar epithelial cells type 1 (ATI) [33, 34].

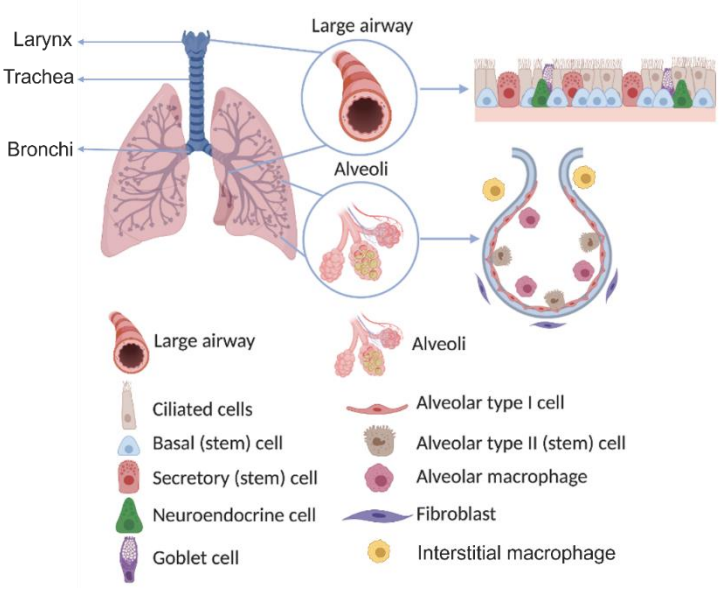

Figure 5: Schema of cellular composition of large airways and alveoli of the lungs. The lower respiratory consists of larynx that continues as trachea and branches into bronchi and bronchioles until the terminal alveoli. The heterogeneity of cellular composition of larger airways and alveoli is shown (Modified from https://www.eurostemcell.org/lung-stem-cells-health-repair-and-disease).

2.2.1 Alveolar epithelial cells

The alveolar epithelium functions in different ways in the lungs. As the epithelial layer forms a natural barrier to the external environment, protecting the body from invading microorganisms and toxins, concomitantly, alveolar epithelial cells also facilitate efficient gas exchange. In the adult lung, the alveolar air space contains alveolar macrophages (AM). The lining epithelium is composed of two epithelial cell types (ATI and ATII cells) and the adjunct interstitium contains fibroblasts and interstitial macrophages (IM) (Figure 4), which are crucial for maintaining lung homeostasis and tissue repair (reviewed in [43]). Around 95 – 98 % of the epithelial lining is filled with flat and elongated ATI cells [33, 36]. ATI cells covering a large cell surface are pivotal cells involved in gas exchange, as they are in close proximity to the interstitium and the endothelial cells of the alveolar capillaries [37, 38]. ATI cells are highly permeable to water, which enables

ion transport and the maintenance of fluid balance in the lung [47]. Specific marker proteins for ATI cells are caveolin, podoplanin, and aquaporin-5 (AQP-5) [48]. AQP-5 belongs to the protein family of aquaporins and is the only member that is found in ATI cells [49]. ATII dysfunction, as a result of repetitive microinjury, leads to the initiation of fibrotic changes by epithelial to mesenchymal transition (EMT) in idiopathic lung fibrosis (reviewed in [50], [51]). While TRPA1 is expressed in both epithelial cell types, its dispensability is already proven in the development of hyperoxia-induced hyperplasia of the epithelium [52]. In chronic obstructive pulmonary disease (COPD), targeting TRPA1 and TRPV1 channels to inhibit cigarette smoke-induced damage in bronchial and alveolar epithelial cells reduced oxidative stress, inflammation, and mitochondrial dysfunction, making them promising therapeutic targets [53]. TRPV4 is essentially required for its function in these epithelial cells and protects the lungs from edema formation in ischemia/reperfusion [2].

2.2.2 Fibroblasts

The lungs are primarily composed of connective tissue housing fibroblasts responsible for the secretion of extracellular matrix (ECM) and maintenance of organ integrity. These mesenchymal cells play central roles in development, wound healing, and immune modulation by secreting ECM proteins, supporting cell functions, and aiding in tissue elasticity (reviewed in [54]). The ECM, comprising various proteins like collagens and fibronectin, provides structural support and signaling cues [55]. Factors like TGF-β1 regulate fibroblast behavior and myofibroblast differentiation crucial for wound closure [56]. Pulmonary fibrosis (PF) can arise from various factors, leading to ECM overproduction and myofibroblast accumulation, impairing lung function [57]. Although medications like pirfenidone and nintedanib improve patient life quality, there is no definite cure for PF [58] . Understanding TRP channels, fibroblasts, and the role of Ca^{2+} in fibrosis offers potential therapies. TGF-β signaling and calcium influx via TRPV4, TRPC6, and TRPM7 contribute to fibrosis progression [35], while TRPA1 activation shows promise in mitigating fibrotic changes [35]. These insights into fibrosis mechanisms provide avenues for therapeutic interventions.

2.3 Lung immunity

As with any healthy organ in the body, our lungs are equipped with a robust immune system, which, in addition to maintaining homeostasis, is also responsible for protection against external or internal danger signals by defenses of varying levels of sensitivity and specificity. The upper respiratory tract efficiently filters out larger particles, while the alveolar and bronchial spaces rely heavily on resident alveolar macrophages for the phagocytosis of finer particulates [59]. The pulmonary immune system, composed of innate and adaptive components, defends against pathogens through various mechanisms such as mucociliary clearance, antimicrobial molecule secretion, and immune cell responses [59]. This defense is extensively provided by monocytes, macrophages, and dendritic cells (DCs) that collectively belong to the mononuclear phagocyte (MNP). The MNP was described in the literature for the very first time in 1968 by Van Furth and Cohn [60]. This heterogeneous system is responsible for functions ranging from immediate immune response to foreign stimuli to antigen presentation and phagocytosis [61]. The tissue-resident monocytes, apart from serving as precursor cells, differ from the circulating monocytes and are important for constant vigilance of the lung parenchyma [62]. DCs specialize in ingesting antigens and activating naïve T cells by migrating to the nearby lymph node [63].

2.3.1 Resident macrophages and their functions

Resident macrophages are the innate immune cells present in every organ of the body mainly responsible for maintaining homeostasis in the local microenvironment. This is achieved by the clearance of dead tissue and excess metabolites from cell functions [64]. The main function of these macrophages is the initiation of the acute response to any signals in the local microenvironment both of exogenous and endogenous nature [65]. The macrophages respond to a wide range of signals that include dead cells, proteins, invading micro-organisms like bacteria and viruses along with toxins secreted by the micro-organisms. In the process of polarization, the macrophages differentiate to a pro-inflammatory M1 state by canonical/classical activation during inflammation or to an anti-inflammatory M2 state by alternative activation post-inflammation as shown in Figure 7 [66]. Here, it is worth mentioning the plasticity of macrophage phenotypes as they can transition between pro- and anti-inflammatory phenotypes based on their microenvironment [67]. Major anti-inflammatory cytokines released by macrophages are IL-10, 11, and 13 [68]. As an immediate response to the signals, the macrophages release pro-inflammatory cytokines like tumor necrosis factor-alpha (TNFα), interleukins (IL)-1, 6, 8 and 12 [69].

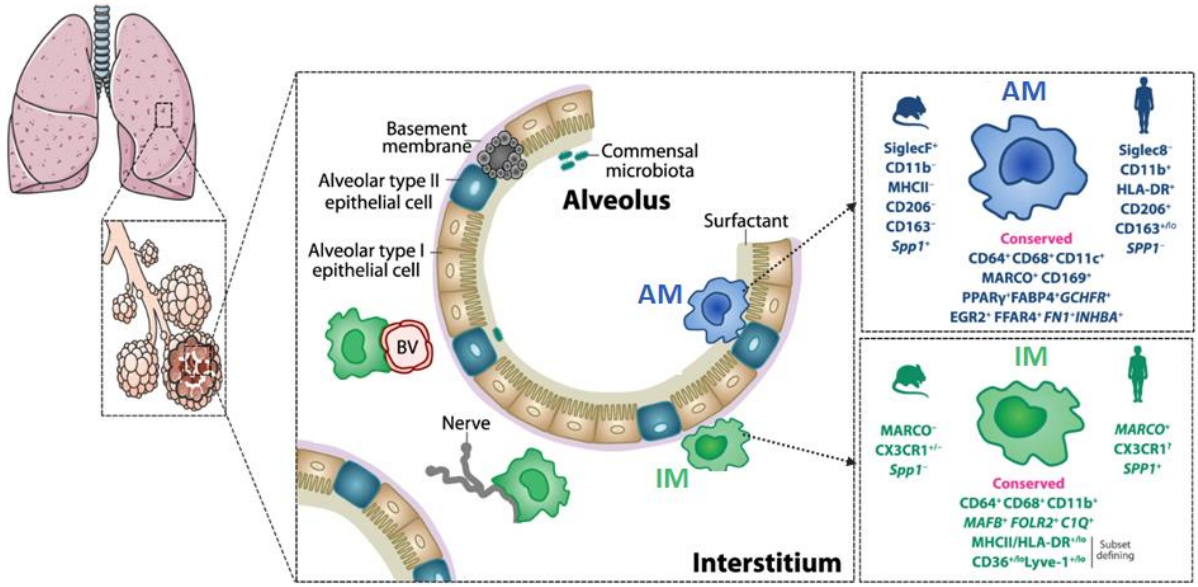

Figure 6: Macrophage heterogeneity of lungs. Schema showing phenotypical characteristics and diverse population of lungs – alveolar macrophage (AMs) and interstitial macrophage (IMs) (modified from [70]).

Unlike other organs in the body, the lungs are equipped with two populations of resident macrophages namely the alveolar macrophages (AMs) and the interstitial macrophages (IMs) (Figure 5,6). These macrophages differ in localization, the cytokines that regulate their growth, and their phenotypes based on the tissue environment that they develop in since birth. Both mouse and human AMs originate from embryonic precursors and occupy the alveolar niche before birth, undergoing minimal proliferation in adulthood [65, 66]. On the other hand, IMs are believed to originate from the yolk sac and are replaced by fetal liver monocytes, with varying rates and extents of replenishment depending on the subtype [73]. Tissue homeostasis relies on a diverse array of functional macrophages, with evidence suggesting that many tissue-resident macrophages are established during embryonic development and persist into adulthood through localized proliferation [71]. Mononuclear phagocytes generated during adult hematopoiesis are recruited to various sites in the body, contributing to tissue repair, inflammation resolution, and disease progression [74].

2.3.2 Alveolar macrophages

Alveolar macrophages (AMs) serve as the primary defense mechanism within the alveolar air space, constantly exposed to inhaled foreign particles. These cells maintain immune equilibrium through efferocytosis and secretion of anti-inflammatory mediators [75]. They also support the generation of T-regulatory cells and respond to epithelial signaling, demonstrating immunosuppressive functions [76]. However, under inflammatory conditions, AMs transition to a pro-inflammatory [77], enhancing phagocytic activity and cytokine production, thereby exacerbating lung inflammation and injury [78]. This dual functionality underscores AMs' pivotal role in modulating pulmonary immune responses. The presence of distinctive surface markers shown in Figure 6, such as CD11c (integrin alpha X) and Siglec F(sialic acid binding Ig like lectin F) and the absence of CD11b (integrin alpha M), differentiate them from other immune cells [79]. Granulocyte-macrophage colony-stimulating factor (GM-CSF/CSF-2) regulates AM growth [80], and its aberrant secretion can lead to AM dysfunction [75, 76]. While, in COPD patients, TRPC6 mRNA expression in AMs was heightened [83], in pulmonary cystic fibrosis (CF), TRPC6 was found to be associated with phagocytic and bactericidal functions of AMs [84]. TRPV2 plays a critical role in phagocytosis by AMs, where defective expression leads to impairment in phagocytotic properties in cystic fibrosis [85]. Along the same lines, TRPV4 facilitates bacterial clearance when studied in an in-vivo model of bacterial pneumonia [86]. All these studies highlight the significance of selective TRP channels in maintaining pulmonary homeostasis and defending against pathogens.

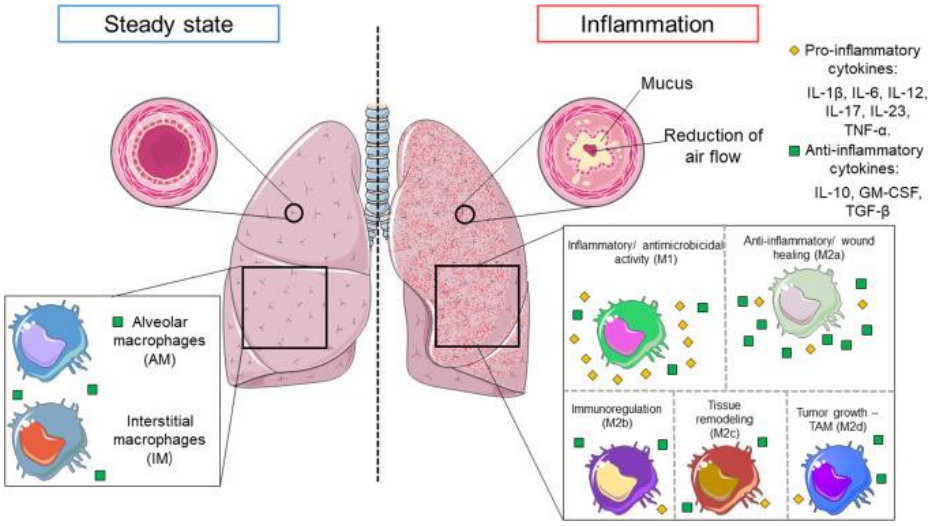

Figure 7: Immune response of AM and IM in inflammation. Macrophages of the lungs polarize to pro-inflammatory M1 by releasing cytokines like interleukins-1, 6, 12, and tumor necrosis factor-alpha (TNFα) and anti-inflammatory M2 state by releasing cytokines like tumor growth factor beta (TGFβ), , granulocyte-macrophage colony stimulating factor (GM-CSF), and interleukin-10 (modified from [87]).

2.3.3 Interstitial macrophages

Lung interstitial macrophages (IMs), initially observed as phagocytic "septal cells" in 1950, were overshadowed by alveolar macrophages until the early 1970s. It was proposed that AMs originated from bone marrow precursors, with an intermediate maturation state in the pulmonary interstitium. Studies comparing AMs and IMs revealed differences in phagocytic potential, receptor expression, and cytokine secretion, suggesting IM as a distinct and fully competent macrophage population, a concept now widely accepted (reviewed in [88]). IMs in both humans and mice exhibit phagocytic activity, serving as the lungs' second line of defense [83, 84, 85]. They possess immunoregulatory functions, including increased secretion of the immunosuppressive cytokine IL-10 upon exposure to bacterial products such as lipopolysaccharide (LPS) and DNA [92], [93].

Research by Moore et al. demonstrated that IM numbers expand in the lung interstitium following in vivo exposure to LPS, suggesting their involvement in inflammation [94]. Recent advancements in single-cell transcriptomics and flow cytometry have revealed the heterogeneity of IM in the lungs, based on distinct surface marker expressions [67, 82, 83]. Common markers across all phenotypes, as depicted in Figure 6, include CD11b, Cx3cr1 (CX3C motif chemokine receptor 1) and Mertk, a tyrosine kinase and differential markers include CD11c and MHCII (major histocompatibility complex II) [90]. Despite their heterogeneity, the functional division of labor among the three different subtypes of IMs remains to be fully elucidated.

Studies on interstitial macrophages (IMs) face significant challenges in isolation and culture maintenance due to marker heterogeneity, low cell counts, and their location deep within the lung parenchyma. However, in 2019, Ogawa et al. introduced a novel approach for IM isolation involving co-culture with stromal cells, offering promise for improved methodologies [95], [96]. Notably, despite increasing research interest, transient receptor potential (TRP) channels in IMs remain largely unexplored, representing a significant gap in our understanding of these cells and their functional regulation. Further investigation into TRP channels could provide valuable insights into IM biology and potential therapeutic targets. Although studies on IMs are on the rise, a major hindrance lies in isolating these macrophages for in-vitro studies and their maintenance in culture. Owing to marker heterogeneity, low counts and remote parenchymal location make the isolation difficult. Most importantly, TRP channels remain completely unexplored in IMs.

2.4 Aim of the thesis

In the first part, the thesis aims to address the gap in understanding TRP channel expression and function in IMs. Specifically, it seeks to:

- Develop methods to isolate murine lung IMs for subsequent in vitro studies.
- Investigate the expression and functional roles of TRP channels in IMs, including their potential contribution to IM polarization.

As TRP channels are highly expressed in the lungs, especially ATII, and fibroblasts, the second part of the thesis aims to study.

- The activity of TRPV4 in isolated ATII cells and changes in morphological changes in WT and TRPV4-/- mice lungs.
- TRP channel expression in primary human lung fibroblasts (HLF) differentiated to myofibroblasts by TGF-β1.

3. Paper I

Received: 7 March 2024 | Accepted: 9 May 2024

DOI: 10.1002/jcp.31322

RESEARCH ARTICLE

Journal of Cellular Physiology WILEY

TRPM2 channels are essential for regulation of cytokine production in lung interstitial macrophages

Suhasini Rajan | Alexey Shalygin | Thomas Gudermann | Vladimir Chubanov | Alexander Dietrich

Walther-Straub-Institute of Pharmacology and Toxicology, Member of the German Center for Lung Research (DZL), LMU-Munich, Munich, Germany

Correspondence
Alexander Dietrich, Walther-Straub-Institute of Pharmacology and Toxicology, Nußbaumstr. 26, 80336 Munich, Germany.
Email: Alexander.Dietrich@lrz.uni-muenchen.de

Funding information
Deutsche Forschungsgemeinschaft; Deutsches Zentrum für Lungenforschung

Abstract

Interstitial macrophages (IMs) are essential for organ homeostasis, inflammation, and autonomous immune response in lung tissues, which are achieved through polarization to a pro-inflammatory M1 and an M2 state for tissue repair. Their remote parenchymal localization and low counts, however, are limiting factors for their isolation and molecular characterization of their specific role during tissue inflammation. We isolated viable murine IMs in sufficient quantities by coculturing them with stromal cells and analyzed mRNA expression patterns of transient receptor potential (TRP) channels in naïve and M1 polarized IMs after application of lipopolysaccharide (LPS) and interferon γ. M-RNAs for the second member of the melastatin family of TRP channels, TRPM2, were upregulated in the M1 state and functional channels were identified by their characteristic currents induced by ADP-ribose, its specific activator. Most interestingly, cytokine production and secretion of interleukin-1α (IL-1α), IL-6 and tumor necrosis factor-α in M1 polarized but TRPM2-deficient IMs was significantly enhanced compared to WT cells. Activation of TRPM2 channels by ADP-ribose (ADPR) released from mitochondria by ROS-produced H_2O_2 significantly increases plasma membrane depolarization, which inhibits production of reactive oxygen species by NADPH oxidases and reduces cytokine production and secretion in a negative feedback loop. Therefore, TRPM2 channels are essential for the regulation of cytokine production in M1-polarized murine IMs. Specific activation of these channels may promote an anti-inflammatory phenotype and prevent a harmful cytokine storm often observed in COVID-19 patients.

KEYWORDS
cytokine storm, IL-1α, IL-6, reactive oxygen species (ROS), TNF-α, TRPM2 deficient mouse model

1 | INTRODUCTION

Our lungs are persistently exposed to pathogens from both sites: the airways and the vasculature. Next to dendritic cells and monocytes, resident macrophages are the most important for innate immune response in lung tissues and were initially differentiated from fetal monocytes or embryonic progenitor cells (Hoeffel et al., 2015; Sheng et al., 2015) reviewed in Gu et al. (2022). While in the airways alveolar macrophages (AMs) serve as a first line of defense, interstitial macrophages (IMs) act as gatekeepers of the vasculature and lung interstitium (see Aegerter et al., 2022; Cheng et al., 2021 for recent reviews). IMs were originally identified in preventing airway allergies like asthma in mice by producing interleukin-10 (IL-10), which has a dampening effect on dendritic cells in the lung (Bedoret et al., 2009). While AMs are easy to isolate from the broncho-alveolar lavage (BAL) fluid and are therefore already extensively studied, the exact roles and functions of IMs are currently unknown due to their remote parenchymal location and low cell counts. Up to three separable and substantially self-renewing populations of IMs were identified in the unchallenged "normal" lung (Gibbings et al., 2017). Although the exact roles of these IMs remain elusive, they exhibit different transcriptional profiles and were shown to be located in the interstitium of the bronchovascular bundles, but not in the alveolar walls (Gibbings et al., 2017). Murine IMs can be distinguished from AMs by the characteristic surface markers like CD11b and CX3CR1, their smaller size, and their irregular-shaped nuclei (reviewed in Gu et al., 2022). Next to their ability of self-renewal, which they share with AMs, IMs can be replenished by circulating monocytes (Gu et al., 2022). Like AMs, IMs form a pro-inflammatory M1 state, expressing tumor necrosis factor-α (TNF-α) and an M2 state for tissue repair, expressing arginase 1 (Arg1), after bacterial infection or an allergic challenge like ovalbumin (Dumigan et al., 2022; Ji et al., 2014; Nie et al., 2017; Peng et al., 2024; Strickland et al., 2023). Most interestingly, after introducing a more efficient way to isolate IMs (Ogawa et al., 2019), it was also possible to polarize isolated IMs in vitro to M1 or M2 states by adding lipopolysaccharide (LPS) and interferon-γ (IFN-γ) or IL-4, respectively (Tsurutani et al., 2021).

Transient receptor potential (TRP) channels are regulators of the intracellular Ca^{2+} concentration $[Ca^{2+}]_i$ in many cells, including vascular smooth muscle, endothelial and immune cells (reviewed in Nilius & Szallasi, 2014). The second member of the TRP melastatin family (Chubanov et al., 2024) (TRPM2) forms tetrameric non-selective cation channels activated directly by ADP-ribose (ADPR) (Fliegert et al., 2017), but also by warm temperatures (Kamm et al., 2021; Song et al., 2016) among others generated during inflammation (Syed Mortadza et al., 2015). TRPM2 controls reactive oxygen species (ROS)-induced chemokine production in monocytes, which is responsible for the recruitment of inflammatory cells to the site of injury (Yamamoto et al., 2008). This channel also regulates inflammatory functions of neutrophils during infections with *Listeria monocytogenes* (Robledo-Avila et al., 2020) and, most interestingly, is also responsible for macrophage polarization and gastric inflammation during *Helicobacter pylori* infections (Beceiro et al., 2017). Next to rather detrimental effects in these tissues, TRPM2 activation can also be beneficial and protects against tissue damage following oxidative stress (reviewed in (Maliougina & El Hiani, 2023; Miller & Cheung, 2016). As TRPM2 channels are also expressed in all three types of IM populations (see supplementary data in Gibbings et al., 2017), we set out to study their role in IM function. After establishing a protocol for the isolation of viable IMs, we identified characteristic currents induced by the TRPM2 activator ADPR. Importantly, TRPM2-deficient IMs polarized after application of LPS and IFN-γ produce and secrete a higher amount of IL-6, IL-1α and TNF-α. TRPM2 activation induces membrane depolarization and less production of ROS resulting in a diminished cytokine secretion. Therefore, TRPM2 regulates cytokine production via a negative feedback loop to prevent massive cytokine secretion similar to a cytokine storm, often observed in COVID-19 patients.

2 | METHODS

2.1 | Animals

TRPM2-deficient (TRPM2-/-) (Yamamoto et al., 2008) and wild-type mice from the same colony were used for all the experiments. All animal experiments were performed in accordance with the guidelines of the European Union for the use of animals.

2.2 | Isolation and propagation of interstitial macrophages and stromal cells

Briefly, the mice were killed by cervical dislocation. Bronchoalveolar lavage with cold phosphate buffer solution (PBS) was performed to remove alveolar macrophages. The thorax was exposed, and the lungs were flushed with warm HBSS by cardiac perfusion. Lungs were harvested, minced, and further subjected to enzymatic digestion with collagenase (4 mg/mL, C1-28; Sigma-Aldrich) in Dulbecco's modified Eagle's medium (DMEM) with no supplements for 50–60 min at 37°C stirred at 100 rpm. The digested lung tissue was homogenized with Pasteur pipette and cell suspension was filtered with 70 µM nylon filter (BD Falcon), followed by centrifuging at 4°C for 5 min at 300 rpm. The cell pellet was resuspended in DMEM (Lonza) supplemented with 10% fetal calf serum (FCS; Invitrogen), 1% penicillin/streptomycin (Lonza) and 50 mg/mL normocin (InvivoGen) and finally seeded in 10 cm cell culture dishes. The IMs were cocultured and propagated with stromal cells according to the method described by Ogawa et al. (2019) and Tsurutani et al. (2021) with some modifications. After 2 days, the supernatant was removed and the cells were washed with warm PBS to remove unattached cells like monocytes, erythrocytes. Treatment with 10 mM ethylene diamine tetra acetic acid (EDTA) in 10 mL DMEM for 20–30 min aided in detaching the cells. Cell suspension was centrifuged and the cells were split at 1:2 and plated with the medium being changed every 3–4 days. Cells were split again following the same method

after 6 days when over-confluent. AMs were isolated by centrifuging the broncho-alveolar lavage at 300 rpm at 4°C for 10 min and plating with Rosewell Park Memorial Institute (RPMI) 1640 medium with 10% FCS. The medium is removed after a day to remove unattached cells and the AMs were used for further analyses.

2.3 | Separation of stromal cells and interstitial macrophages

Cells in the second passage of coculture were detached with 10 mM EDTA after 6 days and centrifuged. The cell pellet suspended in the EasySep™ buffer (Stemcell Technologies; #20144) was subjected to immuno-magnetic separation using EasySep™ mouse CD11b positive selection kit II (Stemcell Technologies; #18970). Separated IMs were either directly used for flow cytometry, RNA isolation or seeded for in-vitro studies.

2.4 | RNA isolation and quantitative reverse transcription (qRT)–PCR analysis

Total RNA was isolated from IMs using RNeasy plus kit (Qiagen), from which first-strand cDNA was synthesized using RevertAid (Thermo Fischer Scientific). Real-time polymerase chain reaction (PCR) was performed using 2 × ABsolute™ QPCR SYBR Green Mix (Thermo Fischer Scientific). The reaction mixture contains 2 µL of cDNA from the first strand synthesis and 10 pmol of each primer pair (Table 1). PCR was carried out in a light-cycler (Roche) by adhering to the following steps: 15 min of initial activation followed by 45 cycles of 12 s at 94°C, 30 s at 50°C, and 30 s at 72°C. Fluorescence intensities were recorded after the extension step at 72°C after each cycle. Crossing points were determined by the software program provided by the manufacturer. Relative gene expression was quantified using the formula: $(2e^{(\text{Crossing point } \beta\text{-actin} - \text{Crossing point } X)}) \times 100 = \%$ of reference gene (β-actin) expression.

2.5 | Flow cytometry

The expression of surface markers for IMs and AMs was detected in a flow cytometer (Guava easyCyte; Merck Millipore) using a cell density of 2×10^5/mL in PBS containing 2% FCS and 0.5 mM EDTA. The cells were blocked with 0.5 µg of anti-mouse FcR (CD16/CD32, 553141; BD Biosciences) for 10 min RT to prevent nonspecific binding of the fluorochrome coupled antibody. The antibodies of interest (Table 2) were incubated for 20 min on ice and later washed twice with PBS to remove unbound antibodies. IMs were tested for macrophage-specific markers like CD11b—integrin αM, Mertk—myeloid epithelial reproductive tyrosine kinase, and Cx3cr1—a CX3C motif chemokine receptor 1. Another marker like MHCII—major histocompatibility complex II present in antigen-presenting cells was also tested. The M1 polarized IMs were examined for M1

TABLE 1 Primer pairs used for qRT-PCR.

Name	Sequence
TRPA1 forward	5′-TCTGCATATTGCCCTGCACA-3′
TRPA1 reverse	5′-TGGAAAATTTGGATCACTTCTTTGC-3′
TRPC1 forward	5′-GCCCCCACCTTTCAACATTA-3′
TRPC1 reverse	5′-GTCGCATGGACGTCAGGTAG-3′
TRPC2 forward	5′-CACGAAAGGAGCCTGAGTTTA-3′
TRPC2 reverse	5′-CCAGCAACTCGAAGCCATAG-3′
TRPC3 forward	5′-AGGCGCAGCGTATGTGGA-3′
TRPC3 reverse	5′-GGCCAAAGCTCTCGTTTGC-3′
TRPC4 forward	5′-CTCCGCCTGATCTCTCTGT-3′
TRPC4 reverse	5′-AAACGCGTTGTTCTGTTTCT-3′
TRPC5 forward	5′-ATGAGGGGCTAACAGAAGA-3′
TRPC5 reverse	5′-TGCAGCCTACATTGAAAGA-3′
TRPC6 forward	5′-CAAGCCTGTCTATTGAGGAA-3′
TRPC6 reverse	5′-CCCAACTCGAGACAAGTTT-3′
TRPC7 forward	5′-CCTACGCCAGGGATAAGTG-3′
TRPC7 reverse	5′-AAGGCCACAAATACCATGA-3′
TRPM2 forward	5′-TACCCACGAGCAACACTT-3′
TRPM2 reverse	5′-GGAGACCCGGACATACTT-3′
TRPM7 forward	5′-GCAAAGCAGAGTGACCTGGTA-3′
TRPM7 reverse	5′-GCCAGTTGGCCAAAATCAT-3′
TRPV2 forward	5′-CACCATAGTTGCCTACCACCA-3′
TRPV2 reverse	5′-GTCGCTTTGATGAGGGAAT-3′
TRPV3 forward	5′-CCACCACCATCTGGAACC-3′
TRPV3 reverse	5′-ATCTCCTTGGAGTGGGCATT-3′
TRPV4 forward	5′-GATGGCCTTTCGCCTCTC-3′
TRPV4 reverse	5′-TCGGATGATGTGCTGAAAGA-3′
Mertk forward	5′-ACGTTGGTGGATACGTGCAT-3′
Mertk reverse	5′-CTCTTCCCACTTCTCGGCAG-3′
Csf1 forward	5′-TACAAGTGGAAGTGGAGGAGCCAT-3′
Csf1 reverse	5′-AGTCCTGTGTGCCCAGCATAGAAT-3′
Csf1r forward	5′-AGGGCCATATACAGGTACACAT-3′
Csf1r reverse	5′-CACAGGCATCCATGTAACAC-3′
Csf2rb forward	5′-GGGCAGGAACACAGGACTTCAGGAC-3′
Csf2rb reverse	5′-CCAGGCCTCTAGCTACCTTGACAGG-3′
CD11b forward	5′-ATGGACGCTGATGGCAATACC-3′
CD11b reverse	5′-TCCCCATTCACGTCTCCCA-3′
Cx3cr1 forward	5′-GAGTATGACGATTCTGCTGAGG-3′
Cx3cr1 reverse	5′-CAGACCGAACGTGAAGACGAG-3′
CD11c forward	5′-CTGGATAGCCTTTCTTCTGCTG-3′

(Continues)

TABLE 1 (Continued)

Name	Sequence
CD11c reverse	5′-GCACACTGTGTCCGAACTCA-3′
Socs3 forward	5′-CGAAGCACGCAGCCAGTT-3′
Socs3 reverse	5′-TCC GTG GGT GGC AAA GAA-3′
CD38 forward	5′-TCTCTAGGAAAGCCCAGATCG-3′
CD38 reverse	5′-GTCCACACCAGGAGTGAGC-3′
CD86 forward	5′-CATGGGCTTGGCAATCCTTA-3′
CD86 reverse	5′-AAATGGGCACGGCAGATATG-3′
iNos forward	5′-GACATTACGACCCCTCCCAC-3′
iNos reverse	5′-GCACATGCAAGGAAGGGAAC-3′
Nox1 forward	5′-GGTTGGGGCTGAACATTTTTC-3′
Nox1 reverse	5′-TCGACACACAGGAATCAGGAT-3′
Nox2 forward	5′-TGTGGTTGGGGCTGAATGTC-3′
Nox2 reverse	5′-CTGAGAAAGGAGAGCAGATTTCG-3′
Nox3 forward	5′-CAAGTGTGTGCTGTAGAGGAC-3′
Nox3 reverse	5′-CTATCCCGTAGGCAACGAGTT-3′
Nox4 forward	5′-AGATTTGCCTGGAAGAACCCA-3′
Nox4 reverse	5′-GCTGCCATCGTTTCTGACAG-3′
β-Actin forward	5′-AAGGCAGTGGAGCAGGTGAA-3′
β-Actin reverse	5′-CCAGCAGACTCAATACACAC-3′

TABLE 2 Fluorochrome coupled antibodies for flow cytometry.

Antibody	Company	Clone	Conjugated fluorophore
CD11b	BioLegend	M1/70	FITC
Mertk	Thermo Fisher Scientific	DS5MMER	PE
CD38	BioLegend	90	FITC
MHCII	BioLegend	M5/114.15.2	APC/cyanine 7
Cx3cr1	BioLegend	SA011F11	PE
CD64	BioLegend	S18017D	PE
CD206 (MMR)	BioLegend	C068C2	FITC

marker CD38, a nicotinamide adenine dinucleotide (NAD+) hydrolase, which is specifically upregulated during inflammation in monocytes and macrophages (Li et al., 2022). Corresponding antibody isotypes were used for all antibodies as negative controls. Flow cytometry data were analyzed, and plots were created using R statistical software (packages—flowcore, ggcyto). Fluorescence intensities were quantified and represented as MFI—median fluorescence intensities.

2.6 | Polarization of IMs

IMs separated from WT and TRPM2-/- stromal cells co-cultures were seeded at a density of 2.5×10^5 in 2 mL of DMEM with supplements in tissue culture treated six-well plates for RNA isolation and non-coated six-well plates for flow cytometry. Cells were allowed to attach for 16 h and subsequently stimulated to M1 polarization state by replacing medium with fresh medium containing 50 ng/mL lipopolysaccharide (LPS; Invitrogen) and 50 ng/mL IFN-γ (PeproTech) (Tsurutani et al., 2021). As a solvent control, 0.1% bovine serum albumin was added to the medium. For M2 polarization, IMs were treated with 20 ng/mL IL-4 (RnD systems). After 24 h of stimulation, cells were harvested for flow cytometry and RNA isolation.

2.7 | Quantification of cytokines by enzyme-linked immunosorbent assay (ELISA)

Supernatants were collected from WT and TRPM2-/- IMs seeded for M1 and M2 polarization, described above, at 1, 3, 6, and 24 h and briefly centrifuged to remove dead cells The supernatants were stored at −80°C. The concentrations of pro-inflammatory cytokines—tumor necrosis factor-α (TNF-α), IL-1α, and IL-6 were detected using a murine Elisa max deluxe set (BioLegend; #430904, #433404, #431304, and #431414, respectively) according to the manufacturer's instructions. The assay diluent without cell supernatant was used as a blank. Finally, absorbance, which was read at 570 nm, was subtracted from the absorbance value at 450 nm. Four-parameter logistic curve-fitting for standards was performed and concentrations of cytokines in unknown samples were interpolated using GraphPad prism (version 10.1).

2.8 | Quantification of reactive oxygen species (ROS)

ROS were indirectly quantified in IMs treated with LPS and IFN-γ using a luminescence-based assay, GSH/GSSG-Glo assay (V6611; Promega), by measuring the levels of glutathione (GSH) and its oxidized form (GSSG) at 0, 10, 20, 30 and 40 min following treatment. The experiment was conducted according to the manufacturer's instructions. In addition, we quantified levels of ROS directly with the use of a fluorogenic probe 2′,7′-dichlorodihydrofluorescein diacetate (H_2DCFDA, 10 μM, D399; Thermo Fischer Scientific), which emits fluorescence only when exposed to ROS. Briefly, 15,000 cells were seeded per well in a 96-well plate in DMEM (without phenol red) for 16 h before the procedure. Cells were treated with 10 μM H2DCFDA for 60 min, followed by 15 min treatment with a selective inhibitor of NOX2 for (GSK2795039, 100 μM, SML2770; Merck). Finally, LPS and IFN-γ were added to cells at certain time points. Phorbol-12-myristat-13-acetate (PMA) (20 μM) was used as a positive control. In both experiments, the treatment was performed in HBSS without

serum. Luminescence for GSH/GSSG-Glo assay and fluorescence emitted by H_2DCFDA were detected using a microplate reader (Fluostar Omega; BMG Labtech).

2.9 | Electrophysiology

Patch-clamp experiments in the whole-cell configuration using voltage clamp or current clamp were performed with an EPC10 HEKA patch-clamp amplifier (Harvard Bioscience) and the Patch-Master software (Version V2x92; Harvard Bioscience) as reported previously (Mederos et al., 2008) with a few modifications. Patch pipettes were made of borosilicate glass (Science Products) and had a resistance of 2.0–3.7 MΩ when filled with the intracellular pipette solution. The extracellular solution contained in mM: 140 NaCl, 2.8 KCl, 1 $CaCl_2$, 2 $MgCl_2$, 10 HEPES-NaOH, and 11 glucose (all from Merck), pH 7.2. For whole-cell recordings of currents voltage ramps from −100 to +100 mV over 50 ms were applied every 2 s (holding potential between ramps was 0 mV). Voltages were corrected for a liquid junction potential of 10 mV. The current amplitudes at −80 and +80 mV were normalized to the cell size and presented as pA/pF. The capacitance was measured using the automated capacitance compensation function of the EPC10 software. Intracellular solution in mM: 140 Cs-glutamate, 8 NaCl, 1 $MgCl_2$, 10 HEPES–CsOH, pH 7.2, and in some experiments 0.2 ADPR (Merck) was applied. Current clamp experiments were performed with an intracellular solution, mM: 140 K glutamate, 8 NaCl, 1 $MgCl_2$, 10 Hepes-NaOH, pH 7.2, and 0.2 ADPR.

2.10 | Data mining and analysis

Transcriptome profile of murine IM by RNA sequencing was downloaded from the Gene Expression Omnibus RNA-seq database (GSE94135) and normalized counts of TRP channels were obtained using DESeq.2 package in R statistical software. Statistical testing and data visualization were performed using GraphPad Prism version 10.1.2 (GraphPad Software). *T*-tests and one-way analysis of variance (ANOVA) were performed for flow cytometry experiments. Two-way ANOVA was performed for the detection of cytokines and oxidative stress. Wilcoxon matched pairs signed rank test was performed for data in Figure 5c. Paired *T*-test was used in Figure 7a. Data are shown as mean ± SEM, with significance denoted as asterisks indicating $p < 0.05$ (*), 0.01 (**), 0.001 (***) and 0.0001 (****).

3 | RESULTS

3.1 | Isolation of lung interstitial macrophages by propagation and magnetic separation

Usually, IMs are isolated by fluorescence-activated cell sorting (FACS) with a range of antibodies specific for IMs. A major disadvantage of this method, however, is the very low cell count of IMs in steady state estimated to be ≈ 9% of extravascular myeloid cells, while it is ≈ 76% for AMs (Gibbings et al., 2017). In 2019, Ogawa et al. proposed an isolation method for resident macrophages not only from the lungs, but also from brain, spleen, and liver (Ogawa et al., 2019). Here, we present an improved version resulting in a higher number of isolated IMs (≈1.2 million cells per mouse compared to ≈ 30,000 cells per mouse after FACS isolation). After growth in a coculture with stromal cells, unstimulated IMs, which express the IM-specific CD11b protein (Gibbings et al., 2017), were isolated by immuno-magnetic separation using CD11b antibodies coupled to magnetic particles (Figure 1a). To validate this method, we characterized IMs for specific cell surface markers that differentiate them from AM by flow cytometry and qRT-PCR. Flow cytometric profiling revealed that IMs were positive for CD11b, Mertk, Cx3cr1, and CD64 (Figure 1b). IMs were mildly positive for MHCII, commonly expressed in antigen presenting cells and negative for CD206 (mannose membrane receptor), which is upregulated during anti-inflammatory conditions (Figure 1b). As a comparison, AMs were positive for Mertk and showed a low expression of CD64 and CD206, but were negative for CD11b, Cx3cr1, and MHCII (Figure 1c). By qRT-PCR experiments, high mRNA levels of CD11b, Cx3cr1, and colony stimulating factor 1 receptor (Csf1r) (Figure 1d) were detected in IMs. Csf1r, a surface protein majorly expressed in microglia (Lei et al., 2020), was recently found to be present in higher levels in IMs when compared to AMs (Meziani et al., 2018). MRNA levels of Mertk were clearly lower and mRNA for AM-specific colony-stimulating factor 2 receptor beta (Csf2rb) (Guilliams et al., 2013) was not detected in IMs (Figure 1d). The IMs isolated using our method, which were propagated with stromal cells and later separated, were therefore $CD11b^+$ $Cx3cr1^+$ $Mertk^+$ $MHCII^{lo}$ $CD64^+$ $CD206^-$as already described before (Gu et al., 2022).

3.2 | Polarization of IMs

Most of the IMs isolated from unchallenged mice are in the unstimulated or naïve state and can be polarized after application of LPS and IFN-γ to the pro-inflammatory M1 state, while incubation with IL-4 results in differentiation to the anti-inflammatory M2 state (Tsurutani et al., 2021) (Figure 2a). We validated the polarization by quantification of mRNA levels for marker proteins specifically upregulated in M1 and M2 states. Along this line, mRNAs for inducible nitric oxide synthase (iNos/Nos2), suppressor of cytokine signaling 3 (Socs3), CD86 were highly expressed in the M1 states (Figure 2b–d), while arginase-1 (Arg-1) and resistin-like alpha (Retnla) were upregulated in the M2 states (Figure 2f,g) (Gibbings et al., 2017), when compared to the unstimulated IMs. Recently, CD38 a surface glycoprotein, has gained more importance as a distinct M1 marker (Jablonski et al., 2015; Li et al., 2022). In bone-marrow-derived macrophages (BMDM), CD38 was expressed in higher quantities in M1 polarized macrophages. Like BMDM, M1 polarized IMs expressed higher levels of CD38 mRNAs (Figure 2e) and were also positive for CD38 protein compared to naïve and M2 polarized IMs (Supporting

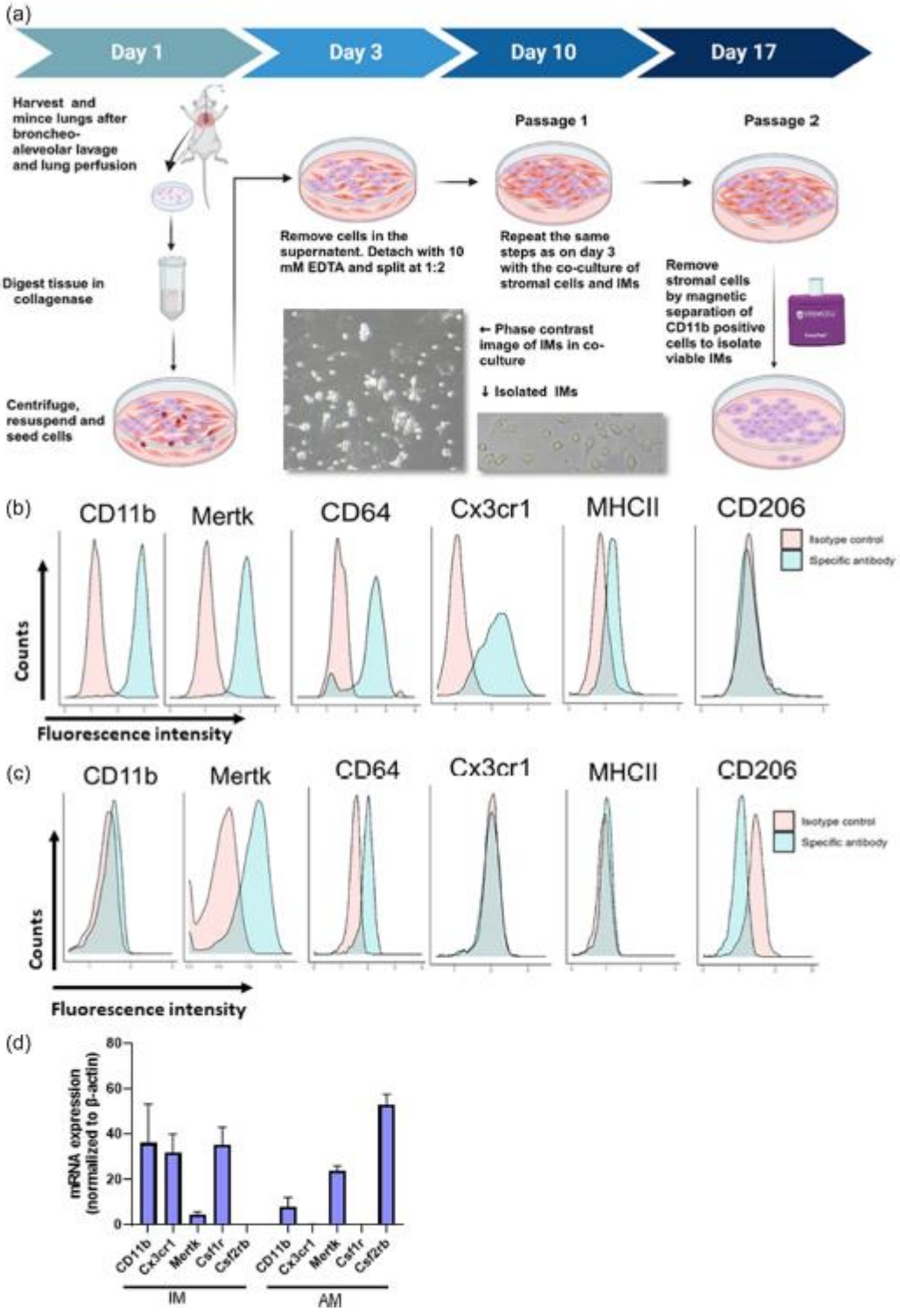

FIGURE 1 (See caption on next page).

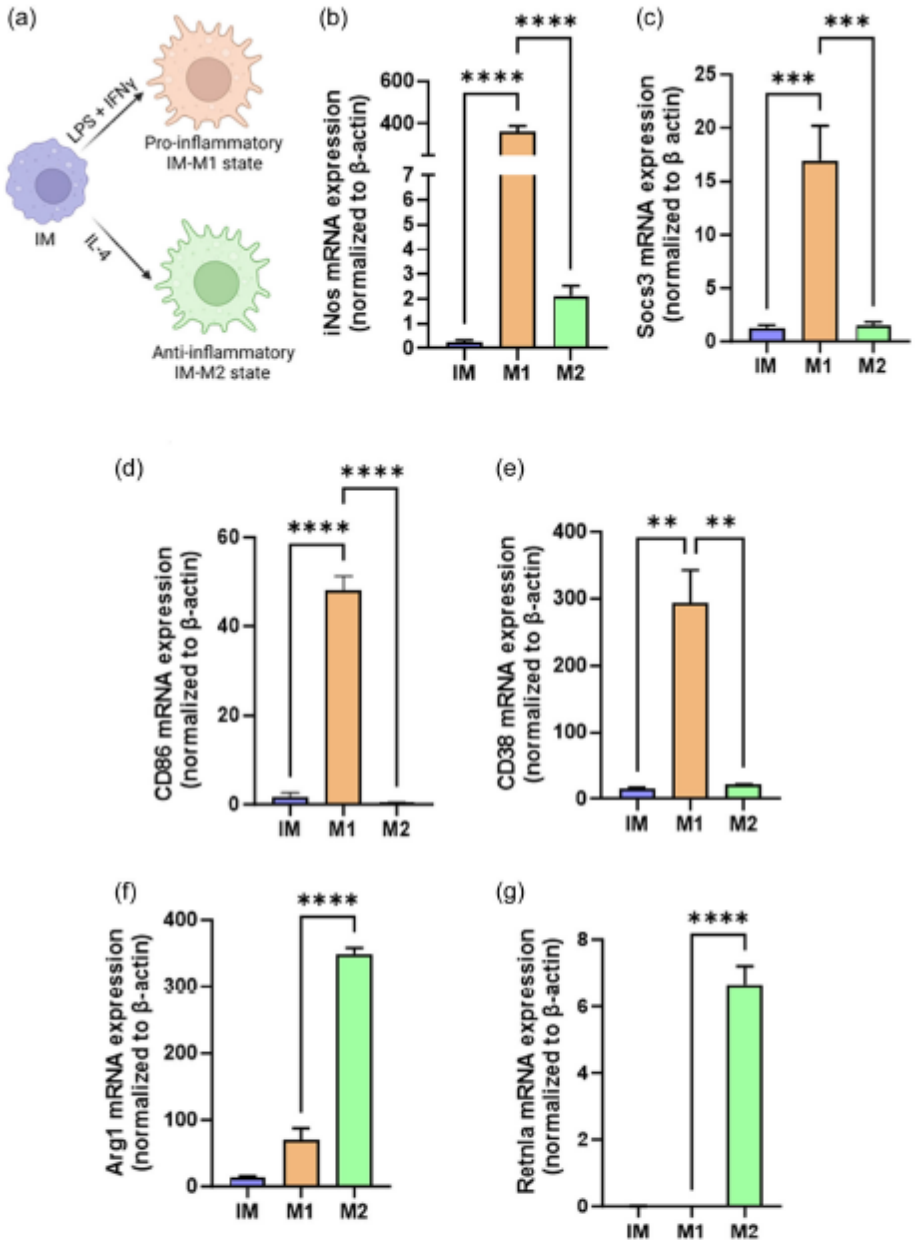

FIGURE 2 IM polarization. (a) Schema of the polarization protocol to obtain IM-M1 state and IM-M2 state cells from unstimulated IMs (IM). MRNA levels of M1-specific marker proteins iNos (b), Socs3 (c), CD86 (d) and CD38 (e) as well as M2-specific marker proteins Arg1 (f) and Retnla (g) in unstimulated IMs, IMs polarized to the M1 state (M1), and IMs polarized to the M2 state (M2). All samples are normalized to the expression of the housekeeping gene β-actin. $n = 3$ samples per group, ** $p < 0.01$, ***$p < 0.001$, ****$p < 0.0001$.

FIGURE 1 Isolation and characterization of IMs from murine lungs. (a) Timeline for isolation of IMs utilizing a coculture with stromal cells and magnetic separation of CD11b positive cells. (b, c) Representative histograms ($n = 3–6$ cell isolations) obtained by application of specific antibodies (in blue) or its corresponding isotype controls (in pink) from flow cytometric analyses of isolated IMs (b) and AMs as control cells (c). (b) Histograms of isolated IMs obtained after application of antibodies directed against typical marker proteins (CD11b, Mertk, CD64, Cx3cr1, MHCII and C206). MHCII is lowly and CD206 is not expressed at the plasma membrane of murine IMs. (c) Histograms of isolated AMs obtained after application of antibodies directed against typical marker proteins (CD11b, Mertk, CD64, Cx3cr1, MHCII, and C206). CD11b, Cx3cr1, and MHCII are not expressed in AMs. (d) mRNA levels of IM-specific marker proteins CD11b, Cx3cr1, and colony-stimulating factor 1 receptor (Csf1r), a general macrophage marker, Mertk, and the AM-specific marker protein (Csf2rb) detected by quantitative RT-PCR in the isolated IMs and AMs. $n = 3–5$ samples per group.

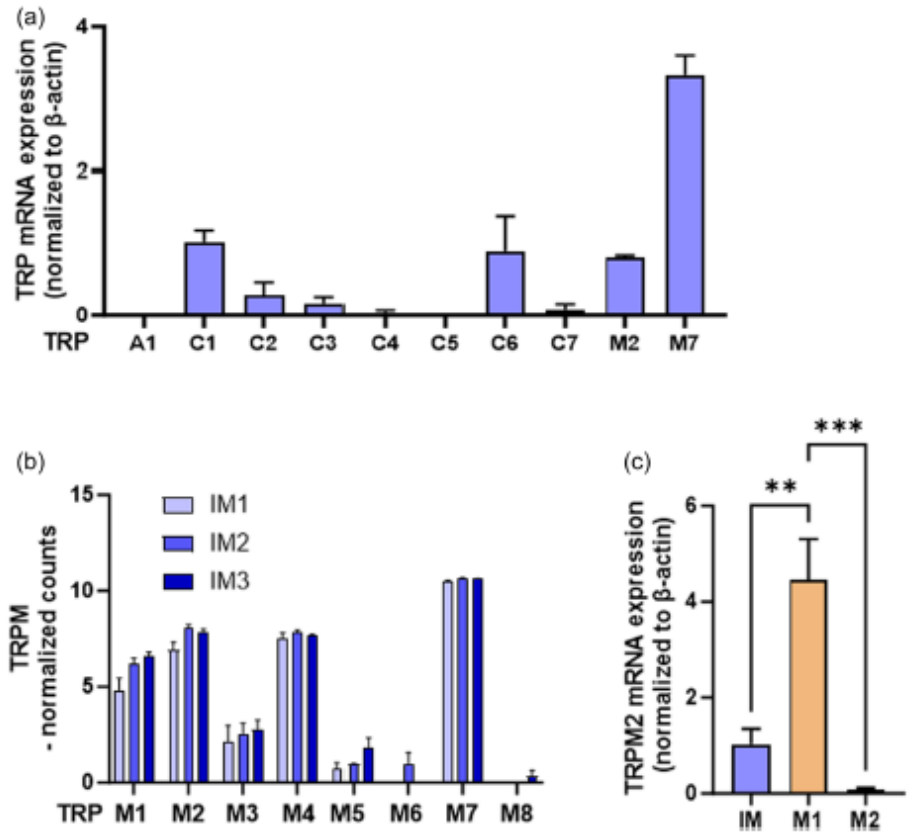

FIGURE 3 TRP expression in IMs. (a) mRNA levels of TRPA1, TRPC, TRPM2 and TRPM7 channels were quantified by quantitative RT-PCR. (b) Data for the mRNA expression of TRPM family genes as normalized counts from the three IM populations extracted from the bulk RNA-seq data set—GSE94135 (Gibbings et al., 2017). (c) Quantitative RT-PCR data for TRPM2 mRNA expression in unstimulated IMs (IM) and IMs polarized to the M1 (M1) or to the M2 state (M2). All samples are normalized to the expression of the housekeeping gene β-actin. $n = 3$ samples per group, $^{**}p < 0.01$, $^{***}p < 0.001$.

Information: Figure S1) denoting a high polarization rate in IMs detected with flow cytometry.

3.3 | TRP channels in IMs

TRP channels play a crucial role in functioning of immune cells in the body (Santoni et al., 2018; Froghi et al., 2021). TRPM2 is essential for monocytes (Yamamoto et al., 2008) as well as neutrophil function (Robledo-Avila et al., 2020), while TRPM7 is ubiquitously expressed in almost all cells of the body (Zou et al., 2019). TRPA1 is predominantly expressed in neuronal cells but was also detected in alveolar type II cells (Kannler et al., 2018). Therefore, we set out to identify TRP channel expression in IMs by quantifying mRNA levels of these TRP proteins (Figure 3a). As expected, no TRPA1 mRNA was detected, while TRPM7 mRNA was highly expressed. TRPC1 and TRPC6 as well as TRPM2 mRNA were identified in similar amounts (Figure 3a). We next analyzed TRPM mRNA expression levels in a publicly available bulk RNA-sequencing data set (NCBI data repository—GSE94135) of the three identified IM species (Gibbings et al., 2017). TRPM2 mRNA showed a similar high expression pattern like TRPM1 and TRPM4 in all three IM species (Figure 3b). As TRPM2 controls polarization of gastric macrophages (Beceiro et al., 2017), we analyzed the mRNA expression of this channel in polarized IMs and identified a highly significant upregulation in the polarized M1 state compared to the unstimulated cells (Figure 3c). Moreover, polarization to the M2 state by IL-4 resulted in a significant downregulation of TRPM2 mRNA compared to unstimulated IM and polarized M1 cells. Therefore, polarization of IMs to the M1 state after application of LPS and IFN-γ induces TRPM2 mRNA expression.

3.4 | CD38 upregulation in TRPM2-/- IM

Next, we quantified mRNAs of IM M1-specific surface marker proteins in TRPM2-deficient cells in comparison to WT cells. While SOCS3 (Figure 4a), CD86 (Figure 4b), and iNos (Figure 4c) were all upregulated in both cell types during M1 polarization in similar

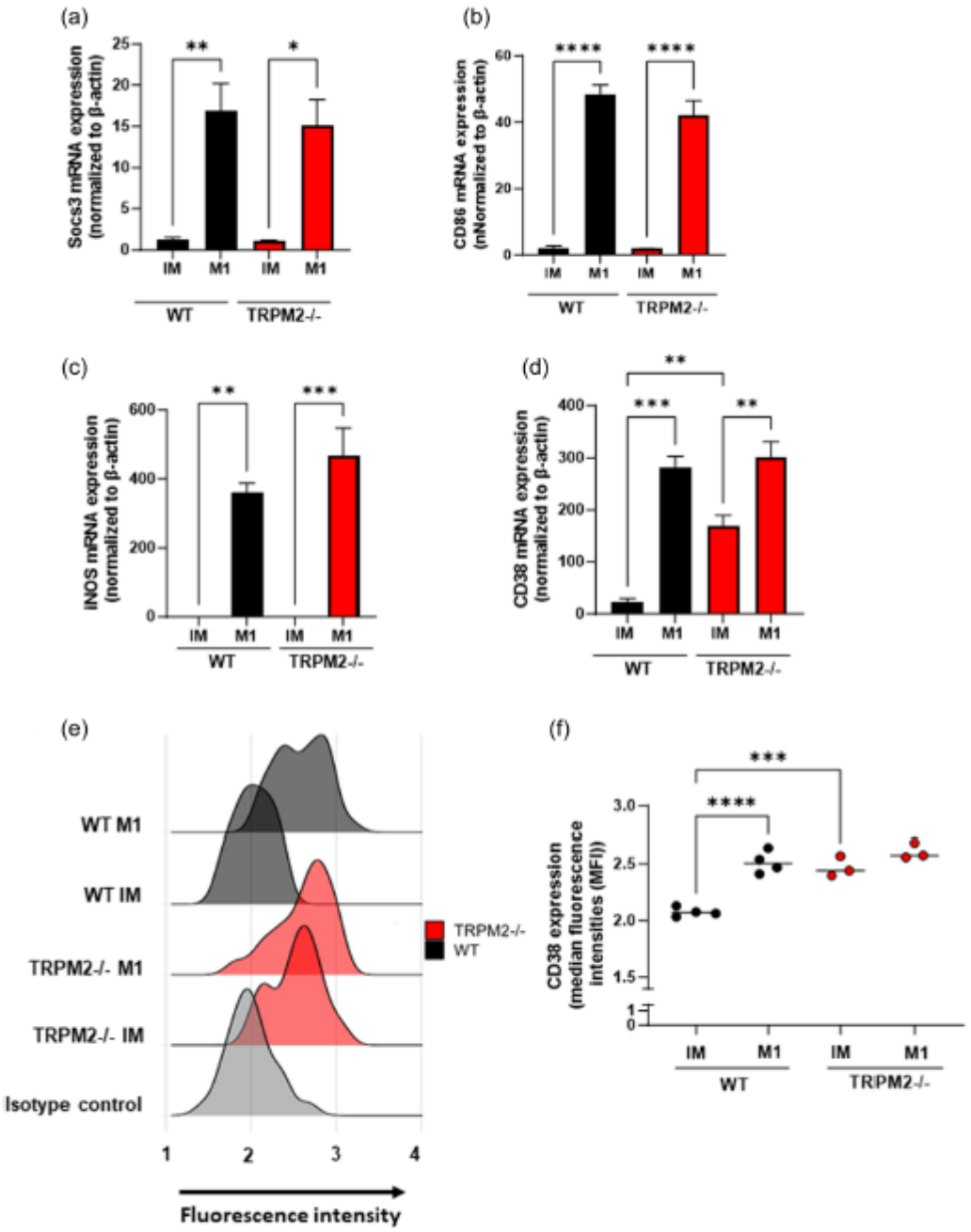

FIGURE 4 Characterization of M1 marker proteins in wild type (WT) and TRPM2-deficient (TRPM2-/-) IMs. (a–d) Quantification of mRNA levels of marker proteins specific for the M1 state (Socs3 (a), CD86 (b), iNos (c), and CD38 (d)) in WT (black) and TRPM2-/- (red) IMs. All samples are normalized to the expression of the housekeeping gene β-actin. (e) Representative histograms in a ridgeline plot obtained by flow cytometry after application of fluorescence-coupled anti CD38 antibodies to WT (in black) or TRPM2-/- (in red) IMs (IM) and IMs polarized to the M1 state (M1). The application of isotype antibodies serves as negative control (in gray). (f) Quantification of CD38 expression by analyzing the median fluorescence intensities (MFI) in flow cytometry experiments shown in (e). $n = 3–4$ samples per group, $^{*}p < 0.05$, $^{**}p < 0.01$, $^{***}p < 0.001$, $^{****}p < 0.0001$.

amounts, CD38 mRNA levels were already high in unstimulated TRPM2-deficient IMs and further increased during M1 polarization (Figure 4d). Most interestingly, CD38 is an ectoenzyme, which converts NAD^+ or cyclic ADP-ribose into ADPR, a specific activator of TRPM2 channels (reviewed in Lund et al., 1998; Numata et al., 2012) and is predominantly expressed in IMs polarized to the M1 state (Supporting Information: Figure S1) with higher levels of TRPM2 mRNA (Figure 3c). In contrast to the qRT-PCR data, CD38 protein levels on the cell surface analyzed by flow cytometry with specific fluorescence-coupled CD38 antibodies in TRPM2-deficient IMs were not significantly different compared to TRPM2-deficient and WT IMs polarized to the M1 state (Figure 4e,f) for yet unknown reasons.

3.5 | Electrophysiology of TRPM2 channels in IM and M1 polarized IMs

To verify TRPM2 activity in these cells, we quantified ADPR-induced currents in unstimulated and M1-polarized WT as well as TRPM2-deficient IMs in voltage clamp experiments. ADPR added from the patch pipette, in general did not increase current densities (pA/pF) in WT IMs in between 80 s after whole-cell break-in ($n = 9$ of 10 cells), similar to TRPM2-/- IMs polarized to the M1 state ($n = 6$ cells) (Figure 5a,c). After polarization of WT IMs to the M1 pro-inflammatory phenotype, ADPR-induced current densities significantly increased ($n = 10$ cells of 22) in contrast to WT IMs and TRPM2-/- IMs polarized to the M1 state, confirming our previous result showing upregulation of TRPM2 in M1 polarized WT IMs (Figure 3c). These results were also evident in the IV (current–voltage) curve depicted in Figure 5b. A fraction (12 of 22 cells) of M1 polarized WT IMs, however, did not develop increased current densities after adding ADPR for unknown reasons.

3.6 | Inflammatory cytokine release in TRPM2-/- IMs

An important function of IMs of the pro-inflammatory M1 state is the production of cytokines to attract other immune cells to the site invaded by pathogens (Aegerter et al., 2022). To test if TRPM2 is involved in the regulation of cytokine release by IMs, we polarized IMs isolated from WT and TRPM2-/- mice to the M1 state after application of LPS and IFN-γ and quantified mRNA levels of inflammatory cytokines like TNF-α, IL-1α and IL-6 using qRT-PCR. As expected, mRNA of levels of all three cytokines were upregulated in the M1 state of WT IMs, but most interestingly, a significantly higher expression was observed in TRPM2-/- IMs (Figure 6a–c). To confirm these results on a protein level, we also quantified the release of cytokines in cell supernatants at 0, 1, 3, 6, and 24 h after polarization using specific ELISAs for all three cytokines. Again, all three cytokines were upregulated in the M1 stated and were secreted in higher levels in TRPM2-/- IMs (Figure 6d–f). While TNF-α secretion was already significantly increased after 3 h in TRPM2-/- IMs after application of LPS and IFN-γ, IL-6 followed after 6 h and IL-1α after 24 h (Figure 6d–f). Therefore, deletion of TRPM2 in IMs, resulted in a higher upregulation of cytokine production and secretion compared to TRPM2-expressing WT cells.

3.7 | ROS production and membrane potentials in IMs

As cytokine production depends on ROS generation by nicotinamide adenine dinucleotide phosphate (NADPH)-oxidase (NOX) (Iles & Forman, 2002), which are closely regulated by the cell's membrane potentials. Our voltage clamp experiments (Figure 5) showed increases in current densities by TRPM2 channels only in M1-polarized WT IMs (Figure 5). Therefore, we analyzed changes in the membrane potential in current-clamp experiments in WT IMs of the M1 state. We were able to identify significantly higher membrane potentials by cation influx through TRPM2 channels after the application of ADPR in M1-polarized WT IMs (Figure 7a). Moreover, mRNA levels of NADPH oxidase 2 (NOX2) as the most predominantly expressed NOX isoform were significantly increased in IMs polarized to M1 from TRPM2-/- mice compared to non-polarized IMs and IMs from WT mice (Figure 7b and Supporting information: Figure S2). Indeed, ROS production detected by a specific fluorescent dye (H_2DCFDA) was significantly higher in TRPM2-/- IMs after 30 and 40 min of treatment with LPS and IFN-γ when compared to WT IMs (Figure 7c). As a consequence of higher ROS production, the ratio of reduced to oxidized glutathione (GSH/GSSG), a well-known marker for oxidative stress, is reduced (Yamada et al., 2006; Zitka et al., 2012). We observed a simultaneous ROS-dependent reduction of GSH/GSSG in both WT and TRPM2-/- IMs. However, the decrease was significantly more pronounced in TRPM2-/- IMs (Figure 7d). Addition of a NOX2 inhibitor, GSK2795039 (Hirano et al., 2015), diminishes the production of ROS in both WT and TRPM2-/- IMs (Figure 7e). Hence, ablation of TRPM2 in IMs leads to higher ROS production, possibly orchestrated by NOX2, accompanied with a decline in GSH/GSSH ratios.

4 | DISCUSSION

Studying IMs was complicated, as viable isolated cell numbers were low, due to their remote location in lung tissues (Aegerter et al., 2022). Therefore, most of the studies characterized IM populations in the lung by fluorescence activated cell sorting followed by single-cell RNA-sequencing techniques (Chakarov et al., 2019; Gibbings et al., 2017; Schyns et al., 2018). However, for a more functional approach, increased numbers of viable cells are essential, which was achieved by coculturing IMs with stromal cells (Ogawa et al., 2019). We improved this published method by reducing the duration of coculture and by a magnetic separation with particles coupled to CD11b antibodies, which is less time-consuming (Figure 1a). It utilizes

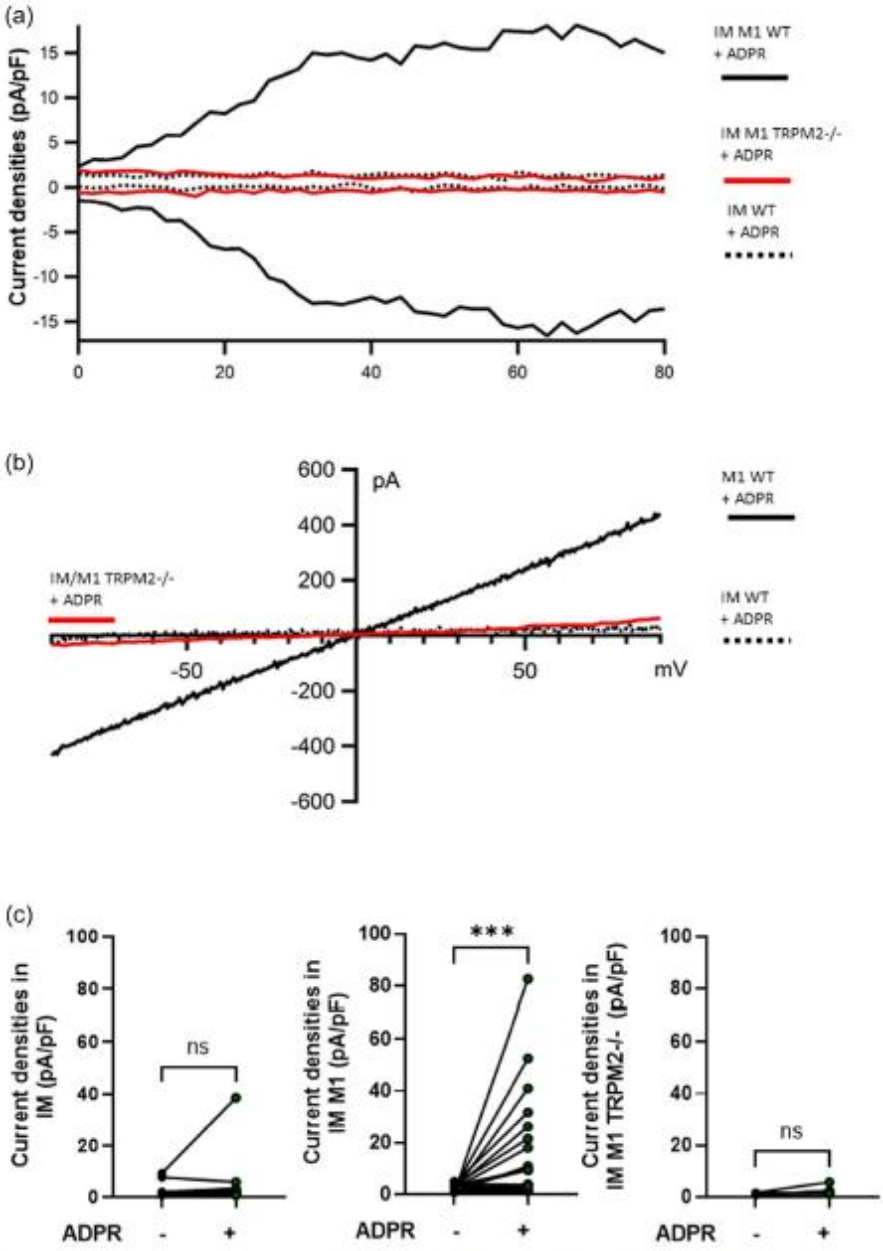

FIGURE 5 Electrophysiological characterization of TRPM2 currents in IMs induced by ADP-ribose (ADPR). (a) Current densities (pA/pF) in presence of ADPR in wild-type (WT) IMs (IM WT, black stippled line), M1 polarized IMs (IM M1 WT, black line), and TRPM2-deficient IMs polarized to the M1 state (IM M1 TRPM2-/-, red line). Data from representative experiments are shown (for IM M1 WT, 10 of 22 cells). (b) IV (current–voltage) curve of maximum currents detected after application of ADPR in WT IMs (IM WT, black stippled line), M1 polarized IMs (IM M1 WT, black line), and TRPM2-deficient IMs polarized to the M1 state (IM M1 TRPM2-/-, red line). Data from representative experiments are shown (for IM M1 WT, 10 of 22 cells). (c) Scatter plots summarizing changes in current densities of WT IMs (IM WT, $n = 10$) WT IMs polarized to the M1 state (IM M1 WT, $n = 22$) and TRPM2-deficient IMs polarized to the M1 state (IM M1 TRPM2-/-, $n = 6$) before (black circles) and after (green circles) application of ADPR. Statistical analysis was performed by a Wilcoxon matched pairs signed rank test. *** $p < 0.001$.

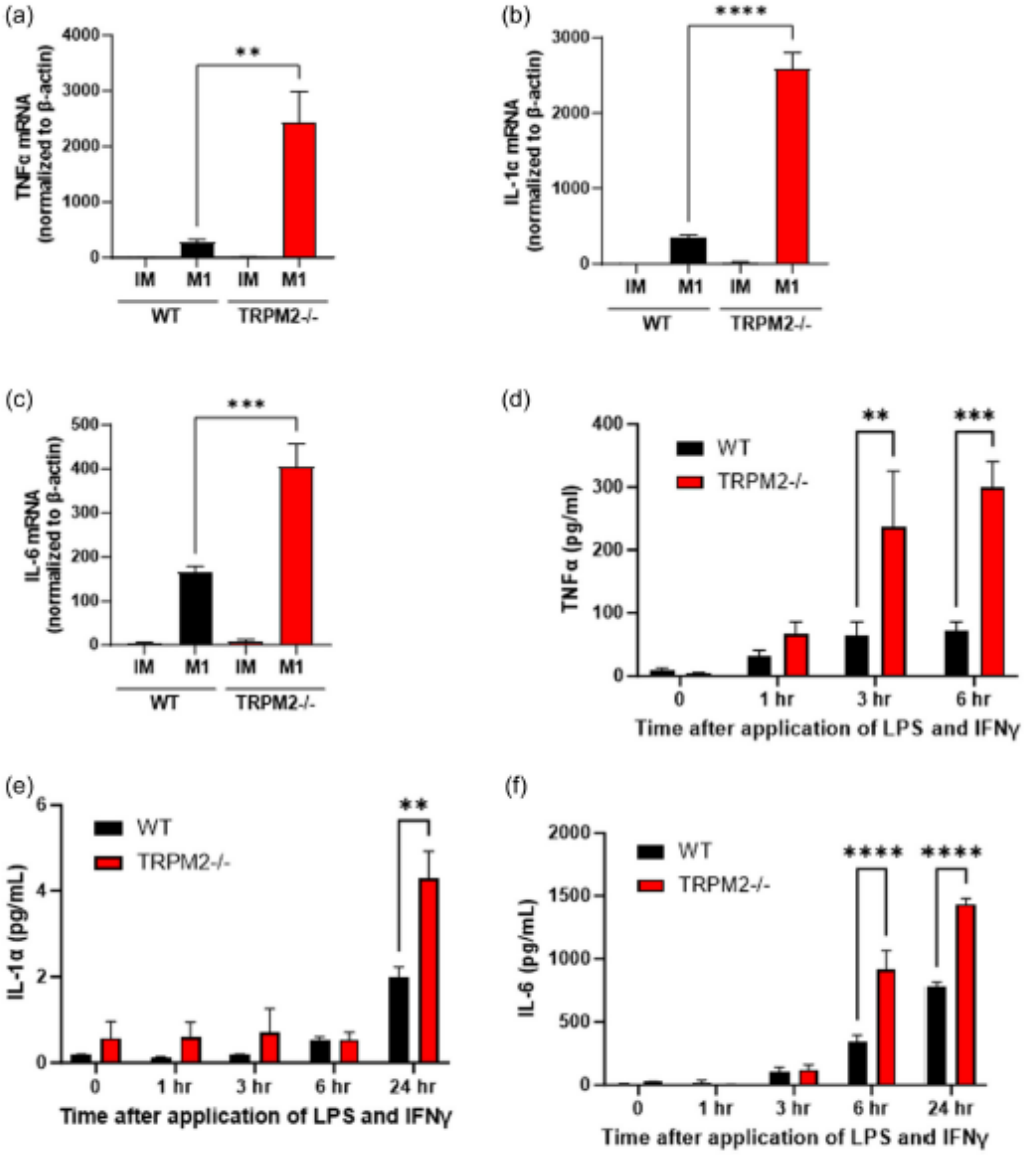

FIGURE 6 Cytokine production and secretion in unstimulated or M1 polarized wild-type (WT) and TRPM2-deficient (TRPM2-/-) IMs. (a) mRNA levels of tumor necrosis factor α (TNF-α), (b) interleukin-1α (IL-1α), (c) Interleukin 6 (IL-6) were measured by quantitative RT-PCR and normalized to the expression of the housekeeping gene β-actin. (d) TNF-α, (e) IL-1α, and (f) IL-6 secretion after application of lipopolysaccharide (LPS) and interferon-γ (IFN-γ) was quantified by enzyme-linked immunosorbent assays (ELISAs) in the culture supernatant. $n = 3–4$ samples per group, $^{**}p < 0.01$, $^{***}p < 0.001$, $^{****}p < 0.0001$.

a murine IM-specific marker (reviewed in Gu et al., 2022), which is not present in closely related alveolar macrophages (AMs) removed by an initial bronchoalveolar lavage (Figure 1b,d). Moreover, mRNA for Csf1r as another IM-specific marker was expressed in our isolated IMs, while mRNA for the AM-specific Csf2rb was not detected (Figure 1e) and closely related dendritic cells do not express CD64 (Figure 1b) (Misharin et al., 2013). Thus, we hope that this isolation procedure, will stimulate research on IM function in the future. Like AMs, IMs can be polarized to a pro-inflammatory M1 state and an anti-inflammatory M2 state for tissue repair (Tsurutani et al., 2021) in vitro to serve the needs of a closely regulated immune response. Successful polarization to both states was verified by an upregulation of mRNA expression of specific marker proteins (Figure 2b–f). Several reports showed evidence that these polarized states of IMs exist in vivo in challenged mice (Dumigan et al., 2022; Ji et al., 2014; Nie et al., 2017; Peng et al., 2024; Strickland et al., 2023), but the

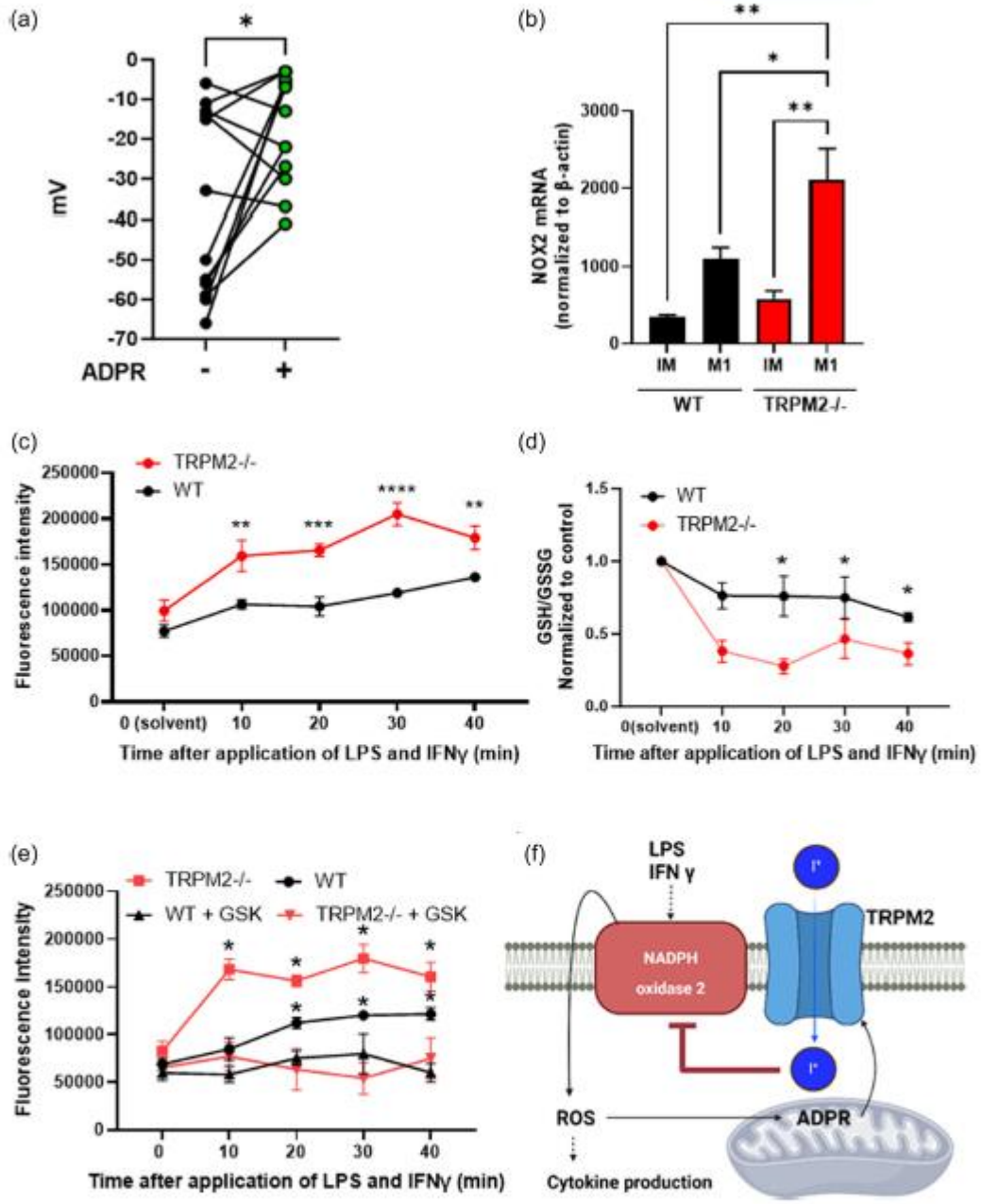

FIGURE 7 Membrane potentials and production of reactive oxygen species (ROS) in IMs. (a) Quantification of membrane potentials in IMs before (black circles) and after application of ADP-ribose (ADPR) (green circles). (b) Quantification of mRNA levels of the NADPH isoform 2 (NOX2) in IMs (IM) and IMs polarized to the M1 state (M1) from wild-type (WT, black columns) and TRPM2-deficient (TRPM2-/-, red columns) mice. All samples are normalized to the expression of the housekeeping gene β-actin. (c) Detection of intracellular ROS levels by measuring fluorescence intensity of 2′,7′-dichlorodihydrofluorescein diacetate (H_2DCFDA), (d) luminescence ratios of reduced to oxidized glutathione (GSH/GSSG), (e) with or without NOX2 inhibitor GSK2795039 following the application of lipopolysaccharide (LPS) and interferon-γ (IFN-γ) at various time points. (f) Schematic presentation of events inducing TRPM2-mediated inhibition of cytokine production and secretion. See text for more details. $n = 3–4$ samples per group, $^*p < 0.05$ (in (e) to all other values), $^{**}p < 0.01$, $^{***}p < 0.001$, $^{****}p < 0.0001$.

exact mechanism of polarization of IMs in lung tissues remains elusive.

TRP channels are expressed in a variety of different cell types and serve multiple functions in the human body (Nilius & Szallasi, 2014). We detected mRNAs of two members of the TRPC family TRPC1 and TRPC6 together with TRPM2 and TRPM7 in the isolated IMs. Using bulk RNA-sequencing data from a publication characterizing three different populations of IMs (Gibbings et al., 2017), we were able to analyze the transcriptome profile of IMs, including members of the TRPM gene family (Chubanov et al., 2024). TRPM2 next to TRPM4 mRNA was highly expressed in all three IM populations (Figure 3b). As TRPM2 serves an important role in monocytes and other immune cells (reviewed in Faouzi & Penner, 2014), we started to study this channel utilizing a TRPM2-deficient mouse model (Yamamoto et al., 2008). TRPM2-/- IM cells were successfully polarized to the M1 state as demonstrated by an upregulation of mRNAs for M1-specific marker proteins (Figure 4a–c). However, CD38 as an additional marker protein was already upregulated in unstimulated IMs (Figure 4d–f). CD38 is an ectoenzyme converting NAD+ in ADPR (reviewed in Chini et al., 2020; Guerreiro et al., 2020), a specific activator of TRPM2 channels (Numata et al., 2012; reviewed in Faouzi & Penner, 2014). ADPR production by CD38, next to generation in mitochondria as well as poly(ADPR) polymerase (PARP) and poly(ADPR) glycohydrolase (PARG) in the nucleus, is indeed able to activate TRPM2 channels in living cells (reviewed in Faouzi & Penner, 2014). Although TRPM2-deficient IMs express higher levels of CD38, changes in other markers like iNos, Socs3, and CD86 remain comparable to WT (Figure 4a–d). Moreover, the basal level of cytokine secretion is still lower than in the stimulated states (Figure 6d-f). Together, these findings denote that TRPM2-/- IMs remain unpolarized in steady-state. Mechanistically, TRPM2 channels might downregulate CD38 in unstimulated IMs by a yet unknown mechanism to avoid over-production of ADPR and over-activation of the channels by a negative feedback loop, which needs to be dissected further. Importantly, TRPM2 mRNA was not only expressed in unstimulated IMs, but significantly upregulated after polarization to the M1, but not to the M2 state (Figure 3c).

As identification of endogenous TRPM2 channels with antibodies remains challenging and can be misleading, we relayed on a functional approach by quantifying TRPM2 currents induced by the well-studied activator ADPR (Perraud et al., 2001). Application of ADPR induced strong currents in IMs polarized to the M1 state, which was significantly lower in unstimulated IMs and absent in TRPM2-/- cells (Figure 5a,b). To the best of our knowledge, we present here the first successful patch-clamp recordings of specific TRPM2 currents in IMs in the whole-cell mode confirming an upregulation of TRPM2 proteins in the M1 state.

The innate immune response of macrophages against invading micro-organisms is the immediate release of pro-inflammatory cytokines. When infected with *H. pylori*, the resident macrophages isolated from the gastric mucosa of TRPM2-/- mice showed augmented levels of pro-inflammatory cytokines (Beceiro et al., 2017). Moreover, on a functional basis, IMs are rather important for cytokine production than for phagocytosis, which is the main task of AMs in the alveolus (Aegerter et al., 2022). Therefore, we quantified cytokine mRNA expression and secretion in unstimulated and M1-polarized IMs. Surprisingly, cytokine production and secretion to the extracellular medium were significantly higher in TRPM2-deficient IMs polarized to the M1 state in comparison to WT cells (Figure 6a–f). When the phagocytes are subjected to oxidative stress, there is an increase in ROS generation which consequently activates the transcription of nuclear factor-kappa-light-chain-enhancer of activated B-cells (NF-κB) as one of its downstream effects. This activation initiates a positive feedback loop of continuous ROS generation by NADPH oxidase (Anrather et al., 2006; Morgan & Liu, 2011) ultimately leading to increased expression of pro-inflammatory cytokines (Lawrence, 2009). Cytokine production is strictly correlated to ROS production via coupling an unbalanced glutathione redox status to activation of NF-κB signaling (reviewed in Filippin et al., 2008). In the initial stages of host defense against infection, circulating neutrophils migrate to the site and eventually, induce respiratory burst to release ROS for bactericidal functions. TRPM2 has already been linked with this process of respiratory burst in neutrophils (Yamamoto et al., 2008). Concomitantly, low-grade respiratory bursts have also been reported in macrophages and rather for intracellular signaling than for killing of bacteria (Iles & Forman, 2002). As TRPM2 is a key player in ROS-mediated signaling in various cell types and pathologies like cancer and ischemic stroke (reviewed in Maliougina & El Hiani, 2023), the next step was to measure the levels of ROS in IMs. LPS and IFN-γ-induced ROS production in M1 polarized IMs was higher (Figure 7c) and GSH/GSSG levels were suppressed in TRPM2-/- cells (Figure 7d). Our study demonstrates that TRPM2 plays an essential role in the regulation of ROS production in IMs and confirms previous data in cardiomyocytes, where Ca^{2+} influx via TRPM2 is essentially required for the reduction of oxidative stress (Hoffman et al., 2015).

As ROS production by NADPH oxidases is inhibited by increases in the cell membrane potential (DeCoursey, 2003; Petheo & Demaurex, 2005), we quantified membrane potentials in IMs before and after application of ADPR. Indeed, membrane potentials were significantly higher in cells after TRPM2 activation by ADPR (Figure 7a), most probably by an enhanced cation influx through the channels. Most interestingly, a similar observation was reported in bone marrow-derived macrophages (BMDMs) after stimulation with LPS (Di et al., 2011). ADPR can be released from mitochondria by ROS, especially by ROS-produced H_2O_2 and activate TRPM2 channels (Ayub & Hallett, 2004; Perraud et al., 2005) to inhibit NADPH oxidase by membrane depolarization. Importantly, mRNA levels of NADPH oxidase 2 (NOX2) as the most predominantly expressed NOX isoform were significantly increased in TRPM2-/- IMs polarized to M1 (Figure 7b), pointing to an inhibitory role of TRPM2 channels also on the transcriptional level. Reduction of NOX expression and activity will reduce the generation of ROS and

cytokine production as well as its secretion (see Figure 7f). Our data are therefore another example of a rather beneficial than detrimental effect of TRPM2 channels following oxidative stress (as reviewed in Maliougina & El Hiani, 2023; Miller & Cheung, 2016).

5 | CONCLUSIONS

In summary, we introduced an efficient method to isolate IMs from mouse models, polarized them to the pro-inflammatory M1 state and were able to identify ADPR-induced TRPM2 currents, but not in TRPM2-deficient IMs. Surprisingly, cytokine production and secretion were exacerbated in TRPM2-/- IMs, pointing to an important regulatory function of the redox-sensitive TRPM2 channels for cytokine release from IMs. Overproduction and secretion of cytokines by immune cells were recently described as a "cytokine storm" in COVID-19 patients, resulting in increased mortality. Therefore, previous data in BMDMs (Di et al., 2011) and our findings in IMs might be the basis for an efficient therapeutic option with TRPM2 channel activators to mitigate cytokine-induced pathologies in these patients in the future.

AUTHOR CONTRIBUTIONS

Alexander Dietrich contributed to the conception, design and funding of the study, interpreted the data, wrote the manuscript, and finally approved the submission. Suhasini Rajan was responsible for most of the experiments, data collection, coordinated its progress and research direction and wrote the manuscript draft. Vladimir Chubanov and Alexey Shalygin were responsible for patch-clamp experiments. Thomas Gudermann reviewed and revised the final manuscript. All authors have read and agreed to submit the final manuscript.

ACKNOWLEDGMENTS

We thank Dr. Yasuo Mori (Kyoto University, Japan) for sharing his TRPM2-deficient mouse model with us. We would like to acknowledge Ananya Kadekar for her assistance in the lab and Raffaele Conca for helping with sorting IMs. A. D., S. R., V. C., and T. G. were supported by the Deutsche Forschungsgemeinschaft (DFG) (TRR 152 [P15, P16] and GRK 2338 RTG [P04, P10]) and the German Center for Lung Research (DZL). Open Access funding enabled and organized by Projekt DEAL.

CONFLICT OF INTEREST STATEMENT

The authors declare no conflict of interest.

ETHICS STATEMENT

Tissue extraction from mouse models was approved by the regional authorities (Regierung Oberbayern).

ORCID

Suhasini Rajan http://orcid.org/0009-0009-6088-0293
Alexander Dietrich http://orcid.org/0000-0002-1168-8707

REFERENCES

Aegerter, H., Lambrecht, B. N., & Jakubzick, C. V. (2022). Biology of lung macrophages in health and disease. *Immunity*, *55*(9), 1564–1580. https://doi.org/10.1016/j.immuni.2022.08.010

Anrather, J., Racchumi, G., & Iadecola, C. (2006). NF-κB regulates phagocytic NADPH oxidase by inducing the expression of gp91. *Journal of Biological Chemistry*, *281*(9), 5657–5667. https://doi.org/10.1074/jbc.M506172200

Ayub, K., & Hallett, M. B. (2004). The mitochondrial ADPR link between Ca^{2+} store release and Ca^{2+} influx channel opening in immune cells. *The FASEB Journal*, *18*(12), 1335–1338. https://doi.org/10.1096/fj.04-1888hyp

Beceiro, S., Radin, J. N., Chatuvedi, R., Piazuelo, M. B., Horvarth, D. J., Cortado, H., Gu, Y., Dixon, B., Gu, C., Lange, I., Koomoa, D. L., Wilson, K. T., Algood, H. M. S., & Partida-Sánchez, S. (2017). TRPM2 ion channels regulate macrophage polarization and gastric inflammation during *Helicobacter pylori* infection. *Mucosal Immunology*, *10*(2), 493–507. https://doi.org/10.1038/mi.2016.60

Bedoret, D., Wallemacq, H., Marichal, T., Desmet, C., Quesada Calvo, F., Henry, E., Closset, R., Dewals, B., Thielen, C., Gustin, P., de Leval, L., Van Rooijen, N., Le Moine, A., Vanderplasschen, A., Cataldo, D., Drion, P. V., Moser, M., Lekeux, P., & Bureau, F. (2009). Lung interstitial macrophages alter dendritic cell functions to prevent airway allergy in mice. *Journal of Clinical Investigation*, *119*(12), 3723–3738. https://doi.org/10.1172/JCI39717

Chakarov, S., Lim, H. Y., Tan, L., Lim, S. Y., See, P., Lum, J., Zhang, X. M., Foo, S., Nakamizo, S., Duan, K., Kong, W. T., Gentek, R., Balachander, A., Carbajo, D., Bleriot, C., Malleret, B., Tam, J. K. C., Baig, S., Shabeer, M., … Ginhoux, F. (2019). Two distinct interstitial macrophage populations coexist across tissues in specific subtissular niches. *Science*, *363*(6432), eaau0964. https://doi.org/10.1126/science.aau0964

Cheng, P., Li, S., & Chen, H. (2021). Macrophages in lung injury, repair, and fibrosis. *Cells*, *10*(2), 436. https://doi.org/10.3390/cells10020436

Chini, C. C. S., Peclat, T. R., Warner, G. M., Kashyap, S., Espindola-Netto, J. M., de Oliveira, G. C., Gomez, L. S., Hogan, K. A., Tarragó, M. G., Puranik, A. S., Agorrody, G., Thompson, K. L., Dang, K., Clarke, S., Childs, B. G., Kanamori, K. S., Witte, M. A., Vidal, P., Kirkland, A. L., … Chini, E. N. (2020). CD38 ecto-enzyme in immune cells is induced during aging and regulates NAD(+) and NMN levels. *Nature Metabolism*, *2*(11), 1284–1304. https://doi.org/10.1038/s42255-020-00298-z

Chubanov, V., Köttgen, M., Touyz, R. M., & Gudermann, T. (2024). TRPM channels in health and disease. *Nature Reviews Nephrology*, *20*(3), 175–187. https://doi.org/10.1038/s41581-023-00777-y

DeCoursey, T. E. (2003). Interactions between NADPH oxidase and voltage-gated proton channels: Why electron transport depends on proton transport. *FEBS Letters*, *555*(1), 57–61. https://doi.org/10.1016/s0014-5793(03)01103-7

Di, A., Gao, X. P., Qian, F., Kawamura, T., Han, J., Hecquet, C., Ye, R. D., Vogel, S. M., & Malik, A. B. (2011). The redox-sensitive cation channel TRPM2 modulates phagocyte ROS production and inflammation. *Nature Immunology*, *13*(1), 29–34. https://doi.org/10.1038/ni.2171

Dumigan, A., Cappa, O., Morris, B., Sá Pessoa, J., Calderon-Gonzalez, R., Mills, G., Lancaster, R., Simpson, D., Kissenpfennig, A., & Bengoechea, J. A. (2022). In vivo single-cell transcriptomics reveal *Klebsiella pneumoniae* skews lung macrophages to promote infection. *EMBO Molecular Medicine*, *14*(12), e16888. https://doi.org/10.15252/emmm.202216888

Faouzi, M., & Penner, R. (2014). Trpm2. *Handbook of Experimental Pharmacology*, *222*, 403–426. https://doi.org/10.1007/978-3-642-54215-2_16

Filippin, L. I., Vercelino, R., Marroni, N. P., & Xavier, R. M. (2008). Redox signalling and the inflammatory response in rheumatoid arthritis.

Clinical and Experimental Immunology, *152*(3), 415–422. https://doi.org/10.1111/j.1365-2249.2008.03634.x

Fliegert, R., Watt, J. M., Schöbel, A., Rozewitz, M. D., Moreau, C., Kirchberger, T., Thomas, M. P., Sick, W., Araujo, A. C., Harneit, A., Potter, B. V. L., & Guse, A. H. (2017). Ligand-induced activation of human TRPM2 requires the terminal ribose of ADPR and involves Arg1433 and Tyr1349. *Biochemical Journal*, *474*(13), 2159–2175. https://doi.org/10.1042/BCJ20170091

Froghi, S., Grant, C. R., Tandon, R., Quaglia, A., Davidson, B., & Fuller, B. (2021). New insights on the role of TRP channels in calcium signalling and immunomodulation: Review of pathways and implications for clinical practice. *Clinical Reviews in Allergy & Immunology*, *60*(2), 271–292. https://doi.org/10.1007/s12016-020-08824-3

Gibbings, S. L., Thomas, S. M., Atif, S. M., McCubbrey, A. L., Desch, A. N., Danhorn, T., Leach, S. M., Bratton, D. L., Henson, P. M., Janssen, W. J., & Jakubzick, C. V. (2017). Three unique interstitial macrophages in the murine lung at steady state. *American Journal of Respiratory Cell and Molecular Biology*, *57*(1), 66–76. https://doi.org/10.1165/rcmb.2016-0361OC

Gu, Y., Lawrence, T., Mohamed, R., Liang, Y., & Yahaya, B. H. (2022). The emerging roles of interstitial macrophages in pulmonary fibrosis: A perspective from scRNA-seq analyses. *Frontiers in Immunology*, *13*:923235. https://doi.org/10.3389/fimmu.2022.923235

Guerreiro, S., Privat, A. L., Bressac, L., & Toulorge, D. (2020). CD38 in neurodegeneration and neuroinflammation. *Cells*, *9*(2), 471. https://doi.org/10.3390/cells9020471

Guilliams, M., De Kleer, I., Henri, S., Post, S., Vanhoutte, L., De Prijck, S., Deswarte, K., Malissen, B., Hammad, H., & Lambrecht, B. N. (2013). Alveolar macrophages develop from fetal monocytes that differentiate into long-lived cells in the first week of life via GM-CSF. *Journal of Experimental Medicine*, *210*(10), 1977–1992. https://doi.org/10.1084/jem.20131199

Hirano, K., Chen, W. S., Chueng, A. L., Dunne, A. A., Seredenina, T., Filippova, A., Ramachandran, S., Bridges, A., Chaudry, L., Pettman, G., Allan, C., Duncan, S., Lee, K. C., Lim, J., Ma, M. T., Ong, A. B., Ye, N. Y., Nasir, S., Mulyanidewi, S., … Rutter, A. R. (2015). Discovery of GSK2795039, a novel small molecule NADPH oxidase 2 inhibitor. *Antioxidants & Redox Signaling*, *23*(5), 358–374. https://doi.org/10.1089/ars.2014.6202

Hoeffel, G., Chen, J., Lavin, Y., Low, D., Almeida, F. F., See, P., Beaudin, A. E., Lum, J., Low, I., Forsberg, E. C., Poidinger, M., Zolezzi, F., Larbi, A., Ng, L. G., Chan, J. K. Y., Greter, M., Becher, B., Samokhvalov, I. M., Merad, M., & Ginhoux, F. (2015). C-Myb(+) erythro-myeloid progenitor-derived fetal monocytes give rise to adult tissue-resident macrophages. *Immunity*, *42*(4), 665–678. https://doi.org/10.1016/j.immuni.2015.03.011

Hoffman, N. E., Miller, B. A., Wang, J., Elrod, J. W., Rajan, S., Gao, E., & Cheung, J. Y. (2015). Ca(2)(+) entry via Trpm2 is essential for cardiac myocyte bioenergetics maintenance. *American Journal of Physiology: Heart and Circulatory Physiology*, *308*(6), H637–H650. https://doi.org/10.1152/ajpheart.00720.2014

Iles, K. E., & Forman, H. J. (2002). Macrophage signaling and respiratory burst. *Immunologic Research*, *26*(1–3), 095–106. https://doi.org/10.1385/IR:26:1-3:095

Jablonski, K. A., Amici, S. A., Webb, L. M., Ruiz-Rosado, J. D., Popovich, P. G., Partida-Sanchez, S., & Guerau-de-Arellano, M. (2015). Novel markers to delineate murine M1 and M2 macrophages. *PLoS One*, *10*(12), e0145342. https://doi.org/10.1371/journal.pone.0145342

Ji, W. J., Ma, Y. Q., Zhou, X., Zhang, Y. D., Lu, R. Y., Sun, H. Y., Guo, Z. Z., Zhang, Z., Li, Y. M., & Wei, L. Q. (2014). Temporal and spatial characterization of mononuclear phagocytes in circulating, lung alveolar and interstitial compartments in a mouse model of bleomycin-induced pulmonary injury. *Journal of Immunological Methods*, *403*(1–2), 7–16. https://doi.org/10.1016/j.jim.2013.11.012

Kamm, G. B., Boffi, J. C., Zuza, K., Nencini, S., Campos, J., Schrenk-Siemens, K., Sonntag, I., Kabaoğlu, B., El Hay, M. Y. A., Schwarz, Y., Tappe-Theodor, A., Bruns, D., Acuna, C., Kuner, T., & Siemens, J. (2021). A synaptic temperature sensor for body cooling. *Neuron*, *109*(20), 3283–3297, e3211. https://doi.org/10.1016/j.neuron.2021.10.001

Kanniler, M., Luling, R., Yildirim, A. O., Gudermann, T., Steinritz, D., & Dietrich, A. (2018). TRPA1 channels: Expression in non-neuronal murine lung tissues and dispensability for hyperoxia-induced alveolar epithelial hyperplasia. *Pflügers Archiv: European Journal of Physiology*, *470*, 1231–1241. https://doi.org/10.1007/s00424-018-2148-6

Lawrence, T. (2009). The nuclear factor NF- B pathway in inflammation. *Cold Spring Harbor Perspectives in Biology*, *1*(6), a001651. https://doi.org/10.1101/cshperspect.a001651

Lei, F., Cui, N., Zhou, C., Chodosh, J., Vavvas, D. G., & Paschalis, E. I. (2020). CSF1R inhibition by a small-molecule inhibitor is not microglia specific; affecting hematopoiesis and the function of macrophages. *Proceedings of the National Academy of Sciences*, *117*(38), 23336–23338. https://doi.org/10.1073/pnas.1922788117

Li, W., Liang, L., Liao, Q., Li, Y., & Zhou, Y. (2022). CD38: An important regulator of T cell function. *Biomedicine & Pharmacotherapy*, *153*):113395. https://doi.org/10.1016/j.biopha.2022.113395

Lund, F. E., Cockayne, D. A., Randall, T. D., Solvason, N., Schuber, F., & Howard, M. C. (1998). CD38: A new paradigm in lymphocyte activation and signal transduction. *Immunological Reviews*, *161*, 79–93. https://doi.org/10.1111/j.1600-065x.1998.tb01573.x

Maliougina, M., & El Hiani, Y. (2023). TRPM2: Bridging calcium and ROS signaling pathways-implications for human diseases. *Frontiers in Physiology*, *14*, 1217828. https://doi.org/10.3389/fphys.2023.1217828

Mederos, Y. S. M., Waring, J., Gudermann, T., & Chubanov, V. (2008). Evolutionary determinants of divergent calcium selectivity of TRPM channels. *FASEB Journal*, *22*, 1540. https://doi.org/10.1096/fj.07-9694com

Meziani, L., Mondini, M., Petit, B., Boissonnas, A., Thomas de Montpreville, V., Mercier, O., Vozenin, M. C., & Deutsch, E. (2018). CSF1R inhibition prevents radiation pulmonary fibrosis by depletion of interstitial macrophages. *European Respiratory Journal*, *51*(3), 1702120. https://doi.org/10.1183/13993003.02120-2017

Miller, B. A., & Cheung, J. Y. (2016). TRPM2 protects against tissue damage following oxidative stress and ischaemia-reperfusion. *The Journal of Physiology*, *594*(15), 4181–4191. https://doi.org/10.1113/JP270934

Misharin, A. V., Morales-Nebreda, L., Mutlu, G. M., Budinger, G. R. S., & Perlman, H. (2013). Flow cytometric analysis of macrophages and dendritic cell subsets in the mouse lung. *American Journal of Respiratory Cell and Molecular Biology*, *49*(4), 503–510. https://doi.org/10.1165/rcmb.2013-0086MA

Morgan, M. J., & Liu, Z. (2011). Crosstalk of reactive oxygen species and NF-κB signaling. *Cell Research*, *21*(1), 103–115. https://doi.org/10.1038/cr.2010.178

Nie, H., Wang, A., He, Q., Yang, Q., Liu, L., Zhang, G., Huang, Y., Ding, X., Yu, H., & Hu, S. (2017). Phenotypic switch in lung interstitial macrophage polarization in an ovalbumin-induced mouse model of asthma. *Experimental and Therapeutic Medicine*, *14*(2), 1284–1292. https://doi.org/10.3892/etm.2017.4699

Nilius, B., & Szallasi, A. (2014). Transient receptor potential channels as drug targets: From the science of basic research to the art of Medicine. *Pharmacological Reviews*, *66*(3), 676–814. https://doi.org/10.1124/pr.113.008268

Numata, T., Sato, K., Christmann, J., Marx, R., Mori, Y., Okada, Y., & Wehner, F. (2012). The ΔC splice-variant of TRPM2 is the hypertonicity-induced cation channel in HeLa cells, and the ecto-enzyme CD38 mediates its activation. *The Journal of Physiology*, *590*(5), 1121–1138. https://doi.org/10.1113/jphysiol.2011.220947

Ogawa, K., Tsurutani, M., Hashimoto, A., & Soeda, M. (2019). Simple propagation method for resident macrophages by co-culture and subculture, and their isolation from various organs. *BMC Immunology*, *20*(1), 34. https://doi.org/10.1186/s12865-019-0314-z

Peng, Y., Qiao, S., Wang, H., Shekhar, S., Wang, S., Yang, J., Fan, Y., & Yang, X. (2024). Enhancement of macrophage immunity against chlamydial infection by natural killer T cells. *Cells*, *13*(2), 133. https://doi.org/10.3390/cells13020133

Perraud, A. L., Fleig, A., Dunn, C. A., Bagley, L. A., Launay, P., Schmitz, C., Stokes, A. J., Zhu, Q., Bessman, M. J., Penner, R., Kinet, J. P., & Scharenberg, A. M. (2001). ADP-ribose gating of the calcium-permeable LTRPC2 channel revealed by nudix motif homology. *Nature*, *411*(6837), 595–599.

Perraud, A. L., Takanishi, C. L., Shen, B., Kang, S., Smith, M. K., Schmitz, C., Knowles, H. M., Ferraris, D., Li, W., Zhang, J., Stoddard, B. L., & Scharenberg, A. M. (2005). Accumulation of free ADP-ribose from mitochondria mediates oxidative stress-induced gating of TRPM2 cation channels. *Journal of Biological Chemistry*, *280*(7), 6138–6148.

Petheo, G. L., & Demaurex, N. (2005). Voltage- and NADPH-dependence of electron currents generated by the phagocytic NADPH oxidase. *Biochemistry Journal*, *388*(Pt 2), 485–491. https://doi.org/10.1042/BJ20041889

Robledo-Avila, F. H., Ruiz-Rosado, J. D., Brockman, K. L., & Partida-Sánchez, S. (2020). The TRPM2 ion channel regulates inflammatory functions of neutrophils during listeria monocytogenes infection. *Frontiers in Immunology*, *11*, 97. https://doi.org/10.3389/fimmu.2020.00097

Santoni, G., Morelli, M. B., Amantini, C., Santoni, M., Nabissi, M., Marinelli, O., & Santoni, A. (2018). "Immuno-Transient receptor potential ion channels": The role in monocyte- and macrophage-mediated inflammatory responses. *Frontiers in Immunology*, *9*, 1273. https://doi.org/10.3389/fimmu.2018.01273

Schyns, J., Bureau, F., & Marichal, T. (2018). Lung interstitial macrophages: Past, present, and future. *Journal of Immunology Research*, *2018*, 5160794. https://doi.org/10.1155/2018/5160794

Sheng, J., Ruedl, C., & Karjalainen, K. (2015). Most Tissue-Resident macrophages except microglia are derived from fetal hematopoietic stem cells. *Immunity*, *43*(2), 382–393. https://doi.org/10.1016/j.immuni.2015.07.016

Song, K., Wang, H., Kamm, G. B., Pohle, J., Reis, F. C., Heppenstall, P., Wende, H., & Siemens, J. (2016). The TRPM2 channel is a hypothalamic heat sensor that limits fever and can drive hypothermia. *Science*, *353*(6306), 1393–1398. https://doi.org/10.1126/science.aaf7537

Strickland, A. B., Chen, Y., Sun, D., & Shi, M. (2023). Alternatively activated lung alveolar and interstitial macrophages promote fungal growth. *iScience*, *26*(5), 106717. https://doi.org/10.1016/j.isci.2023.106717

Syed Mortadza, S. A., Wang, L., Li, D., & Jiang, L. H. (2015). TRPM2 channel-mediated ROS-sensitive Ca(2+) signaling mechanisms in immune cells. *Frontiers in Immunology*, *6*, 407. https://doi.org/10.3389/fimmu.2015.00407

Tsurutani, M., Horie, H., & Ogawa, K. (2021). Cell properties of lung tissue-resident macrophages propagated by co-culture with lung fibroblastic cells from C57BL/6 and BALB/c mice. *Biomedicines*, *9*(9), 1241. https://doi.org/10.3390/biomedicines9091241

Yamada, H., Arai, T., Endo, N., Yamashita, K., Fukuda, K., Sasada, M., & Uchiyama, T. (2006). LPS-induced ROS generation and changes in glutathione level and their relation to the maturation of human monocyte-derived dendritic cells. *Life Sciences*, *78*(9), 926–933. https://doi.org/10.1016/j.lfs.2005.05.106

Yamamoto, S., Shimizu, S., Kiyonaka, S., Takahashi, N., Wajima, T., Hara, Y., Negoro, T., Hiroi, T., Kiuchi, Y., Okada, T., Kaneko, S., Lange, I., Fleig, A., Penner, R., Nishi, M., Takeshima, H., & Mori, Y. (2008). TRPM2-mediated Ca2+influx induces chemokine production in monocytes that aggravates inflammatory neutrophil infiltration. *Nature Medicine*, *14*(7), 738–747. https://doi.org/10.1038/nm1758

Zitka, O., Skalickova, S., Gumulec, J., Masarik, M., Adam, V., Hubalek, J., Trnkova, L., Kruseova, J., Eckschlager, T., & Kizek, R. (2012). Redox status expressed as GSH:GSSG ratio as a marker for oxidative stress in paediatric tumour patients. *Oncology Letters*, *4*(6), 1247–1253. https://doi.org/10.3892/ol.2012.931

Zou, Z. G., Rios, F. J., Montezano, A. C., & Touyz, R. M. (2019). TRPM7, magnesium, and signaling. *International Journal of Molecular Sciences*, *20*(8), 1877. https://doi.org/10.3390/ijms20081877

SUPPORTING INFORMATION

Additional supporting information can be found online in the Supporting Information section at the end of this article.

How to cite this article: Rajan, S., Shalygin, A., Gudermann, T., Chubanov, V., & Dietrich, A. (2024). TRPM2 channels are essential for regulation of cytokine production in lung interstitial macrophages. *Journal of Cellular Physiology*, 1–17. https://doi.org/10.1002/jcp.31322

4. Paper II

JCI insight

RESEARCH ARTICLE

TRPV4 channels are essential for alveolar epithelial barrier function as protection from lung edema

Jonas Weber,[1] Suhasini Rajan,[1] Christian Schremmer,[1] Yu-Kai Chao,[1] Gabriela Krasteva-Christ,[2] Martina Kannler,[1] Ali Önder Yildirim,[3] Monika Brosien,[4] Johann Schredelseker,[1] Norbert Weissmann,[4] Christian Grimm,[1] Thomas Gudermann,[1] and Alexander Dietrich[1]

[1]Walther Straub Institute of Pharmacology and Toxicology, a member of the German Center for Lung Research (DZL), Ludwig Maximilian University of Munich, Munich Germany. [2]Institute of Anatomy and Cell Biology, School of Medicine, Saarland University, Homburg, Germany. [3]Comprehensive Pneumology Center, Institute of Lung Biology and Disease, a member of the DZL, Helmholtz Center Munich, German Research Center for Environmental Health, Munich, Germany. [4]Justus Liebig University Giessen, Cardio-Pulmonary Institute, University of Giessen and Marburg Lung Center, a member of the DZL, Giessen, Germany.

Ischemia/reperfusion-induced edema (IRE), one of the most significant causes of mortality after lung transplantation, can be mimicked ex vivo in isolated perfused mouse lungs (IPL). Transient receptor potential vanilloid 4 (TRPV4) is a nonselective cation channel studied in endothelium; however, its role in the lung epithelium remains elusive. Here, we show enhanced IRE in TRPV4-deficient ($TRPV4^{-/-}$) IPL compared with that of WT controls, indicating a protective role of TRPV4 in maintenance of the alveolar epithelial barrier. By immunohistochemistry, mRNA profiling, and electrophysiological characterization, we detected TRPV4 in bronchial epithelium, alveolar epithelial type I (ATI), and alveolar epithelial type II (ATII) cells. Genetic ablation of TRPV4 resulted in reduced expression of the water-conducting aquaporin-5 (AQP-5) channel in ATI cells. Migration of $TRPV4^{-/-}$ ATI cells was reduced, and cell barrier function was impaired. Analysis of isolated primary $TRPV4^{-/-}$ ATII cells revealed a reduced expression of surfactant protein C, and the TRPV4 activator GSK1016790A induced increases in current densities only in WT ATII cells. Moreover, $TRPV4^{-/-}$ lungs of adult mice developed significantly larger mean chord lengths and altered lung function compared with WT lungs. Therefore, our data illustrate essential functions of TRPV4 channels in alveolar epithelial cells and in protection from edema formation.

Introduction

The alveolar epithelium has multiple functions in the lung. On the one hand, the epithelial layer forms a natural barrier to the external environment, protecting the body from invading microorganisms and toxicants, while, on the other hand, alveolar epithelial cells facilitate gas exchange. In the adult lung, the alveolar epithelium consists of 2 epithelial cell types that are crucial to maintain lung homeostasis and tissue repair (1). Alveolar epithelial type I (ATI) cells are elongated with a large surface area and high barrier function, which facilitates gas exchange in close proximity to endothelial cells of the alveolar capillaries (1). ATI cells are also highly water permeable, allowing for ion transport and maintenance of lung fluid balance (2). Although the latter cells cover the largest surface area of the lung (3), alveolar epithelial type II (ATII) cells, which exhibit a cubic morphology, by far outnumber ATI cells (4). ATII cells are also involved in ion transport and liquid homeostasis (5) and are — most importantly — responsible for the production, storage, secretion, and recycling of pulmonary surfactant. Surfactant lowers the surface tension at the tissue-air barrier to allow proper inflation and deflation of the alveoli during breathing (6). Moreover, ATII cells also serve as progenitors for ATI cells and are capable of long-term self-renewal (7). Although alveolar epithelial cells express a wide variety of ion transporters and channels (8), the exact roles of these proteins for specialized alveolar cell functions have remained elusive.

Transient receptor potential vanilloid 4 (TRPV4) is the fourth cloned member of the vanilloid family of TRP channels (9). Like most TRP channels, TRPV4 harbors an invariant sequence, the TRP box (containing the amino acid sequence EWKFAR), in its intracellular C-terminal tail as well as ankyrin repeats

Authorship note: SR and CS contributed equally to this work.

Conflict of interest: The authors have declared that no conflict of interest exists.

Submitted: October 22, 2019
Accepted: September 9, 2020
Published: September 15, 2020.

Reference information: *JCI Insight*. 2020;5(20):e134464. https://doi.org/10.1172/jci.insight.134464.

in the intracellular N-terminus. The protein is composed of 6 membrane-spanning helices (S1–S6) and a presumed pore-forming loop between S5 and S6 (9, 10). Four of these monomers of the same type preferentially assemble in a functional homotetrameric complex (11), although TRPV4/TRPP2 complexes were also identified in cilia of renal epithelial cells (12). Homotetrameric TRPV4 was originally characterized as a sensor of extracellular osmolarity (13, 14). The channel is functionally expressed in endothelial (15, 16) and epithelial cells of the respiratory system (17–19). TRPV4 channels are thermosensitive in the range of 24°C–38°C and may additionally serve as mechanosensors, because they are activated by membrane and shear stretch as well as by viscous loading (20). As TRPV4 is also involved in pulmonary hypertension (21, 22) and bladder function (23), the channel is an interesting pharmacological target, with numerous modulators already identified (reviewed in ref. 24). Moreover, TRPV4$^{-/-}$ mice were protected from bleomycin-induced pulmonary fibrosis, due to the channel's constitutive expression and function in lung fibroblasts (25). In lung endothelium, where its role was most extensively studied, direct or indirect activation of TRPV4 by mechanical stress (26), high peak inspiratory pressure (27, 28), and high pulmonary venous pressure due to heart failure (29) resulted in the disruption of the endothelial barrier and edema formation. In other tissues, however, the channel maintains physiological cell barrier, for example, in skin (30), the urogenital tract (31), and the corneal epithelium (32). In tracheal epithelial cells, TRPV4 channels regulate ciliary beat frequency (17), and in alveolar epithelial cells, TRPV4 activation by 4α-phorbol esters produced blebs and breaks in lung septa (33) by unknown molecular mechanisms. Moreover, stimulation of TRPV4 by bacterial LPS mounted a protective response (34), whereas TRPV4 inhibition reduced lung edema and inflammation after chlorine exposure (35). Therefore, TRPV4 channels may function as chemosensors of toxicants in the lung epithelium (reviewed in ref. 36), but their exact role in the alveolar epithelium is still elusive.

We have shown that TRPC6, a member of the classical TRP channel family in the endothelium, increases endothelial permeability during ischemia/reperfusion-induced (I/R-induced) edema formation (37), one of the most significant causes of mortality after lung transplantation. However, as outlined above, endothelial permeability is also increased by TRPV4 activation (summarized in ref. 38). Along these lines, we analyzed I/R-induced edema formation in a TRPV4-deficient (TRPV4$^{-/-}$) mouse model. Surprisingly, edema development was increased in TRPV4$^{-/-}$ lungs, but edema development in TRPC6/TRPV4 double-deficient lungs was similar to that of WT lungs. These data indicate a protective role for TRPV4 channels in the other natural cell barrier of the lung, the epithelium. Therefore, we set out to study functions of TRPV4 channels in the alveolar epithelium, capitalizing on the TRPV4$^{-/-}$ mouse model. Enhanced lung edema formation triggered by I/R probably may be due to downregulation of aquaporin-5 (AQP-5) channels in ATI cells, reduced surfactant protein-C (SP-C) production in ATII cells, and/or emphysema-like changes in the overall lung architecture. Our data suggest an essential role of TRPV4 channels in the alveolar epithelium.

Results

Ablation of TRPV4 increases IR-induced edema formation in isolated perfused mouse lungs. To investigate the role of TRPV4 in IR-induced edema formation, we isolated lungs from WT and TRPV4$^{-/-}$ mice. Initial characterization of these mice revealed impaired pressure sensation in dorsal root ganglia (39) and osmotic sensation by exaggerated arginine vasopressin secretion in the brain (40). Loss of TRPV4 protein was confirmed in lung lysates. While in WT controls a protein of appropriately 100 kDa in size was detected by Western blotting with TRPV4-specific antibodies, TRPV4$^{-/-}$ lungs did not express any TRPV4 protein (Figure 1A). Murine embryonic fibroblasts (41), such as pulmonary fibroblasts, express TRPV4 protein (25) and served as an additional positive control. After initial perfusion of isolated lungs for 15 minutes, ischemia was induced for 90 minutes followed by 120 minutes reperfusion. TRPV4$^{-/-}$ lungs showed enhanced lung edema formation, as evidenced by a considerable gain in lung weight, as opposed to WT lungs (Figure 1B), which increased in weight to a similar extent as already described by us previously (37). These results clearly contrast with observations on TRPC6-deficient lungs, which are protected from IR-induced edema due to reduced endothelial permeability (37). Therefore, we generated a TRPV4/TRPC6 double-deficient mouse model (TRPV4/TRPC6$^{-/-}$), which has lungs that lack the increase in IR-induced edema formation but that developed edema, similar to WT mice (Figure 1B). Moreover, lung edema formation in TRPV4$^{-/-}$ lungs was clearly visible by the naked eye (Figure 1C), and, consistently, the wet-to-dry weight ratio increase doubled in TRPV4$^{-/-}$ lungs but only slightly increased in TRPV4/TRPC6$^{-/-}$ lungs (Figure 1D). In conclusion, TRPV4 ablation induces increased IR-induced edema, which

JCI insight

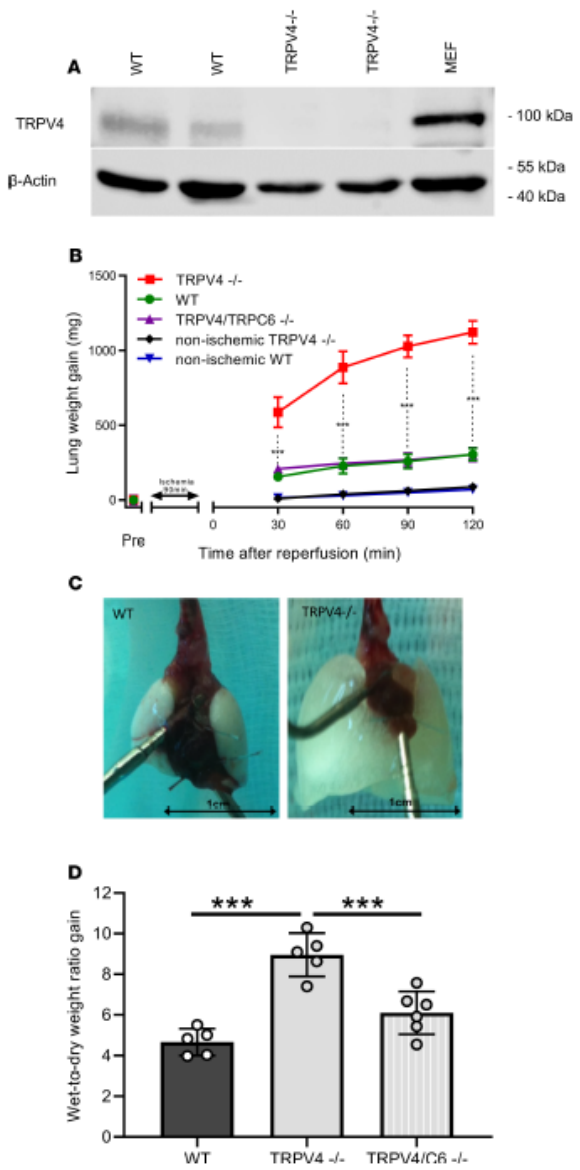

Figure 1. Ablation of TRPV4 increases ischemia-induced edema formation in mouse lungs. (**A**) TRPV4 protein expression in mouse lungs was evaluated by immunoblotting in whole-lung lysates of WT and TRPV4-deficient (TRPV4$^{-/-}$) mice using a TRPV4-specific antiserum. Murine embryonic fibroblasts (MEFs) served as an additional positive control. β-Actin was used as loading control. (**B**) Constant weight measurement of ischemic and nonischemic WT and TRPV4$^{-/-}$ and TRPV4/TRPC6 double-deficient (TRPV4/TRPC6$^{-/-}$) isolated perfused lungs. (**C**) Representative images of WT and TRPV4$^{-/-}$ lungs after ischemia. (**D**) Wet-to-dry weight ratio gains of TRPV4$^{-/-}$ and TRPV4/TRPC6$^{-/-}$ lungs compared with those of WT controls. Data represent mean ± SEM of at least 5 lungs for each genotype. Significance between means was analyzed using ANOVA (**B** and **D**); ***$P < 0.001$.

can be reduced by additional ablation of TRPC6 channels. To identify a possible role for endothelial TRPV4 channels, which might be activated by shear stress due to hydrostatic pressure (42), we decreased initial flow rates (preflow) from 2 ml to 0.5 ml/min. We did not observe any major changes in edema formation in ischemic and nonischemic WT lungs. TRPV4$^{-/-}$ lungs showed a significantly decreased edema

formation only after 90 and 120 minutes of reperfusion for unknown reasons (see Supplemental Figure 1; supplemental material available online with this article; https://doi.org/10.1172/jci.insight.134464DS1).

TRPV4 is expressed in ATI and ATII cells. As TRPV4 is highly expressed in lung endothelium, and its activation results in an increase of endothelial permeability (reviewed in ref. 38), we focused on its possible functions in the epithelium. Epithelial cells represent the second natural barrier regulating edema formation. Analysis of mice carrying an EGFP reporter protein under the control of the TRPV4 promoter/enhancer region revealed expression of TRPV4 protein in endothelium as well as bronchial and alveolar epithelium (Figure 2A). In the bronchial epithelium we detected TRPV4 in ciliated cells by costaining with a β-tubulin IV antibody (Supplemental Figure 2, A–C). Neither club nor neuroendocrine cells showed TRPV4 expression (Supplemental Figure 2, D–I). In the alveoli, costaining experiments with an antibody directed against AQP-5 (Figure 2B), a marker protein of ATI cells, which are involved in lung septa formation (2), revealed a red staining indicative of AQP-5 expression in the plasma membrane and an additional green staining of the cytosol, reflecting TRPV4 expression in these cells (Figure 2B, inset). Moreover, direct quantification of TRPV4 mRNA revealed similar expression levels in ATII cells as in lung endothelial cells, but lower mRNA expression in pulmonary murine lung fibroblasts and precapillary arterial smooth muscle cells (Figure 2C). Therefore, TRPV4 channels are expressed in ATI and ATII cells of the alveolar epithelium.

Loss of TRPV4 resulted in decreased AQP-5 expression in ATI cells. Staining of lung slices with fluorescence-coupled antibodies specific for the water-conducting channel AQP-5 revealed lower total expression levels in ATI cells and reduced plasma membrane localization in TRPV4$^{-/-}$ lungs compared with that in WT lungs (Figure 3, A–E). These results were confirmed by Western blotting of lung lysates probed with an AQP-5–specific antibody (Figure 3, F and G). In clear contrast to these results, protein levels of AQP-1, a major aquaporin channel in the microvascular endothelium, were not significantly different in TRPV4$^{-/-}$ cells compared with WT endothelial cells (Supplemental Figure 3, A–E). Therefore, AQP-5 protein levels in the alveolar epithelium, but not AQP-1 expression in the endothelium is reduced by ablation of TRPV4.

Identification of currents induced by the TRPV4 activator GSK1016790A only in primary ATII cells from WT mice. To investigate the role of TRPV4 on at a cellular level, we first isolated ATII epithelial cells (Figure 4A) from WT and TRPV4$^{-/-}$ mice. We were not able to detect any morphological differences in ATII cells of the different genotypes by phase-contrast microscopy. ATII cells were identified by staining with fluorophore-coupled antibodies directed against directed against prosurfactant protein C (pSP-C) (Figure 4B), which is secreted by ATII cells (reviewed in ref. 5). Patch clamp analysis of primary ATII cells revealed significantly larger currents, which were induced by the selective TRPV4 activator GSK1016790A (GSK, reviewed in ref. 24) only in WT cells, while currents after the application of GSK in TRPV4$^{-/-}$ cells were not significantly different compared with basal currents in WT cells (Figure 4, C and D). Western blotting of protein lysates from ATII cells revealed lower pSP-C levels in TRPV4$^{-/-}$ ATII cells compared with WT cells (Figure 4, E and F). We then differentiated ATII cells to ATI cells by growing them to confluence in plastic cell culture dishes for at least 6 days as described previously (1) (Figure 4G). After 6 days, WT cells expressed AQP-5 protein as an ATI cell marker (Figure 4H). In conclusion, TRPV4 channels are functionally active in ATII cells and are involved in the expression of pSP-C of these alveolar epithelial cells, which can be differentiated to ATI cells in vitro.

TRPV4$^{-/-}$ ATI cells express less AQP-5, show reduced nuclear localization of NFAT, and decreased cell migration and adhesion. As already shown in lung sections of TRPV4$^{-/-}$ mice, translocation of AQP-5 to the plasma membrane was reduced in TRPV4$^{-/-}$ cells (Figure 5, A and B). To test if TRPV4$^{-/-}$ ATII cells are able to differentiate to ATI cells, we analyzed the expression of podoplanin (T1α), another ATI cell marker protein. Notably, podoplanin expression was not significantly different in TRPV4$^{-/-}$ ATII cells differentiated to ATI cells (Figure 5, C and D).To further analyze ATI cell function, we quantified nuclear NFATc1 levels. The translocation of NFATc1 protein to the nucleus was significantly reduced in TRPV4$^{-/-}$ cells (Figure 5, E and F). Moreover, cell migration analyzed by gap closure in in vitro experiments was clearly slowed down in TRPV4$^{-/-}$ ATI cells compared with WT cells (Figure 5, G and H). As an additional line of evidence, we transfected ATII cells with TRPV4-specific or control siRNAs, differentiated them to ATI cells, and quantified cell migration in the same way (Supplemental Figure 4). Most interestingly, we obtained similar results in cells transfected with TRPV4 siRNA, which showed a significantly slower migration compared with nontransfected cells as well as cells transfected with the control siRNAs. As determined by electrical cell impedance sensing (ECIS), subconfluent TRPV4$^{-/-}$ ATI cells showed reduced cell barrier function (Figure 5I).

JCI insight

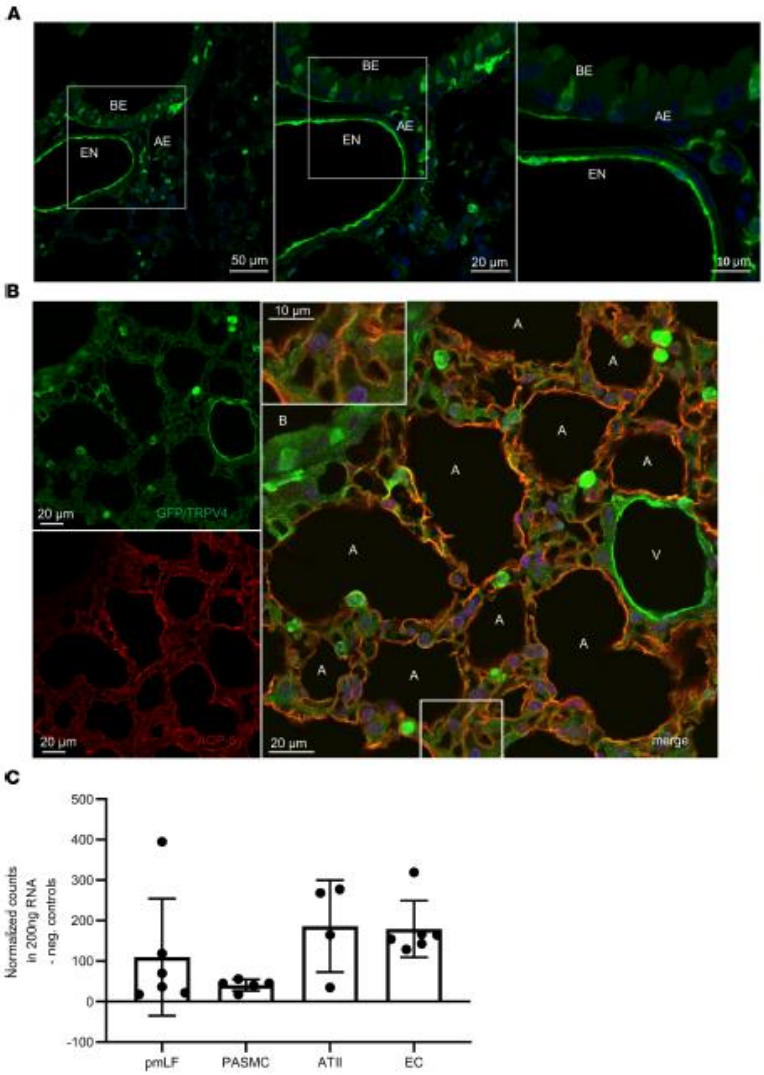

Figure 2. TRPV4 and aquaporin-5 expression in mouse lungs. (**A**) GFP staining (green) by fluorescence-coupled GFP-specific antibodies in lung cryosections of TRPV4EGFP reporter mice reveals expression of TRPV4 in cells of the lung endothelium (EN) as well as in the bronchial (BE) and alveolar epithelium (AE). Nuclei staining was performed with Hoechst dye (blue). Scale bar: 10 µm (right); 20 µm (middle); 50 µm (left). (**B**) Lung cryosections from TRPV4EGFP reporter mice were stained with fluorescence-coupled antisera directed against GFP and aquaporin-5 (AQP-5). Confocal images were obtained after excitation at 488 nm (for EGFP, left top, green) or after excitation at 561 nm (for AQP-5, left bottom, red). Both images were merged (right). Nuclei staining was performed with Hoechst dye (blue). A, alveolus; B, bronchus; V, vasculature. The inset shows the bottom boxed region in at higher magnification. Scale bar: 10 µm (inset); 20 µm. (**C**) TRPV4 mRNA quantification in lung cells using NanoString technology. ATII, alveolar type II cells; EC, endothelial cells; PASMC, precapillary arterial smooth muscle cells; pmLF, primary murine lung fibroblasts. Data represent mean ± SEM from at least 3 independent cell isolations.

Therefore, ablation of TRPV4 induced less AQP-5 expression, reduced nuclear localization of nuclear factor of activated T cells (NFAT), and reduced cell migration and cell barrier function.

TRPV4$^{-/-}$ *mice showed emphysema-like lung structure and altered lung function.* To analyze differences in lung anatomy as a consequence of altered ATI cell function, we quantified mean chord lengths (MCLs) in histological lung sections (Figure 6A). TRPV4 ablation significantly increased MCL of the alveolar lumen in adult (47–52 week old, Figure 6D) mice compared with WT lungs, while young mice (4–6 weeks old) showed no differences (Figure 6B). Lungs from 28- to 30-week-old mice were also prone to larger MCLs (Figure 6C), which, however, were not significantly different compared with those of WT lungs.

JCI insight

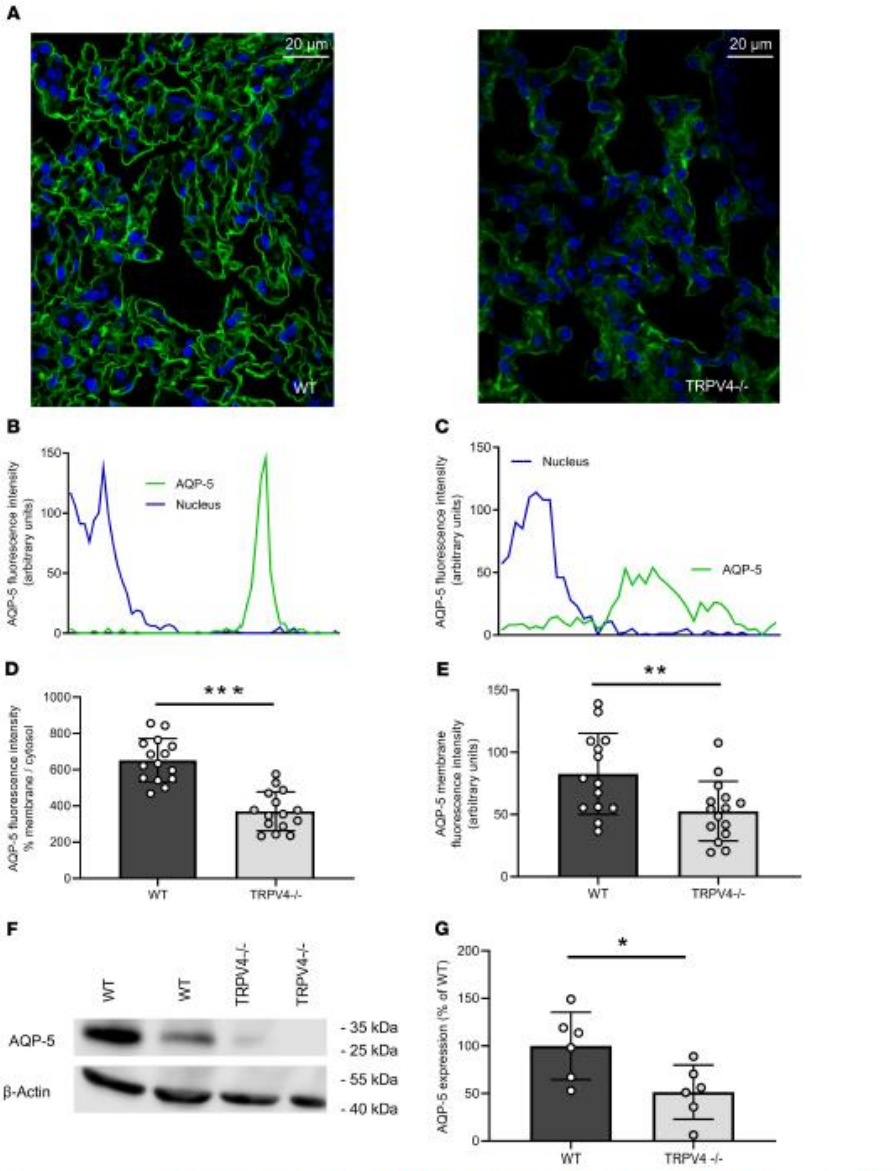

Figure 3. Aquaporin-5 expression and translocation to the plasma membrane in WT and TRPV4$^{-/-}$ alveolar epithelial type I cells. (**A**) Cryosections of WT and TRPV4$^{-/-}$ lungs stained with an aquaporin-5–specific (AQP-5–specific) fluorescence-coupled antibody. Nuclei staining was performed with Hoechst dye (blue). Scale bar: 20 µm. Representative histograms for the quantification of AQP-5 protein in the plasma membrane of WT (**B**) and TRPV4-deficient alveolar epithelial type I (ATI) cells (**C**). (**D** and **E**) Summaries of AQP-5 protein expression in plasma membranes (**D**, percentage of aquaporin-5 membrane/cytosol; **E**, percentage AQP-5 in membranes). Representative Western blot analysis of AQP-5 expression in WT and TRPV4$^{-/-}$ whole-lung lysates (**F**) and summary of AQP-5 expression in lung lysates of TRPV4$^{-/-}$ and WT mice (**G**). Data represent mean ± SEM from at least 6 lungs for each genotype. Significance between means was analyzed using 2-tailed unpaired Student's *t* test; $^{*}P < 0.05$, $^{**}P < 0.01$, $^{***}P < 0.001$.

JCI insight RESEARCH ARTICLE

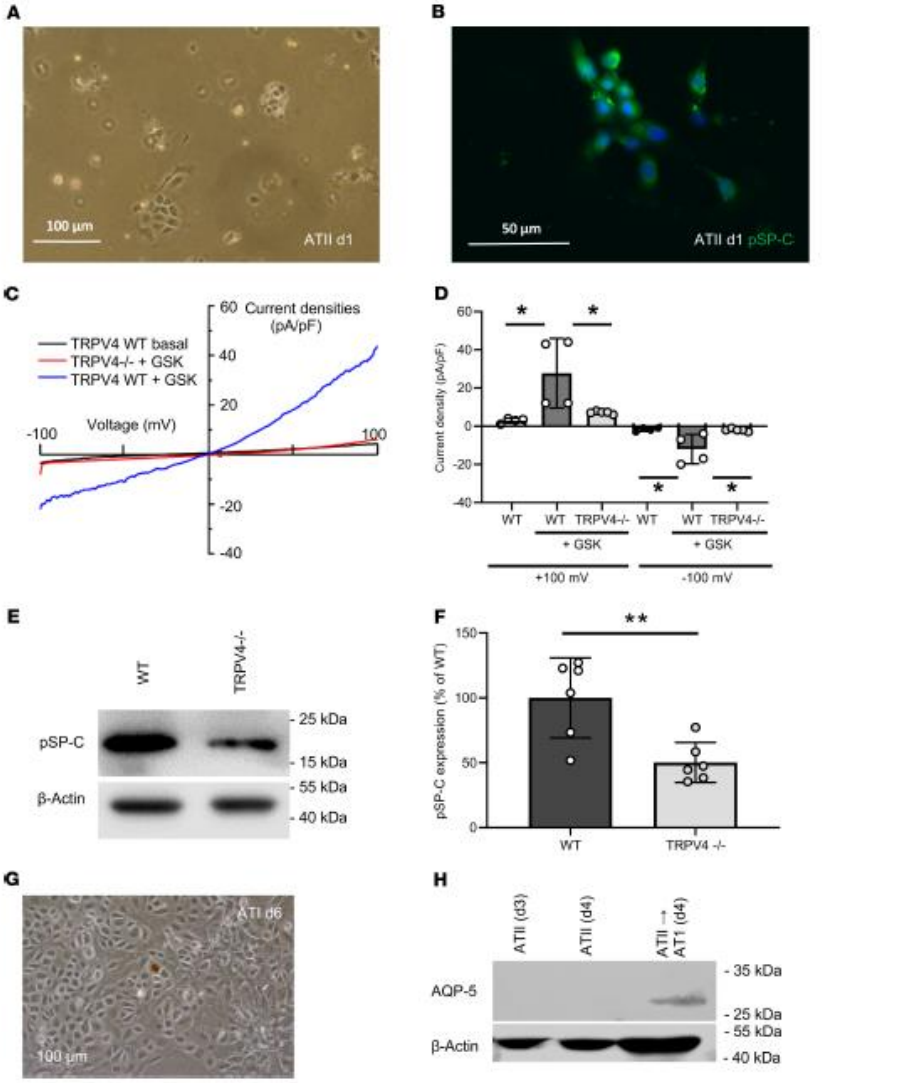

Figure 4. Identification of alveolar epithelial type II cells and differentiation to alveolar epithelial type I cells. Representative cell cluster 1 day after isolation in a phase-contrast image (scale bar: 100 µm) (**A**) and stained with a fluorescence-coupled specific pro-surfactant protein-C (pSP-C) antibody (scale bar: 50 µm) (**B**). Nuclei staining was performed with Hoechst dye (blue). Electrophysiological whole-cell measurements of basal and GSK-induced (GSK-induced) current densities in WT and TRPV4$^{-/-}$ primary alveolar epithelial type II (ATII) cells (**C** and **D**). Representative current density–voltage curves of WT (gray, blue traces) and TRPV4$^{-/-}$ (red trace) ATII cells before (gray trace) and during application of GSK (blue and red traces) (**C**). Summary of current densities at ±100 mV before (white bars) and after application of GSK analyzed in WT (black bars) and TRPV4$^{-/-}$ (gray bars) ATII cells (**D**). Representative Western blot analysis of pSP-C expression in WT and TRPV4$^{-/-}$ ATII cells (**E**) and summary of pSP-C expression in TRPV4$^{-/-}$ and WT ATII cells (**F**). Image of confluent cells on day 6 after ATII cell isolation (scale bar: 100 µm) (**G**) and analysis of AQP-5 expression in cells grown for 3, 4, and 6 days in plastic cell culture dishes by Western blotting (**H**). β-Actin was used as loading control in each blot. Data represent mean ± SEM from at least 3 independent cell preparations of 5 mice each. Significance between means was analyzed using 1-way ANOVA (**C**) or 2-tailed unpaired Student's *t* test (**F**); $^{*}P < 0.05$, $^{**}P < 0.01$.

JCI insight

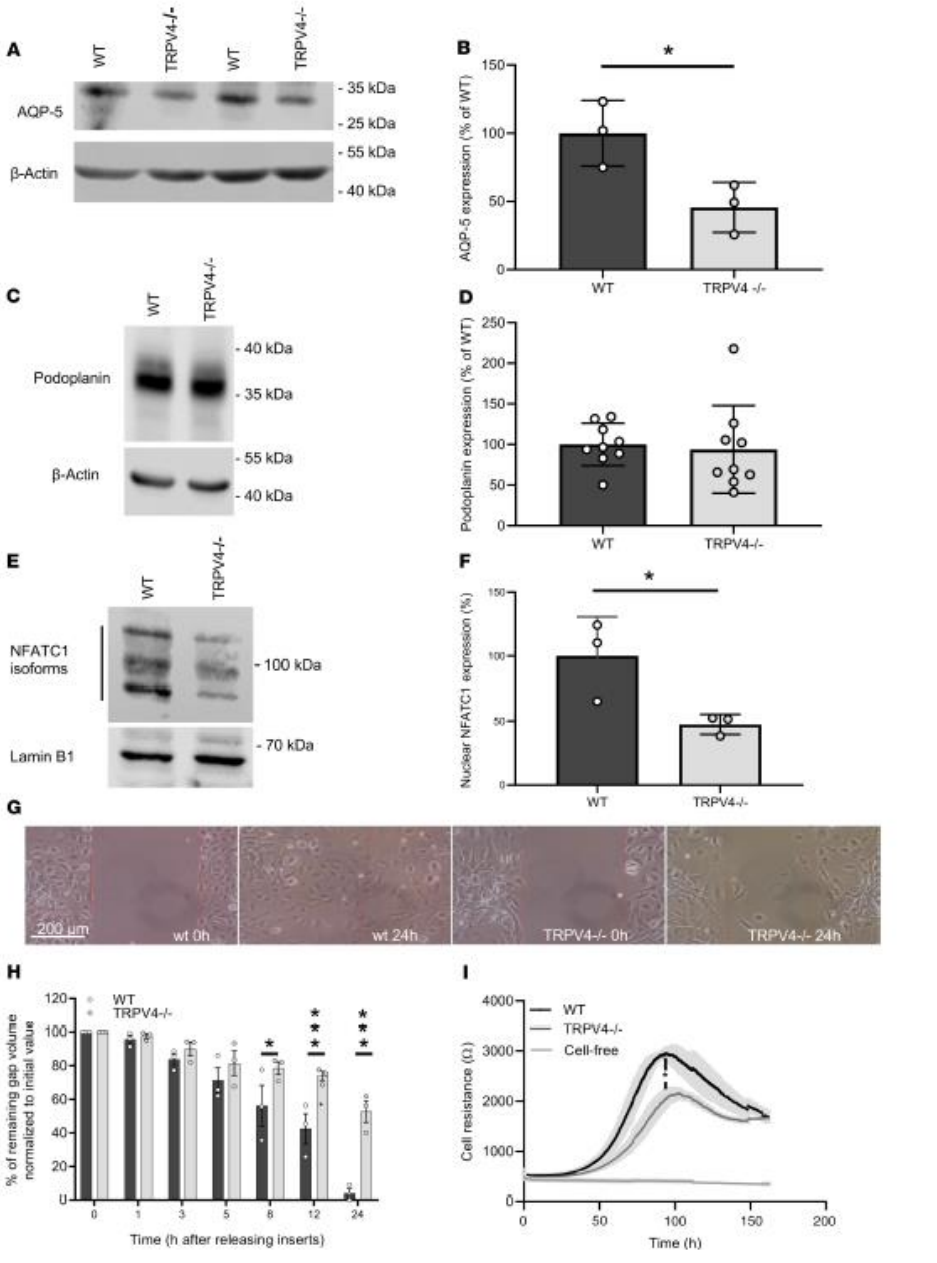
A
WT
TRPV4-/-
WT
TRPV4-/-
AQP-5
β-Actin
- 35 kDa
- 25 kDa
- 55 kDa
- 40 kDa
B
AQP-5 expression (% of WT)
150
100
50
0
*
WT
TRPV4 -/-
C
WT
TRPV4-/-
Podoplanin
β-Actin
- 40 kDa
- 35 kDa
- 55 kDa
- 40 kDa
D
Podoplanin expression (% of WT)
250
200
150
100
50
0
WT
TRPV4-/-
E
WT
TRPV4-/-
NFATC1 isoforms
Lamin B1
- 100 kDa
- 70 kDa
F
Nuclear NFATC1 expression (%)
150
100
50
0
*
WT
TRPV4-/-
G
200 μm
wt 0h
wt 24h
TRPV4-/- 0h
TRPV4-/- 24h
H
WT
TRPV4-/-
% of remaining gap volume normalized to initial value
120
100
80
60
40
20
0
*
* * *
* * *
0
1
3
5
8
12
24
Time (h after releasing inserts)
I
WT
TRPV4-/-
Cell-free
Cell resistance (Ω)
4000
3000
2000
1000
0
0
50
100
150
200
Time (h)

Figure 5. Nuclear localization of nuclear factor of activated T cells in and migration and adhesion of TRPV4-deficient and WT ATI cells. Representative Western blot analysis of AQP-5 expression in WT and TRPV4$^{-/-}$ ATII cells differentiated to ATI cells (**A**) and summary of AQP-5 expression in these cells (**B**). Representative Western blot analysis of podoplanin expression – another ATI cell marker – in WT and TRPV4$^{-/-}$ ATII cells differentiated to ATI cells (**C**) and summary of podoplanin expression in these cells (**D**). Representative Western blot analysis of nuclear NFATc1 localization in WT and TRPV4$^{-/-}$ ATI cells (**E**) and summary of nuclear factor of activated T cells (NFAT) localization in these cells (**F**). Lamin B1 served as loading control. Representative images of a migration assay after removing inserts (scale bar: 200 μm) (**G**). Summary of remaining gap values normalized to initial values quantified in migration assays of TRPV4$^{-/-}$ and WT ATI cells after releasing inserts at 0, 1, 3, 5, 8, 12, and 24 hours (**H**). Electrical cell resistance was quantified with an ECIS device for WT and TRPV4$^{-/-}$ ATI cells for 160 hours. (**I**). Data represent mean ± SEM from at least 3 independent cell preparations of 5 mice each. Significance between means was analyzed using 2-tailed unpaired Student's *t* test; $^{*}P < 0.05$, $^{***}P < 0.001$.

Moreover, lung function was altered (Figure 6, E–H): TRPV4$^{-/-}$ lungs showed increased inspiratory capacity and compliance (Figure 6, E, G, and H) as well as decreased elastance (Figure 6F), which was significantly different from that of WT mice of the same age. In conclusion, adult TRPV4$^{-/-}$ mice showed emphysema-like changes in their lungs, which may be responsible for altered lung function.

Discussion

Although TRPV4 is highly expressed in lungs, its exact function is still elusive (reviewed in ref. 24). Activation of TRPV4 in endothelial cells by mechanical stress, for example, stretching (27, 28, 43), as well as oxidative stress by exposure to H_2O_2 (44) resulted in an increased Ca^{2+} influx mediated by the channel and an increase in endothelial permeability conducive to lung edema (reviewed in ref. 38). Along these lines, pharmacological blockade of TRPV4, for example, by the specific blocker HC-067047, decreased intracellular Ca^{2+} levels in endothelial cells and protected mice from vascular leakage and lung injury (28). Expression and function of TRPV4 channels in the alveolar epithelium, however, has not been studied yet.

Here, we quantified IR-induced edema as one of the most common and significant causes of morbidity and mortality after lung transplantation (45), using the isolated perfused lung model (37). Much to our surprise, TRPV4$^{-/-}$ lungs were not protected from IR-induced lung edema, as observed in TRPC6$^{-/-}$ mice (37). On the contrary, genetic TRPV4 ablation resulted in a robust increase in lung edema (Figure 1B) and a higher wet-to-dry weight ratio increase (Figure 1D) when compared with that of control WT mice. Barrier function was rescued by consecutive breeding of TRPV4$^{-/-}$ mice with TRPC6$^{-/-}$ mice, because lung edema formation in double-deficient mice was similar to that in WT animals (Figure 1B).

As TRPV4 activation in endothelial cells has been shown to result in higher edema formation, we focused on the lung epithelium, another physiological cell barrier in the lung. Recent publications indicate an epithelial function of the channel opposed to that in endothelium, i.e., stabilization of the epithelial barrier in the skin (30), the urogenital tract (31), and the corneal epithelium (32). We demonstrated TRPV4 expression in ATI and ATII cells (Figure 2, B and C). Our further molecular analysis corroborated a functional link between TRPV4 and AQP-5, a water-conducting channel expressed in ATI cells (46). Hypotonic solutions increased the association and surface localization of TRPV4 and AQP-5 in salivary gland cells (47), and AQP-5 expression is regulated by TRPV4 in lung epithelial cells (48). Most interestingly, the expression and plasma membrane translocation of AQP-5 channels in ATI cells were significantly reduced (Figure 3). Therefore, TRPV4 channels increase AQP-5 expression and translocation in ATI cells in clear contrast to human bronchial epithelial cells, where it has been reported that activation of TRPV4 channels by shear stress decreased AQP-5 levels (47). To analyze TRPV4 function on a cellular level, we isolated ATII cells identified by their expression of pSP-C (Figure 4, A and B). We detected significantly larger currents induced by the TRPV4 activator GSK in WT but not in TRPV4$^{-/-}$ ATII cells (Figure 4, C and D). To our knowledge, these data show for the first time that TRPV4 channels are not only expressed, also functional in ATII cells. Quantifying pSP-C levels by Western blotting revealed a reduced expression in TRPV4$^{-/-}$ cells compared with that in WT cells (Figure 4, E and F). The role of surfactant proteins in the prevention of alveolar edema by reducing surface tension as a driving force for fluid flow across the air-blood barrier is still a matter of debate (49) but might also explain exaggerated edema formation in TRPV4$^{-/-}$ mice. Therefore, functional TRPV4 and TRPC6 channels are not only located in different cell types, such as alveolar epithelial and lung endothelial cells, respectively, but may have different roles by decreasing or increasing IR-induced edema. TRPV4 channels aid in epithelial barrier function by supporting SPC production and reducing edema formation in a chronic manner, while TRPC6 channels acutely increase endothelial permeability during IR-induced edema formation (37). Although we cannot exclude a role for endothelial TRPV4 channels, it is unlikely that TRPV4 channels in the endothelium are activated

JCI insight

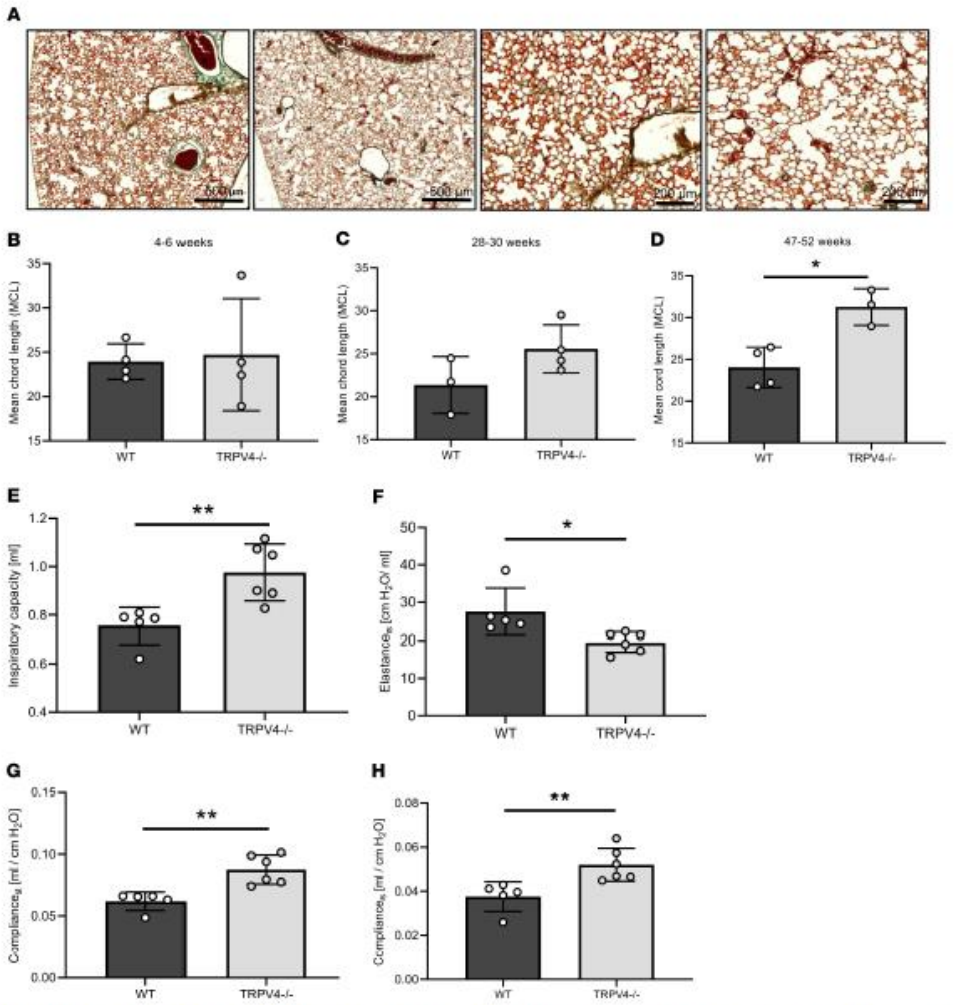

Figure 6. Chord lengths and lung function of WT and TRPV4$^{-/-}$ mice. Representative images of Masson's trichrome–stained lung sections from 52-week-old WT (left, scale bar: 500 µm) and TRPV4$^{-/-}$ mice (right, scale bar: 200 µm) (**A**). Quantification of mean chord lengths of 4- to 6- (**B**), 28- to 30- (**C**), and 47- to 52-week-old (**D**) WT and TRPV4$^{-/-}$ mice. Inspiratory capacity (**E**), elastance of the respiratory system (**F**), static compliance (C_{st}, **G**) and compliance of the respiratory system (C_{rs}, **H**) of 6-month-old WT and TRPV4$^{-/-}$ mice. Data represent mean ± SEM from at least 3 mice. Significance between means was analyzed using 2-tailed unpaired Student's *t* test; $^*P < 0.05$, $^{**}P < 0.01$.

by shear stress due to hydrostatic pressure, as reducing the preflow in the experiments had no effect on IR-induced edema formation (Supplemental Figure 1).

Next, we differentiated ATII cells to ATI cells (1), monitored by the expression of 2 ATI cell markers: AQP-5 and podoplanin. As AQP-5 protein expression was reduced in TRPV4$^{-/-}$ ATI cells (Figure 5, A and B), while podoplanin levels were not altered (Figure 5, C and D), it seems rather unlikely that TRPV4

deficiency and/or a reduction of pSP-C expression results in reduced ATII cell to ATI cell differentiation in general. Plasma membrane translocation of AQP-5 as well as AQP-5 expression may depend on nuclear localization of the transcription factor NFAT by an increase of intracellular Ca^{2+} via TRPV4 similar to TRPC channels (50). Therefore, we quantified nuclear NFAT levels and detected significantly lower levels in TRPV4$^{-/-}$ cells in comparison with that in WT control cells (Figure 5, E and F). A major breakthrough in our understanding of AQP-5 function for water transport across apical membranes of ATI cells was the analysis of AQP-5–deficient mice (51). Although lack of AQP-5 entailed a 10-fold decrease in alveolar permeability in response to an osmotic gradient, AQP-5$^{-/-}$ mice are indistinguishable from WT mice with regard to hydrostatic pulmonary edema as well as isoosmolar fluid transport from the alveolar space (51, 52). Cognizant of this scenario, a role for AQP-5 in the clearance of fluid from the alveolar space after IR-induced lung edema cannot entirely be ruled out, but it appears to be unlikely, and we tried to dissect other additional mechanisms for the vulnerability of TRPV4$^{-/-}$ lungs to edema formation.

As 2 reports demonstrated decreased migration of human epithelial ovarian cancer (53) or endometrial adenocarcinoma cells (54) after downregulation of AQP-5, we set out to quantify cell migration of ATII cells differentiated to ATI cells. TRPV4$^{-/-}$ ATI cells showed a clear deficit in closing gaps by cell migration after releasing inserts compared with WT cells (Figure 5, G and H). In additional experiments, we were able to reproduce these results in cells transfected with TRPV4 siRNAs compared with nontransfected cells as well as cells transfected with control siRNAs (Supplemental Figure 4). These data suggest an important role of TRPV4 channels in cell migration, which needs to be further analyzed in the future. Moreover, cell resistance, as analyzed by ECIS, was significantly reduced in growing TRPV4$^{-/-}$ ATI cells in contrast to that in WT cells (Figure 5I). Both cell types, however, reached confluence after 160 hours, excluding gross changes in their proliferation rates. Changes in cell morphology were also not detected by microscopy.

ATII cells are able to differentiate to ATI cells after lung injury during repair processes in adult mice (7) to reestablish barrier function of the lung alveolus. Therefore, we analyzed lung alveolar histology in WT and TRPV4$^{-/-}$ lungs in young and adult mice. MCL as a measure of alveolar size was increased in adult (47–52 weeks old) but not in young (3 weeks old) TRPV4$^{-/-}$ mice compared with WT mice of the same ages (Figure 6, A–D). We concluded that differences were not caused by defects in embryonic lung development but were due to ongoing growth and repair processes in adult animals. Most interestingly, the emphysema-like changes in lung morphology were also detected in SP-C–deficient mice (55), raising the possibility that reduced SP-C levels in TRPV4$^{-/-}$ ATII cells may also contribute to the phenotype. In the same vein, adult TRPV4$^{-/-}$ mice showed altered lung function, with increased inspiratory capacity and compliance as well as decreased elastance (Figure 6, E–H) compared with WT mice of the same ages. Loss of septa formation because of reduced SP-C levels in adult TRPV4$^{-/-}$ mice may be responsible for decreased clearance of fluid from the alveolar space and may therefore explain higher levels of edema formation in TRPV4$^{-/-}$ lungs.

In summary, loss of TRPV4 channels in alveolar epithelial cells results in decreased pSP-C production in ATII cells and lower AQP-5 expression and membrane localization in ATI cells. The latter proteins are likely to be involved in continuously ongoing repair processes in adult mice, resulting in emphysema-like changes in TRPV4$^{-/-}$ mice. These chronic events may define a protective function of TRPV4 channels against lung edema formation, in clear contrast to their acute detrimental role in endothelial cells.

Methods

Animals. TRPC6$^{-/-}$ (56) and TRPV4$^{-/-}$ (B6.199X1-Trpv4^{tm1Msz} from Riken BioResource Center, RBRC01939) (39, 40) mice were backcrossed 10 times to the C57/BL6J strain. TRPC6/TRPV4$^{-/-}$ mice were obtained by crossing both gene-deficient mouse models. TRPV4EGFP reporter mice (Tg(TRPV4-EGFP)MT43Gsat/Mmucd from MMRC) were bred as previously described (57). Sex- and age-matched mice older than 3 months were used in the experiments, if not mentioned otherwise in the figure legends.

Isolated, perfused mouse lung. Quantification of edema formation in isolated perfused mouse lungs was done as described previously (37). In brief, mice were anesthetized by intraperitoneal injection of ketamine (100 mg/kg BW), xylazine (0.7 mg/kg BW), and anticoagulated with heparin (500 IU/kg BW). Animals were intubated via a small incision in the trachea, ligated, and ventilated with room air using the VCM type 681 (positive end–expiratory pressure, 3 cmH_2O; positive end–inspiratory pressure 3 cmH_2O; respiratory rate was 90 breaths/min). The sternum was opened, the ribs were spread, and the right ventricle was incised

to place the air-free perfusion catheter into the pulmonary artery. After ligation, the perfusion was started with 0.5 ml/min perfusion solution (7.19 g sodium chloride, 0.33 g potassium chloride, 0.27 g magnesium hexahydrate, 0.36 g calcium chloride dihydrate, 0.15 g potassium dihydrogen orthophosphate, 2.67 g glucose monohydrate, 51.28 g hydroxyethyl starch [type 2000000/05] ad 1000 mL with aqua ad iniectabilia, and 0.1848 mg/mL sodium hydrogen carbonate to adjust pH to 7.3) using an ISMATEC Tubing Pump. A second perfusion catheter was introduced in the left ventricle and secured by ligation. The lung, the trachea, and the heart were excised from the thorax in 1 piece and transferred to a 37°C temperature-equilibrated housing chamber for the perfused mouse lung model (IPL-2, Hugo Sachs Elektronik/Harvard Apparatus). The perfusion was slowly raised stepwise to 2 ml/min, and perfusion pressure was monitored with the PLUGSYS TAM-A/P75 type 17111 (Harvard Apparatus). Weight changes were constantly measured with the edema Balance Module/EBM type 713 (Harvard Apparatus). Data were monitored with Pulmodyn software (Harvard Apparatus). The perfusion pressure during the measurements was not significantly different between genotypes as well as before and after ischemia.

Analysis of functional parameters of the respiratory tract. Mice were anesthetized with ketamine (270 mg/kg BW) and xylazin (11 mg/kg BW), intratracheally intubated through a small incision of the trachea, and connected to the flexiVent system (Scireq).

Immunohistochemistry. Mouse lungs were inflated with 2.5% (m/v) glutaraldehyde in PBS and processed for paraffin or O.C.T. compound (Tissue-Tek, Sakura Finetek) embedding. Paraffin-embedded tissue sections (3 μm) were cut using a microtome (Zeiss), mounted on glass slides, deparaffinized in xylene, and rehydrated in graded alcohol. Masson Goldner trichrome staining (Masson Goldner Trichrome Staining Kit, Carl Roth 3459) was done according to the manufacturer's instruction with iron hematoxylin solution for 8 minutes, Goldner's stain 1 for 6 minutes, Goldner's stain 2 for 1 minute, and Goldner's stain 3 for 5 minutes. After dehydration in 100% EtOH and clearing in xylol twice for 1 minute, the sections were mounted in Roti-Histokit II (Carl Roth T160.2). Sections were analyzed by design-based stereology using an Olympus BX51 light microscope equipped with the new Computer Assisted Stereological Toolbox (newCAST, Visiopharm) as described previously (58). For MCL measurements, 10–20 frames were selected randomly across multiple sections by the software, using the ×20 objective, and superimposed by a line grid and points. The intercepts of lines on alveolar wall (Lsepta) and points localized on air space (Pair) were counted and calculated as follows: MCL ($\sum$Pair × L(p)/$\sum$Isepta × 0.5, where L(p) is the line length per point). Cryo-embedded lungs were cut in 10 μm sections on a cryostat (Leica), mounted on glass slides, and surrounded with a hydrophobic pen (Vector Laboratories). After washing with PBS, the sections were blocked for 30 minutes in PBS containing 0.2% Triton X-100 and 5% NGS. Incubation with primary antibody was done at 4°C overnight and secondary antibody at room temperature for 1 hour. Antibodies were diluted in blocking solution. After nuclei staining with Hoechst dye (Thermo Fisher Scientific) (2 μg/mL) for 5 minutes at room temperature followed by sufficient washing the sections were mounted in Roti-Histokit II. The following antibodies and dilutions were used: anti-GFP (chicken, Thermo Fisher Scientific, A10262, 1:200), anti–β-tubulin IV (rabbit monoclonal, Abcam, 179509, 1:1600), anti–AQP-1 (rabbit, Alomone Labs, AQP-001, 1:100), anti–AQP-5 (rabbit, Alomone Labs, AQP-005, 1:100), anti-CC10 (mouse, Santa Cruz Biotechnology, E-11, 1:200), anti-chicken (goat, Thermo Fisher Scientific, A11039, 1:400), anti-CGRP (goat, 1:400, Acris, BP022), anti-rabbit IgG (goat, coupled to Alexa Fluor 488, Thermo Fisher Scientific, A32731, 1:500 and donkey, coupled to Cy3, Merck Millipore, AP182C, 1:1000), and anti-goat IgG (donkey, Life Technologies, A11058, 1:400). For direct labeling of the anti-CC10 antibody, the Zenon Alexa Fluor 546 mouse IgG_1 kit was used according to the manufacturer's recommendations (Invitrogen, 25004). Stained cryosections were analyzed on an epifluorescence microscope (Zeiss Imager.M2, Carl Zeiss) and on a confocal microscope (LSM 880, Carl Zeiss). For membrane localization analysis, staining intensity was analyzed along a line from the nucleus into the cytosol and the plasma membrane.

Primary murine alveolar epithelial cells. Isolation of ATII cells was done as described previously (1, 59, 60). In brief, lungs were flushed via a catheter through the pulmonary artery with 0.9% NaCl solution (B. Braun Melsungen AG), inflated with 1 mL dispase (BD Biosciences), followed by 500 μl 1% low-melting-point agarose (MilliporeSigma), and incubated for 1 hour at room temperature. Subsequently, lung lobes were separated and dissected using 2 forceps; filtered through 100 μm, 20 μm, and 10 μm nylon filters (Sefar); and centrifuged for 10 minutes at 200*g*. Cell pellets were resuspended in DMEM (MilliporeSigma) and plated on CD45- and CD16/32-coated (BD Biosciences) culture dishes

JCI insight

Table 1. List of siRNAs used for downregulation of TRPV4 mRNA

Name	Target sequence
Accell mouse TRPV4 siRNA- SMARTpool	
Accell SMARTpool siRNA A-040742-13	CCAUUGACCUGUUGGAGUC
Accell SMARTpool siRNA A-040742-14	GCAACAUGCGUGAAUUCAU
Accell SMARTpool siRNA A-040742-15	UUACCAGUAUCAAGACUU
Accell SMARTpool siRNA A-040742-16	CUCUUGUGUAUUAUUUAUU
Accell Nontargeting Pool	
Accell Nontargeting Pool D-001910-10-20	UGGUUUACAUGUCGACUAA
	UGGUUUACAUGUUUUCUGA
	UGGUUUACAUGUUUUCCUA
	UGGUUUACAUGUUGUGUGA

for a negative selection of macrophages and lymphocytes and incubated for 30 minutes at 37°C. Non-adherent cells were collected and seeded on uncoated dishes to negatively select fibroblasts at 37°C for 25 minutes. Cells were collected and identified by staining with a fluorescent coupled anti pSP-C antibody (Chemicon International, AB3786, 1:20000). Live cells were counted by trypan blue staining in a Neubauer counting chamber. 2×10^6 cells/well of a 6-well plate were seeded in DMEM containing 10% FCS (Invitrogen), 1% HEPES (Carl Roth), and 1% penicillin/streptomycin (Lonza), and used for analysis or grown for at least 6 days for ATI cell differentiation. ATII cells were transfected with 1 μM Accell SMARTpool siRNA for TRPV4 (in starving medium, 0.1% FCS) 2 days after isolation. On day 6, the cells were washed once and kept in starving medium. A noncoding pool of the Accell siRNA in starving medium served as control (see Table 1 for siRNA sequences).

Patch-clamp recordings of ATII cells. Conventional whole-cell recordings were carried out at room temperature 24 hours after isolation of ATII cells from WT and $TRPV4^{-/-}$ mice. The following bath solution, containing 140 mM NaCl, 1.3 mM $MgCl_2$, 2.4 mM $CaCl_2$, 10 mM glucose, 10 mM HEPES (pH 7.4 with NaOH) and resulting in an osmolality of 310 mOsm/kg, was used for patch-clamp recordings. The pipette solution contained 135 mM CsCl, 2 mM Na-ATP, 1 mM $MgCl_2$, 5 mM EGTA, and 10 mM HEPES (pH 7.2 with CsOH), resulting in an osmolality of 296 mOsm/kg. Patch pipettes made of borosilicate glass (Science Products) had resistances of 2.2–3.5 MΩ for whole-cell measurements. Data were collected with an EPC10 patch clamp amplifier (HEKA) using the Patchmaster software. Current density-voltage relations were obtained before and after application of the TRPV4 activator GSK (1 mM) to the bath solution using voltage ramps from –100 to +100 mV, each lasting 5 seconds. Data were acquired at a frequency of 40 kHz after filtering at 2.8 kHz. The current density-voltage curves and the current density amplitudes at ±100 mV were extracted at minimal or maximal currents, respectively.

Western blot analysis. Western blotting was done as previously described (61). Chemiluminescence was detected in an Odyssey Fc unit (Licor). The following antibodies and dilutions were used: HRP-conjugated anti–β-actin antibody (MilliporeSigma, A3854HRP, 1:10000), anti-TRPV4 (rabbit, Abcam, ab 39260, 1:1000), anti–AQP-5 (rabbit, Alomone AQP-005, 1:1000), anti-Podoplanin (goat, R&D Systems, AF3244, 1:500), secondary anti-goat IgG (whole molecule) peroxidase (MilliporeSigma, A5420-1ML, 1:10000), and secondary anti-rabbit IgG peroxidase (POX) antibody (MilliporeSigma, A6154, 1:10000). One representative of three Western blots is shown in the figures.

NanoString nCounter expression analysis. Direct quantification of TRPV4 mRNA in murine lung cells was done as described previously (62). In brief, total RNA from pulmonary murine cells was isolated using the Qia RNeasy Mini Kit (QIAGEN). Quantity, purity, and integrity of the RNA samples were controlled by spectrophotometry (NanoQuant). Two probes (the reporter and the capture probe) were hybridized to their specific target mRNAs. Then, the target-probe complexes were immobilized in the imaging surface of the nCounter Cartridge by binding of the capture probe. Finally, the sample cartridges were scanned by an automated fluorescence microscope, and molecular barcodes (fluorophores contained in the reporter probe) for each specific target were counted. For expression analysis by nCounter NanoString technology, 200 ng total RNA was hybridized with a NanoString Gene Expression CodeSet and analyzed using the nCounter Digital Analyzer. Background correction was performed and normalization was applied using 4

Table 2. List of oligonucleotides used for nanostring nCounter expression analysis

Name	Primer sequence	Gene Id.
Primer pool A		
β-Actin	AAAAGAGCCTCAGGGCATCGGAACCGCTCGTTGCCAATAGT GATGACCTGCCTCAAGACCTAAGCGACAGCGTGACCTTGTTTCA	NM_007393.1:815
β2-Microglobulin	ATTTGGATTTCAATGTGAGGCGGGTGGAACTGTGTTACGTAGCA GTTCAGCATCCTCTTCTTTTCTTGGTGTTGAGAAGATGCTC	NM_009735.3:177
SdHa	GGCATGCAGTATTAAACCCTGCCTCAGAAAGGCCAAATG CAGCTCGCAAGCACAATTCTGCGGGTTAGCAGGAAGGTTAGGGAAC	NM_023281.1:250
GAPDH	ATCGAAGGTGGAAGAGTGGGAGTTGCTGTTGAAGTCGCA GGAGACAACCTCTGTTGAGATTATTGAGCTTCATCATGACCAGAAG	NM_001001303.1:890
TRPV4	GGCCTCGGTAGTAGATGTCTCTGAAGGGCGAGTTGAT GAATTCACGCATGCATAAAATTGGTTTTGCCTTTCAGCAATTCAACTT	NM_022017.3:776
Primer pool B		
β-Actin	CGAAAGCCATGACCTCCGATCACTCATGTAGTTT CATGGATGCCACAGGATTCCATACCCAAGAAGGAAGGCTGG	NM_007393.1:815
β2-Microglobulin	CGAAAGCCATGACCTCCGATCACTCAGGACATA TCTGACATCTCTACTTTAGGAATTTTTTTCCCGTTCTTCAGC	NM_009735.3:177
SdHa	CGAAAGCCATGACCTCCGATCACTCCTCCCTGTGCTGCA ACAGTATGTGATCGGGTAGGAAAGAGCTTTGTAA	NM_023281.1:250
GAPDH	CGAAAGCCATGACCTCCGATCACTCCAGGAAATGAGC TTGACAAAGTTGTCATTGAGAGCAATGCCAGCCCCGGC	NM_001001303.1:890
TRPV4	CGAAAGCCATGACCTCCGATCACTCCACGTAGTGCTTG CAGCGCCGTTCGATGGCAATGTGCAGGGATGTCT	NM_022017.3:776

SdHa, succinate dehydrogenase subunit A.

different housekeeping genes (succinate dehydrogenase subunit A [Sdha], β2-microglobulin, GAPDH, and β-actin). The DNA sequences used for mRNA expression analysis are summarized in Table 2.

Migration assay. Around 4.4×10^6 ATII cells/well were seeded on a 2-well silicone insert with a 500 μm cell-free gap (ibidi GmbH) and grown in DMEM (10% FCS, 1% HEPES, and 1% penicillin/streptomycin) for 5 days to obtain ATI-like cells. Subsequently, cells were starved in serum-reduced medium (0.1% FCS) for 24 hours before insert detachment to create a defined cell-free gap. Images were taken 0, 1, 3, 5, 8, 12, and 24 hours after gap creation. Migration was analyzed by measuring the remaining gap width with ImageJ software (NIH) in 3 images per time point and replicate.

Isolation of nuclear fractions. Isolation of nuclear protein extracts from ATI-like cells after 6 days of culture was performed with a Nuclear Extract Kit according to the manufacturer's instructions (Active Motif, 40010) as described previously (61). In brief, cells were first washed with PBS containing phosphatase inhibitors. Cytoplasmic protein fractions were collected by adding hypotonic lysis buffer and detergent, causing leakage of cytoplasmic proteins into the supernatant. After centrifugation (14,000*g* for 30 seconds), nuclear protein fractions were obtained by resuspending pellets in detergent-free lysis buffer containing protease inhibitors. NFAT proteins were analyzed by Western blotting as described below using an NFATc1-specific (mouse, Santa Cruz Biotechnology, sc-7294, 1:600) antiserum and lamin B1 (rabbit, Thermo Fisher Scientific, PA5-19468, 1:5000) antibodies as loading controls. Protein bands were normalized to loading controls and quantified by an Odyssey Fc unit (Licor).

Quantification of cell resistance by ECIS. Resistance changes of ATII cells differentiated to ATI cells were analyzed using an ECIS device (Applied Biophysics). Freshly isolated epithelial cells were seeded on ECIS culture ware (8W10E+; Applied Biophysics), which was preincubated with FCS for 3 hours and connected to the ECIS device. A total of 1×10^4 cells was seeded per chamber and grown at 37°C and 5% CO_2 in an incubator. Resistance (Ω) was analyzed at 2000 Hz over 160 hours.

Statistics. All statistical test were performed using GraphPad Prism 7. Numbers of mice and cells as well as statistical tests used are indicated in the figure legends and include 1-way ANOVA and 2-tailed unpaired Student's *t* test. A *P* value of less than 0.05 was considered significant.

Study approval. All animal experiments were approved by the local authority (Regierung Oberbayern, Munich, Germany).

Author contributions

JW and AD conceived the study, analyzed data, and wrote the manuscript. MB, NW, AÖY, JS, and CG aided in the experimental design. JW, YKC, CS, MK, GKC, and SR conducted the experiments. TG aided in critical analysis and in revising the manuscript. All authors read the manuscript and provided critical revisions.

Acknowledgments

The authors thank Bettina Braun for excellent technical assistance and the Riken BioResource Center (RBR) as well as the Mutant Mouse Resource and Research Center for providing the mouse models. This study was funded by the Deutsche Forschungsgemeinschaft (TRR 152, project 16 to AD, project 04 to CG, and project 22 to GKC; GRK 2338, project 04 to AD and project 08 to CG) and the DZL (to AD, MB, NW, and TG).

Address correspondence to: Alexander Dietrich, Walther-Straub-Institute of Pharmacology and Toxicology, Medical Faculty, LMU-Munich, Nussbaumstr. 26, 800336 Munich, Germany. Phone: 011.49.89.2180.73802; Email: alexander.dietrich@lrz.uni-muenchen.de.

1. Mutze K, Vierkotten S, Milosevic J, Eickelberg O, Königshoff M. Enolase 1 (ENO1) and protein disulfide-isomerase associated 3 (PDIA3) regulate Wnt/β-catenin-driven trans-differentiation of murine alveolar epithelial cells. *Dis Model Mech.* 2015;8(8):877–890.
2. Dobbs LG, Johnson MD, Vanderbilt J, Allen L, Gonzalez R. The great big alveolar TI cell: evolving concepts and paradigms. *Cell Physiol Biochem.* 2010;25(1):55–62.
3. Weibel ER. On the tricks alveolar epithelial cells play to make a good lung. *Am J Respir Crit Care Med.* 2015;191(5):504–513.
4. Stone KC, Mercer RR, Freeman BA, Chang LY, Crapo JD. Distribution of lung cell numbers and volumes between alveolar and nonalveolar tissue. *Am Rev Respir Dis.* 1992;146(2):454–456.
5. Fehrenbach H. Alveolar epithelial type II cell: defender of the alveolus revisited. *Respir Res.* 2001;2(1):33–46.
6. Halliday HL. Surfactants: past, present and future. *J Perinatol.* 2008;28 Suppl 1:S47–S56.
7. Desai TJ, Brownfield DG, Krasnow MA. Alveolar progenitor and stem cells in lung development, renewal and cancer. *Nature.* 2014;507(7491):190–194.
8. Hollenhorst MI, Richter K, Fronius M. Ion transport by pulmonary epithelia. *J Biomed Biotechnol.* 2011;2011:174306.
9. Nilius B, Szallasi A. Transient receptor potential channels as drug targets: from the science of basic research to the art of medicine. *Pharmacol Rev.* 2014;66(3):676–814.
10. Dietrich A, Steinritz D, Gudermann T. Transient receptor potential (TRP) channels as molecular targets in lung toxicology and associated diseases. *Cell Calcium.* 2017;67:123–137.
11. Hellwig N, Albrecht N, Harteneck C, Schultz G, Schaefer M. Homo- and heteromeric assembly of TRPV channel subunits. *J Cell Sci.* 2005;118(Pt 5):917–928.
12. Köttgen M, et al. TRPP2 and TRPV4 form a polymodal sensory channel complex. *J Cell Biol.* 2008;182(3):437–447.
13. Liedtke W, et al. Vanilloid receptor-related osmotically activated channel (VR-OAC), a candidate vertebrate osmoreceptor. *Cell.* 2000;103(3):525–535.
14. Strotmann R, Harteneck C, Nunnenmacher K, Schultz G, Plant TD. OTRPC4, a nonselective cation channel that confers sensitivity to extracellular osmolarity. *Nat Cell Biol.* 2000;2(10):695–702.
15. Hill-Eubanks DC, Gonzales AL, Sonkusare SK, Nelson MT. Vascular TRP channels: performing under pressure and going with the flow. *Physiology (Bethesda).* 2014;29(5):343–360.
16. Marziano C, Hong K, Cope EL, Kotlikoff MI, Isakson BE, Sonkusare SK. Nitric oxide-dependent feedback loop regulates transient receptor potential vanilloid 4 (TRPV4) channel cooperativity and endothelial function in small pulmonary arteries. *J Am Heart Assoc.* 2017;6(12):e007157.
17. Lorenzo IM, Liedtke W, Sanderson MJ, Valverde MA. TRPV4 channel participates in receptor-operated calcium entry and ciliary beat frequency regulation in mouse airway epithelial cells. *Proc Natl Acad Sci USA.* 2008;105(34):12611–12616.
18. Li J, et al. TRPV4-mediated calcium influx into human bronchial epithelia upon exposure to diesel exhaust particles. *Environ Health Perspect.* 2011;119(6):784–793.
19. Henry CO, et al. In vitro and in vivo evidence for an inflammatory role of the calcium channel TRPV4 in lung epithelium: Potential involvement in cystic fibrosis. *Am J Physiol Lung Cell Mol Physiol.* 2016;311(3):L664–L675.
20. Goldenberg NM, Ravindran K, Kuebler WM. TRPV4: physiological role and therapeutic potential in respiratory diseases. *Naunyn Schmiedebergs Arch Pharmacol.* 2015;388(4):421–436.
21. Xia Y, et al. TRPV4 channel contributes to serotonin-induced pulmonary vasoconstriction and the enhanced vascular reactivity in chronic hypoxic pulmonary hypertension. *Am J Physiol, Cell Physiol.* 2013;305(7):C704–C715.
22. Goldenberg NM, Wang L, Ranke H, Liedtke W, Tabuchi A, Kuebler WM. TRPV4 is required for hypoxic pulmonary vasoconstriction. *Anesthesiology.* 2015;122(6):1338–1348.
23. Everaerts W, et al. Inhibition of the cation channel TRPV4 improves bladder function in mice and rats with cyclophosphamide-induced cystitis. *Proc Natl Acad Sci USA.* 2010;107(44):19084–19089.
24. Dietrich A. Modulators of transient receptor potential (TRP) channels as therapeutic options in lung disease. *Pharmaceuticals (Basel).* 2019;12(1):E23.
25. Rahaman SO, et al. TRPV4 mediates myofibroblast differentiation and pulmonary fibrosis in mice. *J Clin Invest.* 2014;124(12):5225–5238.
26. Jian MY, King JA, Al-Mehdi AB, Liedtke W, Townsley MI. High vascular pressure-induced lung injury requires P450 epoxygenase-dependent activation of TRPV4. *Am J Respir Cell Mol Biol.* 2008;38(4):386–392.

27. Hamanaka K, et al. TRPV4 initiates the acute calcium-dependent permeability increase during ventilator-induced lung injury in isolated mouse lungs. *Am J Physiol Lung Cell Mol Physiol*. 2007;293(4):L923–L932.
28. Michalick L, Erfinanda L, Weichelt U, van der Giet M, Liedtke W, Kuebler WM. Transient receptor potential vanilloid 4 and serum glucocorticoid-regulated kinase 1 are critical mediators of lung injury in overventilated mice in vivo. *Anesthesiology*. 2017;126(2):300–311.
29. Thorneloe KS, et al. An orally active TRPV4 channel blocker prevents and resolves pulmonary edema induced by heart failure. *Sci Transl Med*. 2012;4(159):159ra148.
30. Akazawa Y, Yuki T, Yoshida H, Sugiyama Y, Inoue S. Activation of TRPV4 strengthens the tight-junction barrier in human epidermal keratinocytes. *Skin Pharmacol Physiol*. 2013;26(1):15–21.
31. Janssen DA, et al. TRPV4 channels in the human urogenital tract play a role in cell junction formation and epithelial barrier. *Acta Physiol (Oxf)*. 2016;218(1):38–48.
32. Martínez-Rendón J, et al. TRPV4 regulates tight junctions and affects differentiation in a cell culture model of the corneal epithelium. *J Cell Physiol*. 2017;232(7):1794–1807.
33. Alvarez DF, King JA, Weber D, Addison E, Liedtke W, Townsley MI. Transient receptor potential vanilloid 4-mediated disruption of the alveolar septal barrier: a novel mechanism of acute lung injury. *Circ Res*. 2006;99(9):988–995.
34. Alpizar YA, et al. TRPV4 activation triggers protective responses to bacterial lipopolysaccharides in airway epithelial cells. *Nat Commun*. 2017;8(1):1059.
35. Balakrishna S, et al. TRPV4 inhibition counteracts edema and inflammation and improves pulmonary function and oxygen saturation in chemically induced acute lung injury. *Am J Physiol Lung Cell Mol Physiol*. 2014;307(2):L158–L172.
36. Steinritz D, Stenger B, Dietrich A, Gudermann T, Popp T. TRPs in Tox: Involvement of transient receptor potential-channels in chemical-induced organ toxicity-a structured review. *Cells*. 2018;7(8):E98.
37. Weissmann N, et al. Activation of TRPC6 channels is essential for lung ischaemia-reperfusion induced oedema in mice. *Nat Commun*. 2012;3:649.
38. Simmons S, Erfinanda L, Bartz C, Kuebler WM. Novel mechanisms regulating endothelial barrier function in the pulmonary microcirculation. *J Physiol (Lond)*. 2019;597(4):997–1021.
39. Suzuki M, Mizuno A, Kodaira K, Imai M. Impaired pressure sensation in mice lacking TRPV4. *J Biol Chem*. 2003;278(25):22664–22668.
40. Mizuno A, Matsumoto N, Imai M, Suzuki M. Impaired osmotic sensation in mice lacking TRPV4. *Am J Physiol, Cell Physiol*. 2003;285(1):C96–101.
41. Kalwa H, et al. Phospholipase C epsilon (PLCε) induced TRPC6 activation: a common but redundant mechanism in primary podocytes. *J Cell Physiol*. 2015;230(6):1389–1399.
42. Mendoza SA, et al. TRPV4-mediated endothelial Ca2+ influx and vasodilation in response to shear stress. *Am J Physiol Heart Circ Physiol*. 2010;298(2):H466–H476.
43. Yin J, et al. Negative-feedback loop attenuates hydrostatic lung edema via a cGMP-dependent regulation of transient receptor potential vanilloid 4. *Circ Res*. 2008;102(8):966–974.
44. Suresh K, et al. Hydrogen peroxide-induced calcium influx in lung microvascular endothelial cells involves TRPV4. *Am J Physiol Lung Cell Mol Physiol*. 2015;309(12):L1467–L1477.
45. de Perrot M, Liu M, Waddell TK, Keshavjee S. Ischemia-reperfusion-induced lung injury. *Am J Respir Crit Care Med*. 2003;167(4):490–511.
46. Dobbs LG, Gonzalez R, Matthay MA, Carter EP, Allen L, Verkman AS. Highly water-permeable type I alveolar epithelial cells confer high water permeability between the airspace and vasculature in rat lung. *Proc Natl Acad Sci USA*. 1998;95(6):2991–2996.
47. Liu X, et al. A role for AQP5 in activation of TRPV4 by hypotonicity: concerted involvement of AQP5 and TRPV4 in regulation of cell volume recovery. *J Biol Chem*. 2006;281(22):15485–15495.
48. Sidhaye VK, Güler AD, Schweitzer KS, D'Alessio F, Caterina MJ, King LS. Transient receptor potential vanilloid 4 regulates aquaporin-5 abundance under hypotonic conditions. *Proc Natl Acad Sci USA*. 2006;103(12):4747–4752.
49. Hills BA. An alternative view of the role(s) of surfactant and the alveolar model. *J Appl Physiol*. 1999;87(5):1567–1583.
50. Pumiputavon K, et al. Cytotoxic and cytostatic effects of four Annonaceae plants on human cancer cell lines. *In Vitro Cell Dev Biol Anim*. 2019;55(9):723–732.
51. Ma T, Fukuda N, Song Y, Matthay MA, Verkman AS. Lung fluid transport in aquaporin-5 knockout mice. *J Clin Invest*. 2000;105(1):93–100.
52. King LS, Nielsen S, Agre P. Aquaporins and the respiratory system: advice for a lung investigator. *J Clin Invest*. 2000;105(1):15–16.
53. Yan C, Zhu Y, Zhang X, Chen X, Zheng W, Yang J. Down-regulated aquaporin 5 inhibits proliferation and migration of human epithelial ovarian cancer 3AO cells. *J Ovarian Res*. 2014;7:78.
54. Jiang XX, et al. Reduced migration of Ishikawa cells associated with downregulation of aquaporin-5. *Oncol Lett*. 2012;4(2):257–261.
55. Glasser SW, Detmer EA, Ikegami M, Na CL, Stahlman MT, Whitsett JA. Pneumonitis and emphysema in sp-C gene targeted mice. *J Biol Chem*. 2003;278(16):14291–14298.
56. Dietrich A, et al. Increased vascular smooth muscle contractility in TRPC6−/− mice. *Mol Cell Biol*. 2005;25(16):6980–6989.
57. Gong S, et al. A gene expression atlas of the central nervous system based on bacterial artificial chromosomes. *Nature*. 2003;425(6961):917–925.
58. John-Schuster G, et al. Cigarette smoke-induced iBALT mediates macrophage activation in a B cell-dependent manner in COPD. *Am J Physiol Lung Cell Mol Physiol*. 2014;307(9):L692–L706.
59. Corti M, Brody AR, Harrison JH. Isolation and primary culture of murine alveolar type II cells. *Am J Respir Cell Mol Biol*. 1996;14(4):309–315.
60. Dobbs LG. Isolation and culture of alveolar type II cells. *Am J Physiol*. 1990;258(4 Pt 1):L134–L147.
61. Hofmann K, et al. Classical transient receptor potential 6 (TRPC6) channels support myofibroblast differentiation and development of experimental pulmonary fibrosis. *Biochim Biophys Acta Mol Basis Dis*. 2017;1863(2):560–568.
62. Kannler M, Lüling R, Yildirim AÖ, Gudermann T, Steinritz D, Dietrich A. TRPA1 channels: expression in non-neuronal murine lung tissues and dispensability for hyperoxia-induced alveolar epithelial hyperplasia. *Pflugers Arch*. 2018;470(8):1231–1241.

5. Paper III

ORIGINAL RESEARCH

An Inhibitory Function of TRPA1 Channels in TGF-β1–driven Fibroblast-to-Myofibroblast Differentiation

Fabienne Geiger[1], Sarah Zeitlmayr[1], Claudia A. Staab-Weijnitz[2], Suhasini Rajan[1], Andreas Breit[1], Thomas Gudermann[1], and Alexander Dietrich[1]

[1]Walther Straub Institute of Pharmacology and Toxicology, Member of the German Center for Lung Research, Ludwig-Maximilians-University Munich, Munich, Germany, and [2]Comprehensive Pneumology Center with the CPC-M BioArchive and Institute of Lung Health and Immunity, Helmholtz Center Munich, Member of the German Center for Lung Research, Munich, Germany

ORCID IDs: 0000-0002-7550-9739 (F.G.); 0000-0002-1211-7834 (C.A.S.-W.); 0000-0002-9343-2798 (A.B.); 0000-0002-1168-8707 (A.D.).

Abstract

TRPA1 (transient receptor potential ankyrin 1) is a nonselective Ca^{2+}-permeable cation channel, which was originally cloned from human lung fibroblasts (HLFs). TRPA1-mediated Ca^{2+} entry is evoked by exposure to several chemicals, including allyl isothiocyanate (AITC), and a protective effect of TRPA1 activation in the development of cardiac fibrosis has been proposed. Yet the function of TRPA1 in TGF-β1 (transforming growth factor-β1)–driven fibroblast-to-myofibroblast differentiation and the development of pulmonary fibrosis remains elusive. TRPA1 expression and function were analyzed in cultured primary HLFs, and mRNA concentrations were significantly reduced after adding TGF-β1. Expression of genes encoding fibrosis markers (e.g., *ACTA2*, *SERPINE1* [plasminogen activator inhibitor 1], *FN1* [fibronectin], *COL1A1* [type I collagen]) was increased after siRNA-mediated downregulation of TRPA1 mRNA in HLFs. Moreover, AITC-induced Ca^{2+} entry in HLFs was decreased after TGF-β1 treatment and by application of TRPA1 siRNAs, while AITC treatment alone did not reduce cell viability or enhance apoptosis. Most interestingly, AITC-induced TRPA1 activation augmented ERK1/2 (extracellular signal–regulated kinase 1/2) and SMAD2 linker phosphorylation, which might inhibit TGF-β-receptor signaling. Our results suggest an inhibitory function of TRPA1 channels in TGF-β1–driven fibroblast-to-myofibroblast differentiation. Therefore, activation of TRPA1 channels might be protective during the development of pulmonary fibrosis in patients.

Keywords: pulmonary fibrosis; extracellular signal–regulated kinase 1/2; mitogen-activated protein kinase p38; PAI-1

Clinical Relevance

Our data in primary human lung fibroblasts point to an important inhibitory function of TRPA1 (transient receptor potential ankyrin 1) channel activity in fibroblast to myofibroblast differentiation, a hallmark of pulmonary fibrosis. Therefore, activation of TRPA1 channels may blaze the trail for new therapeutic options in lung fibrosis.

Lung fibrosis is a chronic progressive disease with limited medical treatment options, leading to respiratory failure and death, with a median overall survival time of 3–5 years after diagnosis (1). The most progressive form of the disease is idiopathic pulmonary fibrosis (IPF) (2), a chronic fibrotic interstitial lung disease of unknown cause, which occurs primarily in older adults (3). The incidence of IPF appears to be higher in North America and Europe (three to nine cases per 100,000 person-years) than in

(Received in original form April 13, 2022; accepted in final form November 15, 2022)

Supported by Deutsches Zentrum für Lungenforschung and Deutsche Forschungsgemeinschaft grants TRR 152 (P15, P16) and GRK2338 (P04, P07, P10).

Author Contributions: Conception and design: F.G. and A.D. Data acquisition and interpretation: F.G., S.Z., C.A.S.-W., S.R., A.B., and A.D. Drafting and revision of manuscript: F.G., S.Z., C.A.S.-W., S.R., A.B., T.G., and A.D.

Correspondence and requests for reprints should be addressed to Alexander Dietrich, Ph.D., Walther-Straub-Institute of Pharmacology and Toxicology, Ludwig-Maximilians-University Munich, Nussbaumstrasse 26, 80336 Munich, Germany. E-mail: alexander.dietrich@lrz.uni-muenchen.de.

This article has a related editorial.

This article has a data supplement, which is accessible from this issue's table of contents at www.atsjournals.org.

Am J Respir Cell Mol Biol Vol 68, Iss 3, pp 314–325, March 2023

Originally Published in Press as DOI: 10.1165/rcmb.2022-0159OC on November 15, 2022
Internet address: www.atsjournals.org

South America and East Asia (fewer than four cases per 100,000 person-years) (4).

The role of inflammation of lung tissues in IPF has been discussed extensively (5). However, multiple and potent antiinflammatory therapies, in particular corticosteroids, have failed to show benefits in patients with IPF (5). Pirfenidone, recently approved in the United States, downregulates the production of growth factors such as TGF-β1 (transforming growth factor-β1) and procollagens, whereas the already established nintedanib is a multi–tyrosine kinase inhibitor. Both compounds slow the decrease of forced vital capacity and also improve patients' quality of life, but they do not increase survival rates (6, 7). Therefore, the need for more causative-acting drugs directed against novel identified pharmacological targets is obvious.

Although the detailed molecular steps of fibrosis development are still elusive, it is now generally believed that after chronic microinjuries, epithelial cells release mediators such as TGF-β1, which induce fibroblast-to-myofibroblast differentiation (1, 2). Myofibroblasts express more α-SMA and secrete extracellular matrix (ECM) proteins (e.g., COL [collagen], FN1 [fibronectin 1], PAI-1) for the recovery of lung barrier function (1, 2). Indeed, IPF is characterized by scattered accumulation of myofibroblasts in fibroproliferative foci with ECM, which results in irreversible destruction of lung architecture and seriously inhibits alveolar gas exchange in patients (1, 7). In addition to fibroblasts, alveolar epithelial cells (8, 9), fibrocytes (10), pericytes (11), and pleural mesothelial cells (12) may also, at least in part, transdifferentiate to myofibroblasts.

The superfamily of TRP (transient receptor potential) channels in vertebrates consists of 28 members in six families fulfilling multiple roles in the living organism (13). While TRPC6 (TRP cation channel subfamily C member 6), the sixth member of the TRPC (classical or canonical TRP) family, is activated by ligand binding (14), TRPV4 (TRP cation channel subfamily V member 4), a channel of the vanilloid family, is thermosensitive in the range from 24°C to 38°C and may serve as mechanosensor because it is activated by membrane and shear stretch (15). Both proteins form tetrameric unselective cation channels, which are expressed in human and mouse fibroblasts (16–18) and increase intracellular Ca^{2+} and Na^{+} concentrations, initiating multiple signal transduction pathways and cellular responses (13). Most interestingly, TRPV4 has already been identified as an important player in pulmonary fibrosis in mice, and its expression was upregulated in lung fibroblasts derived from patients with IPF (18). Moreover, we were able to show that mice lacking TRPC6 were partly protected from bleomycin-induced lung fibrosis (17). TRPC6 channel expression was increased in primary murine lung fibroblasts after application of TGF-β1, and ablation of TRPC6 resulted in reduced α-SMA production, less migration of myofibroblasts, and decreased secretion of ECM (17). Therefore, TRPV4 and TRPC6 are important determinants of TGF-β1–induced myofibroblast differentiation during fibrosis in mice.

Here, we set out to analyze TRP mRNA expression patterns in primary human lung fibroblasts (HLFs) with and without incubation with TGF-β1 in a more translational approach. Although TRPC6 and TRPV4 mRNA expression was not changed, we identified a TGF-β1–mediated downregulation of TRPA1 (TRP ankyrin 1), another member of the TRP superfamily. TRPA1, which is the only member of the TRPA (TRP ankyrin) family, harbors many ankyrin repeat domains in its amino-terminus and opens its pore after exposure to several chemicals, including allyl isothiocyanate (AITC) (19). Most interestingly, steroids and pirfenidone, a drug used as a therapeutic option in patients with lung fibrosis, also activated TRPA1 channels, which resulted in inhibition of trinitrobenzenesulfonic acid–induced colitis (20). Moreover, calcitonin gene–related peptide production after activation of TRPA1 channels in cardiac fibroblasts worked as an endogenous suppressor of cardiac fibrosis (21).

SiRNA-mediated downregulation of TRPA1 mRNA resulted in upregulation of mRNA and protein expression of profibrotic marker proteins. AITC-induced increases in intracellular Ca^{2+} concentration ($[Ca^{2+}]_i$) were reduced. Moreover, TGF-β1 signaling was decreased by AITC-induced TRPA1 activation, probably by ERK (extracellular signal–regulated kinase) and/or MAPK (mitogen-activated protein kinase) p38 phosphorylation and SMAD2 (SMAD family member 2) linker phosphorylation. Therefore, in contrast to TRPC6 and TRPV4, TRPA1 channels are able to inhibit fibroblast-to-myofibroblast differentiation and may serve as pharmacological targets in the development of new therapeutic options for pulmonary fibrosis.

Some of the results of these studies have been previously reported in preprint form (https://biorxiv.org/cgi/content/short/2022.04.12.488008v1).

Methods

Cells

HLFs from healthy donors were obtained from Lonza (#CC-2512), PromoCell (#C-12360), or the CPC-M BioArchive for lung diseases at the Comprehensive Pneumology Center. HLFs were used until passage 8. Ethics statements were provided by the suppliers.

Transcriptomic Analysis by RNA Sequencing

HLFs were incubated with TGF-β1 or solvent as described in the data supplement, and RNA sequencing was performed by IMGM Laboratories on the Illumina NovaSeq 6000 next-generation sequencing system as previously described (22). Data for normalized counts and differential gene expression were obtained using the Bioconductor package DESeq2 (http://www.bioconductor.org/packages/release/bioc/html/DESeq2.html.) (23) and gene enrichment analysis using clusterProfiler (24) in R (https://cran.r-project.org/bin/windows/base/) version 4.1.2. The data set has been deposited in the ArrayExpress database at the European Molecular Biology Laboratory's European Bioinformatics Institute (www.ebi.ac.uk/arrayexpress) under accession number E-MTAB-11629.

Plasmin Assay

To indirectly quantify the secretion of PAI-1 from HLFs, 10 μl of the supernatant of HLFs, 10 μl of 10 mM D-Val-Leu-Lys 7-amido-4-methylcoumarin (D-VLK-AMC) (in 10% DMSO in H_2O) (#V3138; Sigma-Aldrich) as a plasmin substrate (25), and 80 μl Tris/HCl (20 mM, pH 7.4) were incubated for 4 hours at 37°C in 5% CO_2 in a black 96-well plate with a clear bottom. Fluorescence intensity of 7-amido-4-methylcoumarin (AMC) was excited at a wavelength of 380 nm and measured an emission wavelength of 460 nm using a plate reader (Infinite M200 PRO; Tecan). Higher fluorescence values indicate increased concentrations of plasmin processed using tissue plasminogen activator,

as D-VLK-AMC is hydrolyzed by plasmin to AMC (26).

Electroporation and Luciferase Reporter Assay

HLFs were electroporated with the Neon Transfection System (Invitrogen) to achieve plasmid transfection as previously described (27). A total of 250,000 HLFs were resuspended in 100 μl buffer R (Neon Transfection System 100 μl Kit, catalog number MPK10096), and 4 μl of the luciferase reporter plasmid (1 μg/μl pGL3-CAGA[9]-luc) containing the SMAD-sensitive part of the human PAI-1 promotor controlling the luciferase gene (28) was added. Electroporation was performed with two 1,400-V, 20-ms pulses. HLFs were seeded in 4 wells of a 24-well plate in antibiotic-free medium containing 2% (Lonza or PromoCell) or 10% (Deutsches Zentrum für Lungenforschung CPC-M BioArchive) serum. After 24 hours, the cells were treated with TGF-β1 (2 ng/ml) or solvent; medium contained 1% penicillin/streptomycin and 0.1% serum. On the second day, the cells were pretreated with A-967079 (500 nM) or solvent for 30 minutes and stimulated with AITC (10 μM) or DMSO for 120 minutes. The fibroblasts were lysed in 100 μl lysis buffer per well (25 mM Tris/HCl [pH 7.4], 4 mM EGTA, 8 mM $MgCl_2$, 1 mM DTT, and 1% Triton X-100 [Carl Roth, catalog number 3051.2]) for 10 minutes at room temperature. Luminescence was measured upon injection of 20 μl luciferase reporter assay substrate (#E1501; Promega) to each well using an OMEGA (BMG labtech) plate reader.

All other methods are described in the data supplement.

Results

Transcriptional and Functional Downregulation of TRPA1 Channels in HLFs after Application of TGF-β1

To investigate the role of TRP channels in TGF-β1–driven fibroblast-to-myofibroblast differentiation, we cultured primary HLFs from three human donors, applied TGF-β1 (2 ng/ml for 48 h) or solvent, and extracted RNA for a thorough transcriptomic analysis. Although mRNAs coding typical marker proteins for lung fibrosis and signaling pathways for ECM and structure organization were significantly upregulated (*see* Figures E1A and E1B in the data supplement), none of the channels of the TRPC, TRPV (TRP vanilloid), and TRPM (TRP melastatin) families showed significant changes in mRNA expression after the application of TGF-β1 (*see* Figures E1C–E1E). For TRPA1 mRNA, however, there was a clear trend toward TGF-β1–induced downregulation (*see* Figure E1F), which turned out to be significant in a comparison of $\log_2$ fold changes (Table 1). Moreover, this significant reduction of TRPA1 mRNA after application of TGF-β1 was reproducible by repetitive qRT-PCR experiments (Figure 1A). To successfully manipulate TRPA1 expression in lung fibroblasts, we tested an siRNA pool directed against TRPA1 mRNA and identified an 84.4% downregulation of TRPA1 mRNA, whereas a scrambled control siRNA showed no significant changes (Figure 1A). We tested four TRPA1 antisera, including two monoclonal antibodies reported to be selective for TRPA1 channels (29). However, in our hands these batches of antibodies showed no selectivity for the TRPA1 protein in human embryonic kidney 293 (HEK) cells stably expressing the channel (*see* Figure E2). Therefore, TRPA1 function was analyzed using Ca^{2+} imaging of fibroblasts.

Table 1. $\log_2$ Fold Changes and *P* Values for Transient Receptor Potential Channel mRNA Expression Obtained by Transcriptomic Analysis of Human Lung Fibroblasts Treated with Transforming Growth Factor-β1 or Solvent

TRP Channel	$\log_2$ Fold Change	*P* Value	Adjusted *P* Value
TRPA1	−1.649	**0.003**	**0.047**
TRPC1	−0.437	0.262	0.675
TRPC2	N/A	N/A	N/A
TRPC3	0.173	0.842	0.969
TRPC4	−0.788	0.523	0.860
TRPC5	0.528	0.807	N/A
TRPC6	−0.205	0.728	0.939
TRPC7	N/A	N/A	N/A
TRPM1	−1.531	0.705	N/A
TRPM2	1.239	0.761	N/A
TRPM3	−0.868	0.499	N/A
TRPM4	0.037	0.932	0.992
TRPM5	N/A	N/A	N/A
TRPM6	−0.793	0.700	N/A
TRPM7	0.001	0.997	1.000
TRPM8	−0.525	0.755	N/A
TRPV1	−0.048	0.931	0.991
TRPV2	−0.618	0.433	0.809
TRPV3	1.693	0.214	N/A
TRPV4	0.259	0.821	0.964
TRPV5	N/A	N/A	N/A
TRPV6	1.239	0.761	N/A

Definition of abbreviations: N/A = not available; TRP = transient receptor potential; TRPA = transient receptor potential ankyrin 1; TRPC = canonical transient receptor potential; TRPM = transient receptor potential melastatin; TRPV = transient receptor potential vanilloid.
P values <0.05 are indicated in boldface type.

Application of the specific TRPA1 activator AITC resulted in a transient increase in $[Ca^{2+}]_i$, which was reduced in cells transfected with TRPA1 siRNAs (Figures 1B and 1C). Most interestingly, fibroblasts treated with TGF-β1 showed significantly reduced AITC-induced increases in $[Ca^{2+}]_i$ in comparison with control cells incubated with solvent only (Figures 1D and 1E). We obtained similar results with another specific activator of TRPA1 channels, JT010 (30) (*see* Figures E3A and E3B). Therefore, TRPA1 expression and function are reduced after application of TGF-β1 to primary human fibroblasts. This AITC-induced increase in $[Ca^{2+}]_i$ was blocked by a specific TRPA1 inhibitor, A-967079, in the absence and presence of TGF-β1 (*see* Figures E3C and E3D).

Downregulation of TRPA1 mRNA Increases Expression of Fibrosis Markers in HLFs

TGF-β1–induced fibroblast-to-myofibroblast differentiation is a key event in the development of lung fibrosis and results in upregulation of gene expression of *ACTA2*, *COL1A1* (type I collagen), *FN1*, and *SERPINE1* (plasminogen activator inhibitor 1),

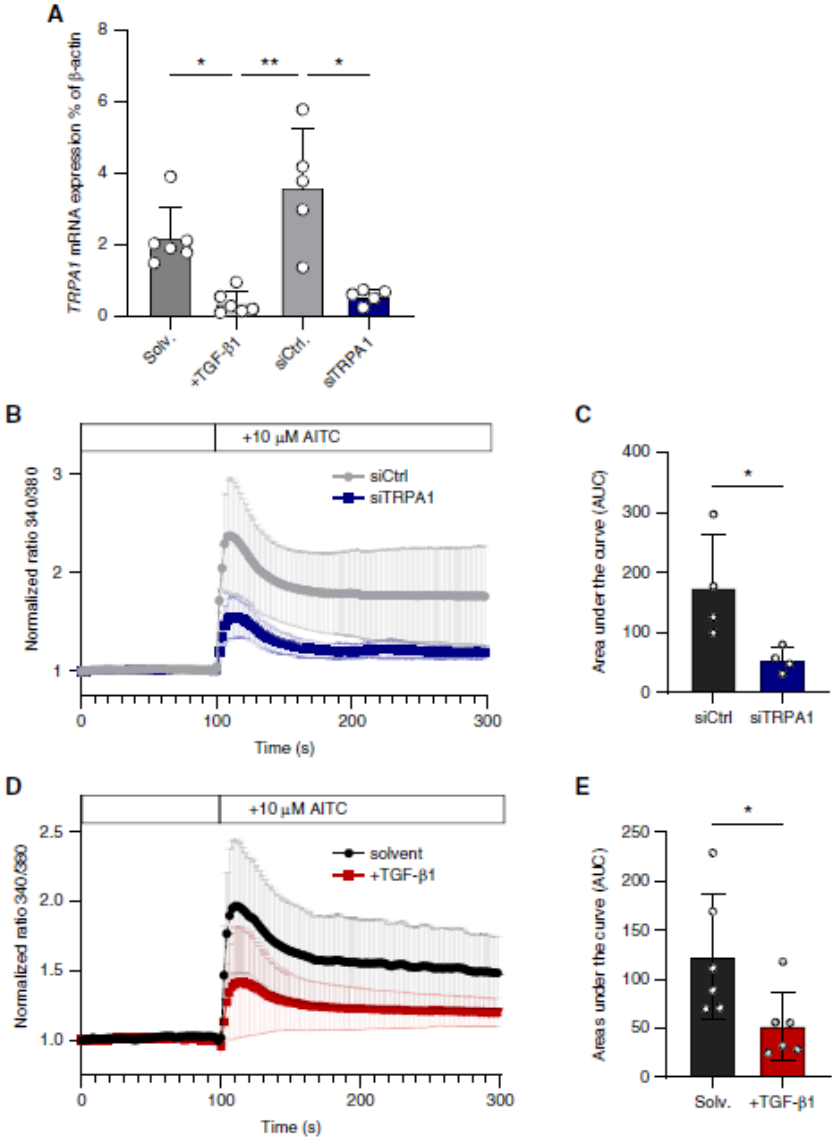

Figure 1. qRT-PCR and Ca^{2+} imaging in primary human lung fibroblasts (HLFs) cultured with TGF-β1 (transforming growth factor-β1) or transfected with TRPA1 (transient receptor potential ankyrin 1)–specific siRNAs. (*A*) TRPA1 mRNA expression quantified by qRT-PCR experiments in HLFs cultured with TGF-β1 (+TGF-β1) or transfected with TRPA1-specific siRNAs (siTRPA1). Solvent (Solv) or scrambled siRNAs (siCtrl) served as a control. (*B*) HLFs were transfected with siTRPA1 (blue line) or siCtrl (gray line) as a control, and intracellular Ca^{2+} concentrations were quantified as normalized ratios 340/380 nm after adding the TRPA1 activator allyl isothiocyanate (AITC) (10 μM), as described in METHODS. Light gray areas represent SEM. (*C*) Areas under the curves (AUCs) were calculated and plotted as bars (siTRPA1, blue bar; siCtrl, black bar). (*D*) HLFs were cultured with TGF-β1 (red line) or Solv (black line) as a control, and intracellular Ca^{2+} concentrations were quantified as normalized ratios 340/380 nm after adding the TRPA1 activator AITC (10 μM), as described in the data supplement. Light gray areas represent SEM. (*E*) AUCs were calculated and plotted as bars (+TGF-β1, red bar; Solv, black bar). Data were analyzed using a Kruskal-Wallis test (*A*) or a Mann-Whitney test (*C* and *E*) and are presented as mean ± SEM. qRT-PCR and calcium imaging experiments were performed with $n \geq 5$ independent cell isolations each. For all graphs, $^{*}P < 0.05$ and $^{**}P < 0.01$ versus the value in cells treated with Solv or siCtrl alone.

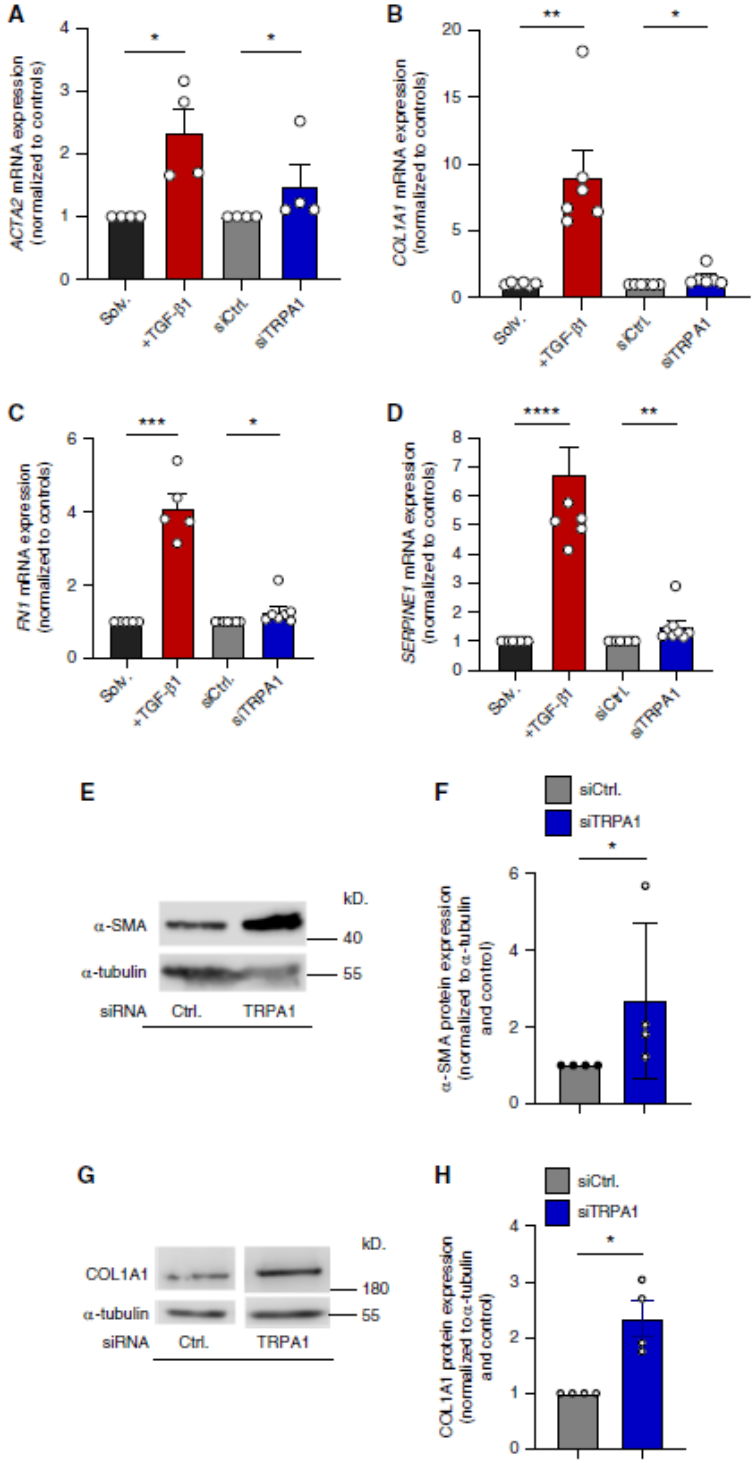

Figure 2. qRT-PCR and western blotting experiments for expression of fibrotic marker genes in HLFs cultured with TGF-β1 or transfected with siTRPA1. (*A*) Quantification of mRNA concentrations of *ACTA2* in HLFs cultured with TGF-β1 or Solv and transfected with siTRPA1 or siCtrl as a control. (*B*) Quantification of mRNA concentrations of *COL1A1* (collagen 1A1) in HLFs cultured with TGF-β1 or Solv and transfected with

encoding the fibrotic marker proteins α-SMA, the α(1) chain of type I collagen (COL1A1), FN-1, and PAI-1, respectively. As expected, application of TGF-β1 resulted in upregulation of mRNA expression from these genes (*see* Figure E1A). Most interestingly, transfection of cells by the specific TRPA1 siRNA but not a control siRNA was also able to increase mRNA expression of fibrotic marker proteins in the absence of TGF-β1 (Figures 2A–2D). To evaluate these small but significant increases in mRNA concentrations on a protein level, we performed quantitative western blotting of protein lysates from fibroblasts transfected with TRPA1-specific or control siRNA. Expression of both proteins α-SMA and COL1A1 increased after downregulation of TRPA1 channels (Figures 2E–2H). However, TRPA1-specific siRNA was not effective if cells were simultaneously incubated with TGF-β1 (*see* Figures E4A and E4B). Thus, in turn, TRPA1 expression and function seem to suppress expression of profibrotic genes.

Downregulation of TRPA1 mRNA Increases and Application of TRPA1 Activators Decreases Function of Profibrotic Proteins in HLFs

To further evaluate the effects of TRPA1 channels on protein expression and function, we performed several assays. Detection of α-SMA by binding of an α-SMA–specific antibody followed by a fluorophore-coupled secondary antibody revealed increased protein concentrations after TGF-β1 induction in HLFs, which were also identified after application of the TRPA1 siRNA (Figures 3A and 3B). Phalloidin staining to detect F-actin was also enhanced after incubation of cells with TGF-β1 or TRPA1 siRNA (Figures 3C and 3D). TGF-β1–induced upregulation of α-SMA and COL1A1 was detected using western blotting in HLFs and was significantly downregulated by the TRPA1 activator AITC (Figures 3E–3H). We obtained similar results in the presence of the other specific TRPA1 activator, ƒT010, and cotreatment with TGF-β1 (*see* Figures E4C–E4F). PAI-1 is able to inhibit tissue plasminogen activator or urokinase-induced production of plasmin, which results in degradation of fibrin clots (Figure 4A). This process is quantified by cleaving of D-VLK-AMC by plasmin and increased emission of fluorescence from free AMC (Figure 4B) (26). As expected, plasmin-induced fluorescence of the HLF medium was decreased after incubation of cells with TGF-β1. Transfection of cells with TRPA1 siRNA was also able to decrease fluorescence, although to a lesser extent (Figure 4C). Application of the TRPA1 activator AITC (Figure 4D) or ƒT010 (*see* Figure E4G) also resulted in a lesser or no decrease in plasmin activity, respectively. In conclusion, downregulation of TRPA1 results in higher expression and activity of profibrotic marker proteins, whereas treatment of HLFs with TRPA1 activators rescued plasmin activity compared to TGF-β1 treatment alone, most probably by reduced expression of PAI-1.

TRPA1-induced MAPK Phosphorylation Inhibits TGF-β1–mediated Transcription of Fibrotic Marker Proteins

To understand TRPA1 channel and TGF-β1 function on cellular transcription, we established a luciferase assay. A construct containing luciferase cDNA under the control of *SERPINE1* (encoding PAI-1) core promoter region (pGL3-CAGA[9]-luc) (28) was transfected in HLFs. Cells were treated with TGF-β1, AITC, the TRPA1 inhibitor A-967079, or a combination of all three compounds (Figure 5A), and luciferase activity was quantified. As expected, application of TGF-β1 resulted in increased PAI-1 promoter–induced luciferase activity compared with treatment with solvent only. Incubation of cells with AITC for 2 hours, however, reduced TGF-β1–induced luciferase activity, which returned to initial degrees if A-967079 was applied (Figure 5B). This inhibition of gene transcription was not due to cell apoptosis or reduced cell viability, as caspase and water-soluble tetrazolium salt assays showed no increased apoptosis or reduced cell viability by AITC treatment, respectively (*see* Figure E8). TGF-β1 signaling via SMAD isoforms and inhibition of SMAD-dependent transcription by the MAPK signaling pathway have been reported in a fetal lung epithelial cell line (31, 32). Moreover, increased expression of profibrotic markers by ERK inhibition was recently shown in dermal fibroblasts (33). Therefore, we quantified ERK1/2 and MAPK p38 phosphorylation in response to application of TGF-β1, AITC, and TRPA1 siRNA by western blot analysis using a phospho-specific ERK1/2 antibody. AITC was able to increase ERK1/2 phosphorylation, as reported before (34), as well as MAPK p38, which was reduced to basal concentrations after preincubation with TRPA1 siRNA (Figures 5C and 5D; *see* Figures E5A and E5B). Preincubation with TGF-β1 resulted in ERK1/2 and MAPK p38 phosphorylation after application of TRPA1 siRNA or AITC, which, however, were not significantly different (*see* Figures E5C–E5F). Removal of extracellular Ca^{2+} reduced AITC-induced ERK1/2 and MAPK p38 phosphorylation to basal degrees (*see* Figure E6A–E6D). TGF-β1–regulated transcription is mediated by carboxyterminal phosphorylation of SMAD2/3 proteins, which are subsequently translocated to the nucleus. Additional phosphorylation of serine residues (245, 250, and 255) in the linker region of SMAD2 proteins, however, results in inhibition of nuclear translocation (31, 32; reviewed in Ref. 35). To dissect the signaling pathway mediating TRPA1-induced inhibition of TGF-β1 signaling in human fibroblasts, we analyzed linker phosphorylation of SMAD2 proteins in HLFs after stimulation by AITC by Ser245/250/255–specific phospho-SMAD2 antibodies. Most interestingly, application of AITC (3 μM) for 10 minutes resulted in an increase in SMAD2 linker phosphorylation, which was found to be reduced after a longer incubation time of 30 minutes and by simultaneous application of the TRPA1 inhibitor A967079 (Figures 5E and 5F).

Figure 2. (*Continued*). siTRPA1 or siCtrl as a control. (*C*) Quantification of mRNA concentrations of *FN1* (fibronectin) in HLFs cultured with TGF-β1 or Solv and transfected with siTRPA1 or siCtrl as a control. (*D*) Quantification of mRNA concentrations of *SERPINE1* (plasminogen activator inhibitor) in HLFs cultured with TGF-β1 or Solv and transfected with siTRPA1 or scrambled siCtrl as a control. (*E* and *F*) Quantification of α-SMA protein concentrations in HLFs transfected with siTRPA1 (siRNA TRPA1) or siCtrl (siRNA Ctrl) as control by quantitative western blotting. (*G* and *H*) Quantification of COL1A1 protein concentrations in HLFs transfected with siRNA TRPA1 or scrambled siRNA Ctrl. as a control by quantitative western blotting. Data were analyzed using a Kruskal-Wallis test (*A–D*) or a Mann-Whitney test (*F* and *H*) and are presented as mean ± SEM. Cells are from at least three independent donors ($n \geq 4$). For all graphs, $^{*}P < 0.05$, $^{**}P < 0.01$, $^{***}P < 0.001$, and $^{****}P < 0.0001$ versus the value in cells treated with Solv or siCtrl alone.

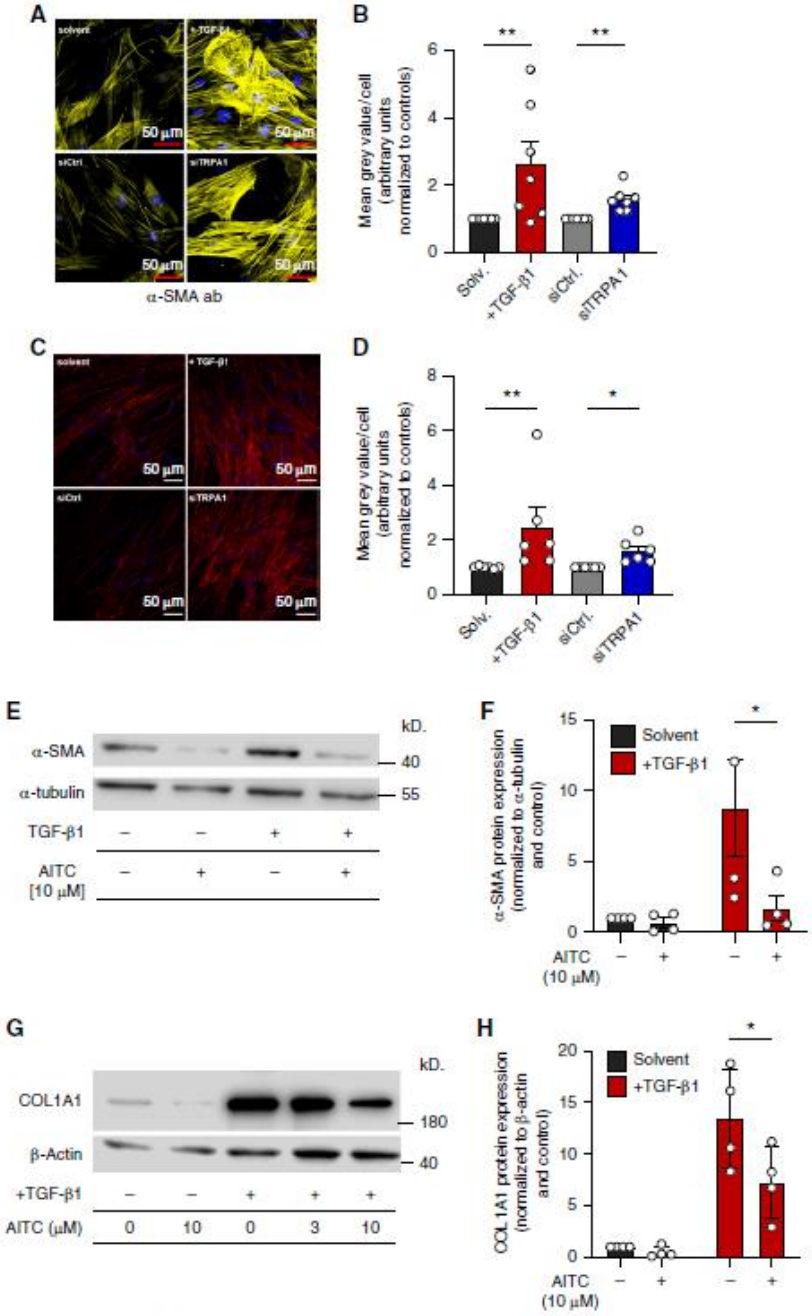

Figure 3. Quantification of expression of fibrotic marker proteins in HLFs cultured with or without TGF-β1 and transfected with siTRPA1 or stimulated with the TRPA1 activator AITC. (*A*) Representative confocal laser microscopy images of HLF cultured with Solv, TGF-β1, siCtrl, or siTRPA1 and stained with fluorophore-tagged anti α-SMA antibodies (α-SMA ab). Scale bars, 50 μm. (*B*) Summary of mean gray values obtained from images shown in *A*. (*C*) Representative confocal laser microscopy images of HLFs cultured with Solv, TGF-β1, siCtrl, or siTRPA1 and stained with fluorophore-tagged phalloidin for detection of F-actin. Scale bars, 50 μm. (*D*) Summary of mean gray values obtained from images shown in *C*. (*E*) α-SMA protein expression was quantified by western blotting using a specific antiserum in HLFs cultured with or without TGF-β1 and/or treated with the TRPA1 activator AITC. α-Tubulin served as a loading control. (*F*) Summary of α-SMA protein expression normalized to β-actin in HLFs cultured with or without TGF-β1 and/or treated with the TRPA1 activator AITC in the indicated concentrations.

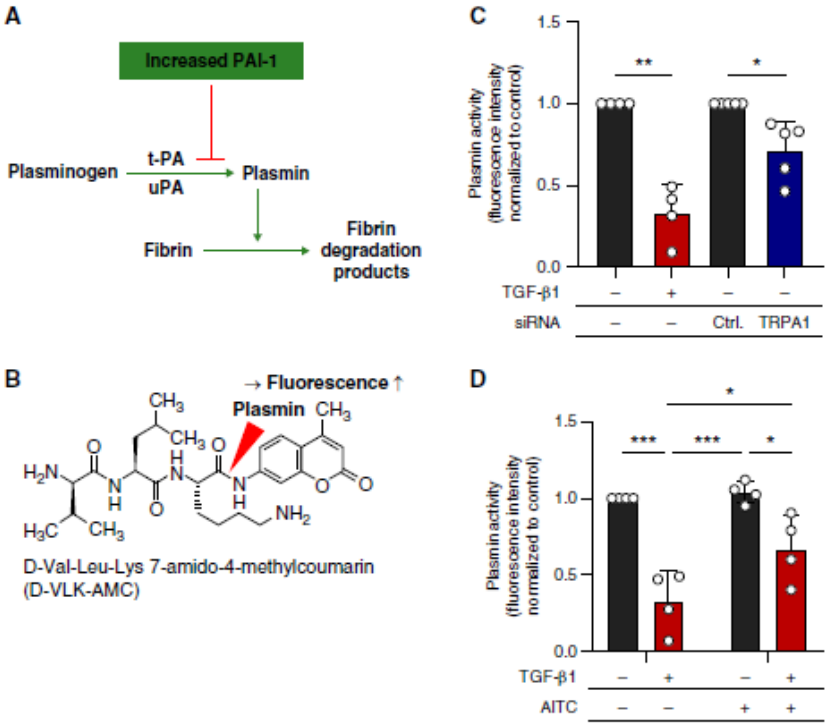

Figure 4. Indirect quantification of expression of PAI-1 activity in HLFs cultured with TGF-β1 or transfected with siTRPA1. (*A*) Schematic picture of PAI-1 inhibits cleavage of plasminogen in plasmin by tissue plasminogen activator (t-PA). Plasmin is able to degrade fibrin clots during fibrinolysis. (*B*) Hydrolysis of D-VLK-AMC by plasmin results in free 7-amido-4-methylcoumarin (AMC), which is quantified by fluorometric detection (excitation wavelength 380 nm, emission wavelength 460 nm). (*C*) Plasmin activity quantified by AMC fluorescence in the medium of HLFs cultured with Solv or TGF-β1 and transfected with siCtrl or siTRPA1. (*D*) Plasmin activity quantified by AMC fluorescence in the medium of HLFs cultured with (+) or without (−) TGF-β1 and with (+) or without (−) application of the TRPA1 activator AITC. Data were analyzed using a Kruskal-Wallis test (*C*) or two-way ANOVA (*D*) and are presented as mean ± SEM. Cells are from at least three independent donors, and the number of experiments is ≥4. For all graphs, $^{*}P < 0.05$, $^{**}P < 0.01$, and $^{***}P < 0.001$; in *C*, for the value of cells treated with control versus cells treated with TGF-β1 or siCtrl alone, and in *D*, control versus AITC-treated cells. D-VLK-AMC = D-Val-Leu-Lys 7-amido-4-methylcoumarin; uPA = urokinase.

Preincubation with TGF-β1 also resulted in changes in SMAD2 linker phosphorylation after application of AITC, which, however, were not significantly different (*see* Figure E7A). Removal of extracellular Ca^{2+} reduced AITC-induced SMAD2 linker phosphorylation to basal degrees (*see* Figures E7B and E7C). Previous studies revealed that sustained stimulation of MRC-5 cells or HLFs with TGF-β1 reduced total protein concentrations of SMAD3 (36, 37). We also observed a profound reduction of cytosolic SMAD3 concentrations after TGF-β1 stimulation of HLFs (*see* Figures E7D and E7E). Interestingly, application of AITC significantly increased basal SMAD3 concentrations (*see* Figures E7D and E7E), confirming an important function of TRPA1 activation also on SMAD3.

In conclusion, our data favor a mechanistic model in which TRPA1-mediated ERK phosphorylation inhibits TGF-β1–induced transcription and fibroblast-to-myofibroblast differentiation by linker phosphorylation of SMAD2 proteins (Figure 6).

Discussion

Pulmonary fibrosis is a devastating disease with only a few treatment options. Although detailed molecular aspects of the development of lung fibrosis are still elusive, it is commonly believed that fibroblast-to-myofibroblast differentiation is a decisive step. The identification of new target proteins mediating this process is therefore an important step toward establishing new biomarkers and future therapeutic options. TRP channels are expressed and essential for

Figure 3. (*Continued*). (*G*) COL1A1 protein expression was quantified by western blotting using a specific antiserum in HLFs cultured with or without TGF-β1 and/or treated with the TRPA1 activator AITC in the indicated concentrations. β-actin served as a loading control. (*H*) Summary of COL1A1 protein expression normalized to β-actin in HLFs cultured with or without TGF-β1 and/or treated with the TRPA1 activator AITC in the indicated concentrations. Data were analyzed using a Kruskal-Wallis test (*B* and *D*) or two-way ANOVA (*F* and *H*) and are presented as mean ± SEM. Cells in *A*–*F* are from at least three independent donors, and the number of experiments is ≥4. For all graphs, $^{*}P < 0.05$ and $^{**}P < 0.01$ versus the value in cells treated with Solv or siCtrl alone.

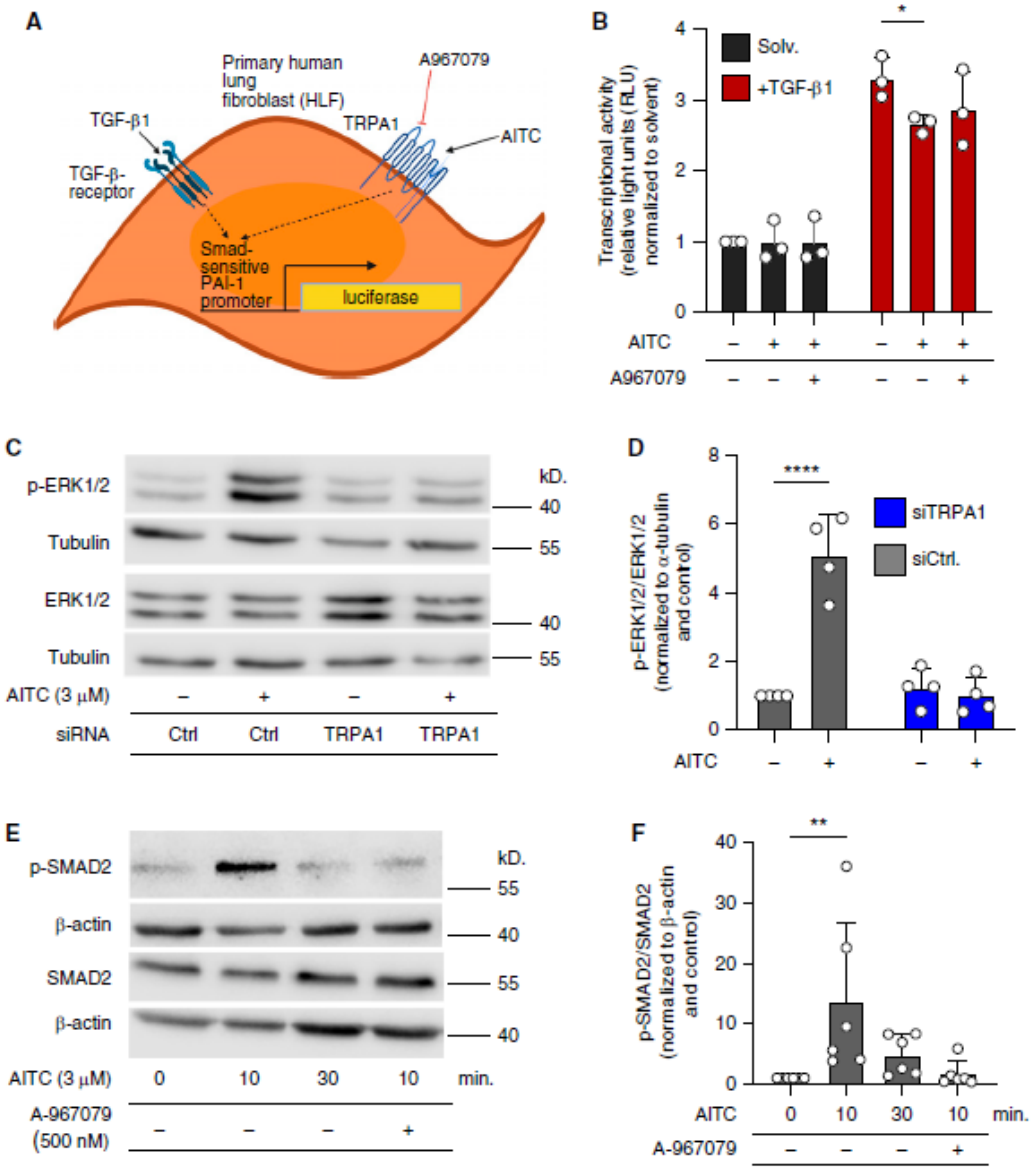

Figure 5. Identification of proteins involved in TRPA1-mediated inhibition of TGF-β1–induced transcription. (*A*) Schematic presentation of luciferase reporter assay. HLFs were transfected with a plasmid containing the luciferase gene under the control of the SMAD-sensitive part of the human PAI-1 promoter. TGF-β1 agonist for activation of SMAD transcription and AITC as a TRPA1 activator or A-967079 as a channel inhibitor were added, and luciferase activity was quantified. (*B*) SMAD transcriptional activity in HLFs quantified after culturing in Solv (black bars) or TGF-β1 (red bars) as well as treatment with AITC or A-967079. (*C*) Lysates from fibroblasts transfected with siRNA TRPA1 or siRNA Ctrl and treated with (+) or without (−) AITC were incubated in a western blot with specific antibodies directed against ERK1/2 (extracellular signal–regulated kinase 1/2) and phosphorylated ERK1/2 (pERK1/2). α-Tubulin served as a loading control. (*D*) Summary of the pERK1/2/ERK1/2 quantification normalized to α-tubulin by western blotting in HLFs transfected with siTRPA1 (blue bars) or siCtrl (gray bars) incubated with (+) or without (−) AITC. (*E*) Lysates from fibroblasts pretreated with (+) or without (−) A-967079 and stimulated with (+) or without (−) AITC for the indicted times(minutes) were incubated in a western blot with specific antibodies directed against SMAD2 (SMAD family member 2) and linker phosphorylated SMAD2 (pSMAD2). β-Actin served as a loading control. (*F*) Summary of the pSMAD2/SMAD2 quantification normalized to β-actin by western blotting in HLFs pretreated with (+) or without (−) A-967079 and incubated with (+) or without (−) AITC. Data were analyzed using two-way ANOVA (*B* and *D*) or a Kruskal-Wallis test (*F*) and are presented as mean ± SEM. Cells in *A–F* are from at least three independent donors ($n \geq 3$). For all graphs, $^{*}P < 0.05$, $^{**}P < 0.01$, and $^{****}P < 0.0001$ versus the value in cells treated with Solv alone.

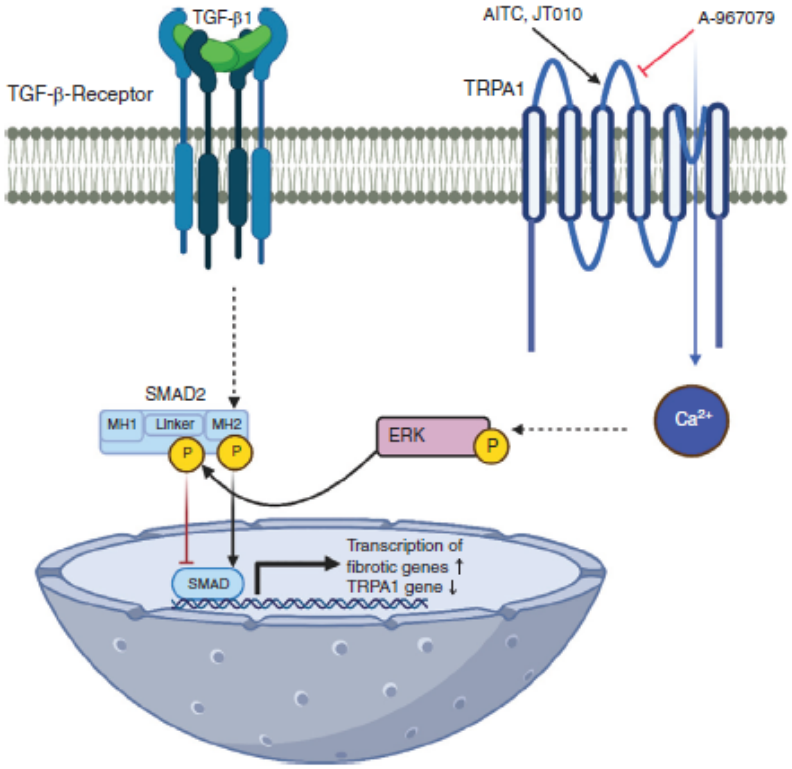

Figure 6. Proposed signaling pathway for TRPA1-mediated inhibition of TGF-β1–induced SMAD-mediated transcription. Ca^{2+} influx through AITC- or JT010-activated TRPA1 channels increases ERK1/2 phosphorylation, which induces linker phosphorylation of SMAD2. In contrast to the carboxyterminal phosphorylation of SMAD2, which enhances nuclear SMAD-induced transcription by activated TGF-β receptors, linker phosphorylation of SMAD2 reduces TGF-β1–induced transcription of profibrotic genes. A TRPA1 inhibitor (A-967079) is able to reverse the inhibitory effect of TRPA1-induced Ca^{2+} influx. Moreover, TRPA1 gene expression is inhibited by TGF-β1 activation of HLFs by a still unknown mechanism.

Ca^{2+} homeostasis in many cells, including fibroblasts (17, 38). We were able to demonstrate an essential role of TRPC6 in murine fibroblast-to-myofibroblast differentiation (17). On a molecular level, TRPC6 mRNA and protein concentrations were upregulated in myofibroblasts compared with fibroblasts, and TRPC6-deficient mice were partially protected from bleomycin-induced pulmonary fibrosis (17). Moreover, expression of TRPV4, a member of the vanilloid family of TRP channels, was upregulated in lung fibroblasts derived from patients with IPF (18). However, after a thorough transcriptomic comparison of primary human fibroblasts with TGF-β1–differentiated myofibroblasts, we were not able to identify significantly different degrees of TRPC6 or TRPV4 mRNA expression. Most interestingly and unlike mRNAs of all other TRP proteins, TRPA1 mRNA was found to be significantly downregulated (Table 1). TRPA1 channels were originally identified in human fibroblasts (19). In addition, they are important sensor molecules for toxicants (39, 40). Although the exact triggers for the development of lung fibrosis are still not known, it is believed that microinjuries of epithelial cells by chronic exposure to lung toxicants are an important predisposition for the disease (1, 7).

For the first time, we present evidence for an inhibitory role of TRPA1 channels in primary HLF to myofibroblast differentiation by TGF-β1. Preincubation of cells with TGF-β1 decreased AITC-induced increases in $[Ca^{2+}]_i$ (Figures 1D and 1E). A specific knockdown of TRPA1 expression increased mRNA (Figures 2A–2D) and protein expression (Figures 2E–2H) of important profibrotic marker proteins, reduced AITC-induced increases in $[Ca^{2+}]_i$ (Figures 1B and 1C). Most interestingly, we were able to monitor basal TRPA1 activity in HLFs, probably protecting these cells from myofibroblast differentiation. Of note, preapplication of TGF-β1 and TRPA1 siRNA had no additive effect on the expression of fibrotic genes (e.g., α-SMA, COL1A1) (*see* Figures E4A and E4B), as TRPA1 mRNA might be already downregulated in cells treated with TGF-β1. However, coapplication of TGF-β1 and AITC or JT010 activated TRPA1 channels in the cell membrane with high efficacy and reduced TGF-β1–mediated gene transcription and PAI-1 activity (Figures 4D, 5B, and E4G), as well as expression of fibrotic proteins (e.g., COL1A1 and α-SMA in Figures 3E–3H and E4C–E4F). On a molecular level, TRPA1 channel activation by AITC induced ERK1/2 phosphorylation (Figures 5C and 5D) and SMAD2 linker phosphorylation (Figures 5E and 5F), which reduces nuclear translocation and activation

of transcription (32; reviewed in Ref. 35). Downregulation by specific TRPA1 siRNAs or a TRPA1 inhibitor reversed these effects (Figures 5C–5F). Moreover, depletion of extracellular Ca^{2+} reduced AITC-induced phosphorylation of ERK1/2, MAPK p38, and the SMAD2 linker region, supporting the notion that phosphorylation of these proteins depends on AITC-mediated increase in $[Ca^{2+}]_i$. These findings highlight an inhibitory role of TRPA1 in the development of human myofibroblasts triggered by TGF-β1. In a recent study, a similar effect was shown in MRC-5 and HF19 cell lines, which are both isolated from lungs of human fetuses and resemble some of the characteristics of human fibroblasts (41). TGF-β1 significantly downregulated TRPA1 expression and AITC enhanced α-SMA gene and protein expression in these cell lines (41). HC-030031 as a TRPA1 antagonist, however, failed to suppress the AITC-induced downregulation of α-SMA and seemed to work synergistically with AITC (41). Only combined inhibition of ERK1/2 MAPK and NERF (nuclear factor of erythroid 2–related factor) reversed the AITC-induced α-SMA suppression (41).

While this work was in progress, another research group investigated TRPA1 channels in human lung myofibroblasts (HLMFs) and TGF-β1–mediated profibrotic responses (42). The researchers reported that the expression and function of TRPA1 channels in both healthy subjects and patients with IPF were reduced by application of TGF-β1 (42). TRPA1 overexpression or activation induced HLMF apoptosis, and TRPA1 activation by H_2O_2 induced necrosis. TRPA1 inhibition resulting from TGF-β1 downregulation or pharmacological inhibition protected HLMFs from both apoptosis and necrosis (42). They concluded that TGF-β1 induces resistance of HLMFs to TRPA1 agonist–mediated and H_2O_2-mediated cell death via downregulation of TRPA1 (42). These data in human myofibroblasts confirm our results, underscoring an inhibitory role of TRPA1 in profibrotic events governing fibroblast-to-myofibroblast differentiation at an early stage of lung fibrosis. However, there are also clear differences in the role of TRPA1 channels in HLFs versus HMLFs. We did not observe any reduction in cell viability or increases in apoptosis in HLFs after activation of TRPA1 by the specific activator AITC (*see* Figure E8), while overexpression of TRPA1 in HLMFs increased apoptosis (42). However, we did not use H_2O_2, as this compound also activates TRPM2 channels and can induce cell death per se (43).

There is also evidence that TRP channels cluster with other signaling molecules in compartments formed by proteins such as caveolins (44). In these caveolae as microdomains of calcium signaling (45), Ca^{2+} influx through TRPA1 channels might indeed inhibit fibroblast-to-myofibroblast differentiation, whereas in others Ca^{2+} influx through TRPV4 channels might promote lung fibrosis (18).

Conclusions

As it is generally accepted that fibroblasts contribute mainly to the progression of pulmonary fibrosis by differentiating to myofibroblasts and secreting excessive amounts of ECM (46), our data in HLFs and the results of others in HLMFs point to an important inhibitory function of TRPA1 channels in fibroblast-to-myofibroblast differentiation and HLMF survival. Therefore, activation of TRPA1 channels may blaze the trail for new therapeutic options in lung fibrosis. Future studies will show if TRPA1 activators are successful in fibrosis models, despite their effects on other cells (e.g., neurons) in which TRPA1 channels are also expressed. ■

Author disclosures are available with the text of this article at www.atsjournals.org.

Acknowledgment: The authors thank Bettina Braun and Astrid Bauer for excellent technical assistance and Anna Litovskikh for her great help in the analysis of transcriptomic data using R. The authors acknowledge the provision of human primary fibroblasts from the CPC-M BioArchive and its partners at the Asklepios Biobank Gauting, Klinikum der Universität München, and Ludwig-Maximilians-Universität München. Figures 5A and 6 were created using BioRender.com.

References

1. King TE Jr, Pardo A, Selman M. Idiopathic pulmonary fibrosis. *Lancet* 2011;378:1949–1961.
2. Lederer DJ, Martinez FJ. Idiopathic pulmonary fibrosis. *N Engl J Med* 2018;378:1811–1823.
3. Raghu G, Collard HR, Egan JJ, Martinez FJ, Behr J, Brown KK, *et al.*; ATS/ERS/JRS/ALAT Committee on Idiopathic Pulmonary Fibrosis. An official ATS/ERS/JRS/ALAT statement: idiopathic pulmonary fibrosis. Evidence-based guidelines for diagnosis and management. *Am J Respir Crit Care Med* 2011;183:788–824.
4. Hutchinson J, Fogarty A, Hubbard R, McKeever T. Global incidence and mortality of idiopathic pulmonary fibrosis: a systematic review. *Eur Respir J* 2015;46:795–806.
5. Selman M, King TE, Pardo A; American Thoracic Society; European Respiratory Society; American College of Chest Physicians. Idiopathic pulmonary fibrosis: prevailing and evolving hypotheses about its pathogenesis and implications for therapy. *Ann Intern Med* 2001;134:136–151.
6. Selvaggio AS, Noble PW. Pirfenidone initiates a new era in the treatment of idiopathic pulmonary fibrosis. *Annu Rev Med* 2016;67:487–495.
7. Martinez FJ, Collard HR, Pardo A, Raghu G, Richeldi L, Selman M, *et al.* Idiopathic pulmonary fibrosis. *Nat Rev Dis Primers* 2017;3:17074.
8. Tanjore H, Cheng DS, Degryse AL, Zoz DF, Abdolrasulnia R, Lawson WE, *et al.* Alveolar epithelial cells undergo epithelial-to-mesenchymal transition in response to endoplasmic reticulum stress. *J Biol Chem* 2011;286:30972–30980.
9. Bartis D, Mise N, Mahida RY, Eickelberg O, Thickett DR. Epithelial-mesenchymal transition in lung development and disease: does it exist and is it important? *Thorax* 2014;69:760–765.
10. Hashimoto N, Jin H, Liu T, Chensue SW, Phan SH. Bone marrow-derived progenitor cells in pulmonary fibrosis. *J Clin Invest* 2004;113:243–252.
11. Hung C, Linn G, Chow YH, Kobayashi A, Mittelsteadt K, Altemeier WA, *et al.* Role of lung pericytes and resident fibroblasts in the pathogenesis of pulmonary fibrosis. *Am J Respir Crit Care Med* 2013;188:820–830.
12. Mubarak KK, Montes-Worboys A, Regev D, Nasreen N, Mohammed KA, Faruqi I, *et al.* Parenchymal trafficking of pleural mesothelial cells in idiopathic pulmonary fibrosis. *Eur Respir J* 2012;39:133–140.
13. Nilius B, Szallasi A. Transient receptor potential channels as drug targets: from the science of basic research to the art of medicine. *Pharmacol Rev* 2014;66:676–814.
14. Chen X, Sooch G, Demaree IS, White FA, Obukhov AG. Transient receptor potential canonical (TRPC) channels: then and now. *Cells* 2020;9:1983.
15. Goldenberg NM, Ravindran K, Kuebler WM. TRPV4: physiological role and therapeutic potential in respiratory diseases. *Naunyn Schmiedebergs Arch Pharmacol* 2015;388:421–436.

16. Davis J, Burr AR, Davis GF, Birnbaumer L, Molkentin JDA. A TRPC6-dependent pathway for myofibroblast transdifferentiation and wound healing in vivo. *Dev Cell* 2012;23:705–715.
17. Hofmann K, Fiedler S, Vierkotten S, Weber J, Klee S, Jia J, *et al.* Classical transient receptor potential 6 (TRPC6) channels support myofibroblast differentiation and development of experimental pulmonary fibrosis. *Biochim Biophys Acta Mol Basis Dis* 2017;1863:560–568.
18. Rahaman SO, Grove LM, Paruchuri S, Southern BD, Abraham S, Niese KA, *et al.* TRPV4 mediates myofibroblast differentiation and pulmonary fibrosis in mice. *J Clin Invest* 2014;124:5225–5238.
19. Hu F, Song X, Long D. Transient receptor potential ankyrin 1 and calcium: interactions and association with disease (review). *Exp Ther Med* 2021;22:1462.
20. Kurahara LH, Hiraishi K, Hu Y, Koga K, Onitsuka M, Doi M, *et al.* Activation of myofibroblast TRPA1 by steroids and pirfenidone ameliorates fibrosis in experimental Crohn's disease. *Cell Mol Gastroenterol Hepatol* 2017;5:299–318.
21. Li W, Zhang Z, Li X, Cai J, Li D, Du J, *et al.* CGRP derived from cardiac fibroblasts is an endogenous suppressor of cardiac fibrosis. *Cardiovasc Res* 2020;116:1335–1348.
22. Webert L, Faro D, Zeitlmayr S, Gudermann T, Breit A. Analysis of the glucose-dependent transcriptome in murine hypothalamic cells. *Cells* 2022;11:639.
23. Love MI, Huber W, Anders S. Moderated estimation of fold change and dispersion for RNA-seq data with DESeq2. *Genome Biol* 2014;15:550.
24. Yu G, Wang LG, Han Y, He QY. clusterProfiler: an R package for comparing biological themes among gene clusters. *Omics* 2012;16:284–287.
25. Wu SR, Lin CH, Shih HP, Ko CJ, Lin HY, Lan SW, *et al.* HAI-2 as a novel inhibitor of plasmin represses lung cancer cell invasion and metastasis. *Br J Cancer* 2019;120:499–511.
26. Zeitlmayr S, Zierler S, Staab-Weijnitz CA, Dietrich A, Geiger F, Horgen FD, *et al.* TRPM7 restrains plasmin activity and promotes transforming growth factor-β1 signaling in primary human lung fibroblasts. *Arch Toxicol* 2022;96:2767–2783.
27. Zhou W, Pal AS, Hsu AY, Gurol T, Zhu X, Wirbisky-Hershberger SE, *et al.* MicroRNA-223 suppresses the canonical NF-κB pathway in basal keratinocytes to dampen neutrophilic inflammation. *Cell Rep* 2018;22:1810–1823.
28. Dennler S, Itoh S, Vivien D, ten Dijke P, Huet S, Gauthier JM. Direct binding of Smad3 and Smad4 to critical TGF beta-inducible elements in the promoter of human plasminogen activator inhibitor-type 1 gene. *EMBO J* 1998;17:3091–3100.
29. Virk HS, Rekas MZ, Biddle MS, Wright AKA, Sousa J, Weston CA, *et al.* Validation of antibodies for the specific detection of human TRPA1. *Sci Rep* 2019;9:18500.
30. Takaya J, Mio K, Shiraishi T, Kurokawa T, Otsuka S, Mori Y, *et al.* A potent and site-selective agonist of TRPA1. *J Am Chem Soc* 2015;137:15859–15864.
31. Kretzschmar M, Doody J, Massagué J. Opposing BMP and EGF signalling pathways converge on the TGF-beta family mediator Smad1. *Nature* 1997;389:618–622.
32. Kretzschmar M, Doody J, Timokhina I, Massagué J. A mechanism of repression of TGFbeta/ Smad signaling by oncogenic Ras. *Genes Dev* 1999;13:804–816.
33. Dolivo DM, Larson SA, Dominko T. Crosstalk between mitogen-activated protein kinase inhibitors and transforming growth factor-β signaling results in variable activation of human dermal fibroblasts. *Int J Mol Med* 2019;43:325–335.
34. Schaefer EA, Stohr S, Meister M, Aigner A, Gudermann T, Buech TR. Stimulation of the chemosensory TRPA1 cation channel by volatile toxic substances promotes cell survival of small cell lung cancer cells. *Biochem Pharmacol* 2013;85:426–438.
35. Kamato D, Do BH, Osman N, Ross BP, Mohamed R, Xu S, *et al.* Smad linker region phosphorylation is a signalling pathway in its own right and not only a modulator of canonical TGF-β signalling. *Cell Mol Life Sci* 2020;77:243–251.
36. Breton JD, Heydet D, Starrs LM, Veldre T, Ghildyal R. Molecular changes during TGFβ-mediated lung fibroblast-myofibroblast differentiation: implication for glucocorticoid resistance. *Physiol Rep* 2018;6:e13669.
37. Staab-Weijnitz CA, Fernandez IE, Knüppel L, Maul J, Heinzelmann K, Juan-Guardela BM, *et al.* FK506-binding protein 10, a potential novel drug target for idiopathic pulmonary fibrosis. *Am J Respir Crit Care Med* 2015;192:455–467.
38. Bendiks L, Geiger F, Gudermann T, Feske S, Dietrich A. Store-operated Ca^{2+} entry in primary murine lung fibroblasts is independent of classical transient receptor potential (TRPC) channels and contributes to cell migration. *Sci Rep* 2020;10:6812.
39. Achanta S, Jordt SE. Transient receptor potential channels in pulmonary chemical injuries and as countermeasure targets. *Ann N Y Acad Sci* 2020;1480:73–103.
40. Steinritz D, Stenger B, Dietrich A, Gudermann T, Popp T. TRPs in tox: involvement of transient receptor potential-channels in chemical-induced organ toxicity—a structured review. *Cells* 2018;7:98.
41. Yap JMG, Ueda T, Kanemitsu Y, Takeda N, Fukumitsu K, Fukuda S, *et al.* AITC inhibits fibroblast-myofibroblast transition via TRPA1-independent MAPK and NRF2/HO-1 pathways and reverses corticosteroids insensitivity in human lung fibroblasts. *Respir Res* 2021;22:51.
42. Virk HS, Biddle MS, Smallwood DT, Weston CA, Castells E, Bowman VW, *et al.* TGFβ1 induces resistance of human lung myofibroblasts to cell death via down-regulation of TRPA1 channels. *Br J Pharmacol* 2021;178:2948–2962.
43. Faouzi M, Penner R. Trpm2. *Handb Exp Pharmacol* 2014;222:403–426.
44. Samapati R, Yang Y, Yin J, Stoerger C, Arenz C, Dietrich A, *et al.* Lung endothelial Ca^{2+} and permeability response to platelet-activating factor is mediated by acid sphingomyelinase and transient receptor potential classical 6. *Am J Respir Crit Care Med* 2012;185:160–170.
45. Pani B, Singh BB. Lipid rafts/caveolae as microdomains of calcium signaling. *Cell Calcium* 2009;45:625–633.
46. Henderson NC, Rieder F, Wynn TA. Fibrosis: from mechanisms to medicines. *Nature* 2020;587:555–566.

References

[1] S. Rajan, A. Shalygin, T. Gudermann, V. Chubanov, and A. Dietrich, ‘TRPM2 channels are essential for regulation of cytokine production in lung interstitial macrophages’, *J Cell Physiol*, May 2024, doi: 10.1002/jcp.31322.

[2] J. Weber *et al.*, ‘TRPV4 channels are essential for alveolar epithelial barrier function as protection from lung edema’, *JCI Insight*, vol. 5, no. 20, pp. e134464, 134464, Oct. 2020, doi: 10.1172/jci.insight.134464.

[3] F. Geiger *et al.*, ‘An Inhibitory Function of TRPA1 Channels in TGF-β1-driven Fibroblast-to-Myofibroblast Differentiation’, *Am J Respir Cell Mol Biol*, vol. 68, no. 3, pp. 314–325, Mar. 2023, doi: 10.1165/rcmb.2022-0159OC.

[4] K. Hofmann *et al.*, ‘Classical transient receptor potential 6 (TRPC6) channels support myofibroblast differentiation and development of experimental pulmonary fibrosis’, *Biochim Biophys Acta Mol Basis Dis*, vol. 1863, no. 2, pp. 560–568, Feb. 2017, doi: 10.1016/j.bbadis.2016.12.002.

[5] D. J. Cosens and A. Manning, ‘Abnormal Electroretinogram from a Drosophila Mutant’, *Nature*, vol. 224, no. 5216, pp. 285–287, Oct. 1969, doi: 10.1038/224285a0.

[6] C. Montell and G. M. Rubin, ‘Molecular characterization of the Drosophila trp locus: a putative integral membrane protein required for phototransduction’, *Neuron*, vol. 2, no. 4, pp. 1313–1323, Apr. 1989, doi: 10.1016/0896-6273(89)90069-x.

[7] F. Wong, E. L. Schaefer, B. C. Roop, J. N. LaMendola, D. Johnson-Seaton, and D. Shao, ‘Proper function of the Drosophila trp gene product during pupal development is important for normal visual transduction in the adult’, *Neuron*, vol. 3, no. 1, pp. 81–94, Jul. 1989, doi: 10.1016/0896-6273(89)90117-7.

[8] B. Nilius and A. Szallasi, ‘Transient Receptor Potential Channels as Drug Targets: From the Science of Basic Research to the Art of Medicine’, *Pharmacol Rev*, vol. 66, no. 3, pp. 676–814, Jul. 2014, doi: 10.1124/pr.113.008268.

[9] A. Samanta, T. E. T. Hughes, and V. Y. Moiseenkova-Bell, ‘Transient Receptor Potential (TRP) Channels’, *Subcell Biochem*, vol. 87, pp. 141–165, 2018, doi: 10.1007/978-981-10-7757-9_6.

[10] M. Kashio and M. Tominaga, ‘TRP channels in thermosensation’, *Current Opinion in Neurobiology*, vol. 75, p. 102591, Aug. 2022, doi: 10.1016/j.conb.2022.102591.

[11] ‘PERMEATION AND SELECTIVITY OF TRP CHANNELS | Annual Reviews’. Accessed: Mar. 19, 2024. [Online]. Available: https://www.annualreviews.org/content/journals/10.1146/annurev.physiol.68.040204.101406

[12] M. J. Berridge, M. D. Bootman, and H. L. Roderick, ‘Calcium signalling: dynamics, homeostasis and remodelling’, *Nat Rev Mol Cell Biol*, vol. 4, no. 7, pp. 517–529, Jul. 2003, doi: 10.1038/nrm1155.

[13] E. Carafoli, ‘Calcium signaling: a tale for all seasons’, *Proc Natl Acad Sci U S A*, vol. 99, no. 3, pp. 1115–1122, Feb. 2002, doi: 10.1073/pnas.032427999.

[14] M. Zhang, Y. Ma, X. Ye, N. Zhang, L. Pan, and B. Wang, ‘TRP (transient receptor potential) ion channel family: structures, biological functions and therapeutic interventions for diseases’, *Sig Transduct Target Ther*, vol. 8, no. 1, pp. 1–38, Jul. 2023, doi: 10.1038/s41392-023-01464-x.

[15] A. Dietrich, ‘Transient Receptor Potential (TRP) Channels in Health and Disease’, *Cells*, vol. 8, no. 5, p. 413, May 2019, doi: 10.3390/cells8050413.

[16] ‘Advances in TRP channel drug discovery: from target validation to clinical studies - PubMed’. Accessed: Mar. 19, 2024. [Online]. Available: https://pubmed.ncbi.nlm.nih.gov/34526696/

[17] Y. Huang, R. Fliegert, A. H. Guse, W. Lü, and J. Du, ‘A structural overview of the ion channels of the TRPM family’, *Cell Calcium*, vol. 85, p. 102111, Jan. 2020, doi: 10.1016/j.ceca.2019.102111.

[18] V. Chubanov, M. Köttgen, R. M. Touyz, and T. Gudermann, ‘TRPM channels in health and disease’, *Nat Rev Nephrol*, vol. 20, no. 3, pp. 175–187, Mar. 2024, doi: 10.1038/s41581-023-00777-y.

[19] M. Maliougina and Y. El Hiani, ‘TRPM2: bridging calcium and ROS signaling pathways-implications for human diseases’, *Front Physiol*, vol. 14, p. 1217828, 2023, doi: 10.3389/fphys.2023.1217828.

[20] P. Zong, Q. Lin, J. Feng, and L. Yue, ‘A Systemic Review of the Integral Role of TRPM2 in Ischemic Stroke: From Upstream Risk Factors to Ultimate Neuronal Death’, *Cells*, vol. 11, no. 3, p. 491, Jan. 2022, doi: 10.3390/cells11030491.

[21] A. Sumoza-Toledo and R. Penner, ‘TRPM2: a multifunctional ion channel for calcium signalling’, *J Physiol*, vol. 589, no. Pt 7, pp. 1515–1525, Apr. 2011, doi: 10.1113/jphysiol.2010.201855.

[22] B. Tóth, I. Iordanov, and L. Csanády, ‘Putative chanzyme activity of TRPM2 cation channel is unrelated to pore gating’, *Proc Natl Acad Sci U S A*, vol. 111, no. 47, pp. 16949–16954, Nov. 2014, doi: 10.1073/pnas.1412449111.

[23] I. Iordanov, C. Mihályi, B. Tóth, and L. Csanády, ‘The proposed channel-enzyme transient receptor potential melastatin 2 does not possess ADP ribose hydrolase activity’, *eLife*, vol. 5, p. e17600, doi: 10.7554/eLife.17600.

[24] K. Togashi *et al.*, ‘TRPM2 activation by cyclic ADP-ribose at body temperature is involved in insulin secretion’, *The EMBO Journal*, vol. 25, no. 9, pp. 1804–1815, May 2006, doi: 10.1038/sj.emboj.7601083.

[25] I. Lange, S. Yamamoto, S. Partida-Sanchez, Y. Mori, A. Fleig, and R. Penner, ‘TRPM2 Functions as a Lysosomal Ca2+-Release Channel in β Cells’, *Sci Signal*, vol. 2, no. 71, p. ra23, May 2009, doi: 10.1126/scisignal.2000278.

[26] E. FONFRIA, P. R. MURDOCK, F. S. CUSDIN, C. D. BENHAM, R. E. KELSELL, and S. MCNULTY, ‘Tissue Distribution Profiles of the Human TRPM Cation Channel Family’, *Journal of Receptors and Signal Transduction*, vol. 26, no. 3, pp. 159–178, Jan. 2006, doi: 10.1080/10799890600637506.

[27] C. Xu *et al.*, ‘TRPM2 variants and bipolar disorder risk: confirmation in a family-based association study’, *Bipolar Disord*, vol. 11, no. 1, pp. 1–10, Feb. 2009, doi: 10.1111/j.1399-5618.2008.00655.x.

[28] R. A. Pumroy, E. C. Fluck, T. Ahmed, and V. Y. Moiseenkova-Bell, ‘Structural insights into the gating mechanisms of TRPV Channels’, *Cell Calcium*, vol. 87, p. 102168, May 2020, doi: 10.1016/j.ceca.2020.102168.

[29] N. M. Goldenberg, K. Ravindran, and W. M. Kuebler, ‘TRPV4: physiological role and therapeutic potential in respiratory diseases’, *Naunyn-Schmiedeberg’s Arch Pharmacol*, vol. 388, no. 4, pp. 421–436, Apr. 2015, doi: 10.1007/s00210-014-1058-1.

[30] S. Negri, P. Faris, R. Berra-Romani, G. Guerra, and F. Moccia, ‘Endothelial Transient Receptor Potential Channels and Vascular Remodeling: Extracellular Ca2 + Entry for Angiogenesis, Arteriogenesis and Vasculogenesis’, *Front. Physiol.*, vol. 10, Jan. 2020, doi: 10.3389/fphys.2019.01618.

[31] D. F. Alvarez, J. A. King, D. Weber, E. Addison, W. Liedtke, and M. I. Townsley, ‘Transient Receptor Potential Vanilloid 4–Mediated Disruption of the Alveolar Septal Barrier’, *Circulation Research*, vol. 99, no. 9, pp. 988–995, Oct. 2006, doi: 10.1161/01.RES.0000247065.11756.19.

[32] D. Dryn, M. Melnyk, I. Kizub, H. Hu, A. Soloviev, and A. Zholos, ‘THE ROLE OF TRPV4 CATION CHANNELS IN THE REGULATION OF PHENYLEPHRINE-INDUCED CONTRACTION OF RAT PULMONARY ARTER’, *Fiziol Zh (1994)*, vol. 62, no. 2, pp. 79–86, 2016, doi: 10.15407/fz62.02.079.

[33] M. Kumar, Md. K. Zaman, S. Das, D. Goyary, M. P. Pathak, and P. Chattopadhyay, ‘Transient Receptor Potential Vanilloid (TRPV4) channel inhibition: A novel promising approach for the treatment of lung diseases’, *Biomedicine & Pharmacotherapy*, vol. 163, p. 114861, Jul. 2023, doi: 10.1016/j.biopha.2023.114861.

[34] W. Zhen, Z. Zhao, S. Chang, X. Chen, Y. Wan, and F. Yang, ‘Structural basis of ligand activation and inhibition in a mammalian TRPV4 ion channel’, *Cell Discov*, vol. 9, no. 1, pp. 1–4, Jul. 2023, doi: 10.1038/s41421-023-00579-3.

[35] I. Müller, P. Alt, S. Rajan, L. Schaller, F. Geiger, and A. Dietrich, ‘Transient Receptor Potential (TRP) Channels in Airway Toxicity and Disease: An Update’, *Cells*, vol. 11, no. 18, p. 2907, Sep. 2022, doi: 10.3390/cells11182907.

[36] D. Jaquemar, T. Schenker, and B. Trueb, ‘An Ankyrin-like Protein with Transmembrane Domains Is Specifically Lost after Oncogenic Transformation of Human Fibroblasts *’, *Journal of Biological Chemistry*, vol. 274, no. 11, pp. 7325–7333, Mar. 1999, doi: 10.1074/jbc.274.11.7325.

[37] L. Landini, D. Souza Monteiro de Araujo, M. Titiz, P. Geppetti, R. Nassini, and F. De Logu, ‘TRPA1 Role in Inflammatory Disorders: What Is Known So Far?’, *International Journal of Molecular Sciences*, vol. 23, no. 9, Art. no. 9, Jan. 2022, doi: 10.3390/ijms23094529.

[38] Nassenstein, ‘Expression and function of the ion channel TRPA1 in vagal afferent nerves innervating mouse lungs’, doi: 10.1113/jphysiol.2007.148379.

[39] B. J. Canning, N. Mori, and S. B. Mazzone, ‘Vagal afferent nerves regulating the cough reflex’, *Respir Physiol Neurobiol*, vol. 152, no. 3, pp. 223–242, Jul. 2006, doi: 10.1016/j.resp.2006.03.001.

[40] J. R. Rock *et al.*, ‘Basal cells as stem cells of the mouse trachea and human airway epithelium’, *Proc Natl Acad Sci U S A*, vol. 106, no. 31, pp. 12771–12775, Aug. 2009, doi: 10.1073/pnas.0906850106.

[41] T. Volckaert and S. De Langhe, ‘Lung epithelial stem cells and their niches: Fgf10 takes center stage’, *Fibrogenesis Tissue Repair*, vol. 7, p. 8, 2014, doi: 10.1186/1755-1536-7-8.

[42] D. Zheng *et al.*, ‘Differentiation of Club Cells to Alveolar Epithelial Cells In Vitro’, *Sci Rep*, vol. 7, p. 41661, Jan. 2017, doi: 10.1038/srep41661.

[43] L. Knudsen and M. Ochs, ‘The micromechanics of lung alveoli: structure and function of surfactant and tissue components’, *Histochem Cell Biol*, vol. 150, no. 6, pp. 661–676, 2018, doi: 10.1007/s00418-018-1747-9.

[44] K. C. Stone, R. R. Mercer, P. Gehr, B. Stockstill, and J. D. Crapo, ‘Allometric relationships of cell numbers and size in the mammalian lung’, *Am J Respir Cell Mol Biol*, vol. 6, no. 2, pp. 235–243, Feb. 1992, doi: 10.1165/ajrcmb/6.2.235.

[45] J. Bhattacharya and M. A. Matthay, ‘Regulation and repair of the alveolar-capillary barrier in acute lung injury’, *Annu Rev Physiol*, vol. 75, pp. 593–615, 2013, doi: 10.1146/annurev-physiol-030212-183756.

[46] E. R. Weibel, ‘On the tricks alveolar epithelial cells play to make a good lung’, *Am J Respir Crit Care Med*, vol. 191, no. 5, pp. 504–513, Mar. 2015, doi: 10.1164/rccm.201409-1663OE.

[47] L. G. Dobbs, M. D. Johnson, J. Vanderbilt, L. Allen, and R. Gonzalez, 'The great big alveolar TI cell: evolving concepts and paradigms', *Cell Physiol Biochem*, vol. 25, no. 1, pp. 55–62, 2010, doi: 10.1159/000272063.

[48] S. Wang and R. D. Hubmayr, 'Type I alveolar epithelial phenotype in primary culture', *Am J Respir Cell Mol Biol*, vol. 44, no. 5, pp. 692–699, May 2011, doi: 10.1165/rcmb.2009-0359OC.

[49] L. G. Dobbs, R. Gonzalez, M. A. Matthay, E. P. Carter, L. Allen, and A. S. Verkman, 'Highly water-permeable type I alveolar epithelial cells confer high water permeability between the airspace and vasculature in rat lung', *Proc Natl Acad Sci U S A*, vol. 95, no. 6, pp. 2991–2996, Mar. 1998, doi: 10.1073/pnas.95.6.2991.

[50] P. Confalonieri *et al.*, 'Regeneration or Repair? The Role of Alveolar Epithelial Cells in the Pathogenesis of Idiopathic Pulmonary Fibrosis (IPF)', *Cells*, vol. 11, no. 13, p. 2095, Jun. 2022, doi: 10.3390/cells11132095.

[51] S. Moimas *et al.*, 'miR-200 family members reduce senescence and restore idiopathic pulmonary fibrosis type II alveolar epithelial cell transdifferentiation', *ERJ Open Res*, vol. 5, no. 4, pp. 00138–02019, Dec. 2019, doi: 10.1183/23120541.00138-2019.

[52] M. Kannler, R. Lüling, A. Ö. Yildirim, T. Gudermann, D. Steinritz, and A. Dietrich, 'TRPA1 channels: expression in non-neuronal murine lung tissues and dispensability for hyperoxia-induced alveolar epithelial hyperplasia', *Pflugers Arch*, vol. 470, no. 8, pp. 1231–1241, Aug. 2018, doi: 10.1007/s00424-018-2148-6.

[53] M. Wang *et al.*, 'Roles of TRPA1 and TRPV1 in cigarette smoke -induced airway epithelial cell injury model', *Free Radic Biol Med*, vol. 134, pp. 229–238, Apr. 2019, doi: 10.1016/j.freeradbiomed.2019.01.004.

[54] M. V. Plikus *et al.*, 'Fibroblasts: origins, definitions, and functions in health and disease', *Cell*, vol. 184, no. 15, pp. 3852–3872, Jul. 2021, doi: 10.1016/j.cell.2021.06.024.

[55] E. S. White, 'Lung Extracellular Matrix and Fibroblast Function', *Ann Am Thorac Soc*, vol. 12, no. Suppl 1, pp. S30–S33, Mar. 2015, doi: 10.1513/AnnalsATS.201406-240MG.

[56] V. J. Thannickal *et al.*, 'Myofibroblast Differentiation by Transforming Growth Factor-β1 Is Dependent on Cell Adhesion and Integrin Signaling via Focal Adhesion Kinase *', *Journal of Biological Chemistry*, vol. 278, no. 14, pp. 12384–12389, Apr. 2003, doi: 10.1074/jbc.M208544200.

[57] M. S. Wilson and T. A. Wynn, 'Pulmonary fibrosis: pathogenesis, etiology and regulation', *Mucosal Immunol*, vol. 2, no. 2, pp. 103–121, Mar. 2009, doi: 10.1038/mi.2008.85.

[58] C. C. Moor *et al.*, 'Patient expectations, experiences and satisfaction with nintedanib and pirfenidone in idiopathic pulmonary fibrosis: a quantitative study', *Respir Res*, vol. 21, p. 196, 2020, doi: 10.1186/s12931-020-01458-1.

[59] I. Gopallawa, R. Dehinwal, V. Bhatia, V. Gujar, and N. Chirmule, 'A four-part guide to lung immunology: Invasion, inflammation, immunity, and intervention', *Front Immunol*, vol. 14, p. 1119564, Mar. 2023, doi: 10.3389/fimmu.2023.1119564.

[60] R. van Furth and Z. A. Cohn, 'The origin and kinetics of mononuclear phagocytes', *J Exp Med*, vol. 128, no. 3, pp. 415–435, Sep. 1968, doi: 10.1084/jem.128.3.415.

[61] F. Baharom, G. Rankin, A. Blomberg, and A. Smed-Sörensen, 'Human Lung Mononuclear Phagocytes in Health and Disease', *Front Immunol*, vol. 8, p. 499, 2017, doi: 10.3389/fimmu.2017.00499.

[62] M. P. Rodero *et al.*, 'Immune surveillance of the lung by migrating tissue monocytes', *eLife*, vol. 4, p. e07847, Jul. 2015, doi: 10.7554/eLife.07847.

[63] P. C. Cook and A. S. MacDonald, 'Dendritic cells in lung immunopathology', *Semin Immunopathol*, vol. 38, no. 4, pp. 449–460, 2016, doi: 10.1007/s00281-016-0571-3.

[64] C. S. Zent and M. R. Elliott, ‘Maxed out macs: physiologic cell clearance as a function of macrophage phagocytic capacity’, *FEBS J*, vol. 284, no. 7, pp. 1021–1039, Apr. 2017, doi: 10.1111/febs.13961.

[65] X. Zhang and D. Mosser, ‘Macrophage activation by endogenous danger signals’, *J Pathol*, vol. 214, no. 2, pp. 161–178, Jan. 2008, doi: 10.1002/path.2284.

[66] C. Atri, F. Z. Guerfali, and D. Laouini, ‘Role of Human Macrophage Polarization in Inflammation during Infectious Diseases’, *Int J Mol Sci*, vol. 19, no. 6, p. 1801, Jun. 2018, doi: 10.3390/ijms19061801.

[67] W. Xu, X. Zhao, M. R. Daha, and C. van Kooten, ‘Reversible differentiation of pro- and anti-inflammatory macrophages’, *Mol Immunol*, vol. 53, no. 3, pp. 179–186, Mar. 2013, doi: 10.1016/j.molimm.2012.07.005.

[68] J.-M. Zhang and J. An, ‘Cytokines, Inflammation and Pain’, *Int Anesthesiol Clin*, vol. 45, no. 2, pp. 27–37, 2007, doi: 10.1097/AIA.0b013e318034194e.

[69] G. Arango Duque and A. Descoteaux, ‘Macrophage Cytokines: Involvement in Immunity and Infectious Diseases’, *Front Immunol*, vol. 5, p. 491, Oct. 2014, doi: 10.3389/fimmu.2014.00491.

[70] C. C. Bain and A. S. MacDonald, ‘The impact of the lung environment on macrophage development, activation and function: diversity in the face of adversity’, *Mucosal Immunol*, vol. 15, no. 2, pp. 223–234, Feb. 2022, doi: 10.1038/s41385-021-00480-w.

[71] E. Evren, E. Ringqvist, and T. Willinger, ‘Origin and ontogeny of lung macrophages: from mice to humans’, *Immunology*, vol. 160, no. 2, pp. 126–138, Jun. 2020, doi: 10.1111/imm.13154.

[72] G. Hoeffel *et al.*, ‘C-Myb(+) erythro-myeloid progenitor-derived fetal monocytes give rise to adult tissue-resident macrophages’, *Immunity*, vol. 42, no. 4, pp. 665–678, Apr. 2015, doi: 10.1016/j.immuni.2015.03.011.

[73] S. Chakarov *et al.*, ‘Two distinct interstitial macrophage populations coexist across tissues in specific subtissular niches’, *Science*, vol. 363, no. 6432, p. eaau0964, Mar. 2019, doi: 10.1126/science.aau0964.

[74] M. F. Gutknecht and A. H. Bouton, ‘Functional significance of mononuclear phagocyte populations generated through adult hematopoiesis’, *J Leukoc Biol*, vol. 96, no. 6, pp. 969–980, Dec. 2014, doi: 10.1189/jlb.1RI0414-195R.

[75] A. Ortega-Gómez, M. Perretti, and O. Soehnlein, ‘Resolution of inflammation: an integrated view’, *EMBO Mol Med*, vol. 5, no. 5, pp. 661–674, May 2013, doi: 10.1002/emmm.201202382.

[76] M. M. Coleman, D. Ruane, B. Moran, P. J. Dunne, J. Keane, and K. H. G. Mills, ‘Alveolar macrophages contribute to respiratory tolerance by inducing FoxP3 expression in naive T cells’, *Am J Respir Cell Mol Biol*, vol. 48, no. 6, pp. 773–780, Jun. 2013, doi: 10.1165/rcmb.2012-0263OC.

[77] C.-F. Tsai, J.-H. Chen, and W.-L. Yeh, ‘Pulmonary fibroblasts-secreted CXCL10 polarizes alveolar macrophages under pro-inflammatory stimuli’, *Toxicol Appl Pharmacol*, vol. 380, p. 114698, Oct. 2019, doi: 10.1016/j.taap.2019.114698.

[78] S. Soni *et al.*, ‘Alveolar macrophage-derived microvesicles mediate acute lung injury’, *Thorax*, vol. 71, no. 11, pp. 1020–1029, Nov. 2016, doi: 10.1136/thoraxjnl-2015-208032.

[79] A. V. Misharin, L. Morales-Nebreda, G. M. Mutlu, G. R. S. Budinger, and H. Perlman, ‘Flow Cytometric Analysis of Macrophages and Dendritic Cell Subsets in the Mouse Lung’, *Am J Respir Cell Mol Biol*, vol. 49, no. 4, pp. 503–510, Oct. 2013, doi: 10.1165/rcmb.2013-0086MA.

[80] C. Draijer, L. R. K. Penke, and M. Peters-Golden, ‘Distinctive Effects of GM-CSF and M-CSF on Proliferation and Polarization of Two Major Pulmonary Macrophage Populations’, *J Immunol*, vol. 202, no. 9, pp. 2700–2709, May 2019, doi: 10.4049/jimmunol.1801387.

[81] J. A. Huffman Reed, W. R. Rice, Z. K. Zsengellér, S. E. Wert, G. Dranoff, and J. A. Whitsett, ‘GM-CSF enhances lung growth and causes alveolar type II epithelial cell hyperplasia in transgenic mice’, *Am J Physiol*, vol. 273, no. 4, pp. L715-725, Oct. 1997, doi: 10.1152/ajplung.1997.273.4.L715.

[82] Y. D. Woo, D. Jeong, and D. H. Chung, ‘Development and Functions of Alveolar Macrophages’, *Mol Cells*, vol. 44, no. 5, pp. 292–330, May 2021, doi: 10.14348/molcells.2021.0058.

[83] T. K. Finney-Hayward *et al.*, ‘Expression of Transient Receptor Potential C6 Channels in Human Lung Macrophages’, *Am J Respir Cell Mol Biol*, vol. 43, no. 3, pp. 296–304, Sep. 2010, doi: 10.1165/rcmb.2008-0373OC.

[84] V. Riazanski *et al.*, ‘TRPC6 channel translocation into phagosomal membrane augments phagosomal function’, *Proceedings of the National Academy of Sciences*, vol. 112, no. 47, pp. E6486–E6495, Nov. 2015, doi: 10.1073/pnas.1518966112.

[85] M. Lévêque *et al.*, ‘Phagocytosis depends on TRPV2-mediated calcium influx and requires TRPV2 in lipids rafts: alteration in macrophages from patients with cystic fibrosis’, *Sci Rep*, vol. 8, no. 1, p. 4310, Mar. 2018, doi: 10.1038/s41598-018-22558-5.

[86] R. G. Scheraga *et al.*, ‘TRPV4 Protects the Lung from Bacterial Pneumonia via MAPK Molecular Pathway Switching’, *J Immunol*, vol. 204, no. 5, pp. 1310–1321, Mar. 2020, doi: 10.4049/jimmunol.1901033.

[87] E. M. Melo, V. L. S. Oliveira, D. Boff, and I. Galvão, ‘Pulmonary macrophages and their different roles in health and disease’, *The International Journal of Biochemistry & Cell Biology*, vol. 141, p. 106095, Dec. 2021, doi: 10.1016/j.biocel.2021.106095.

[88] J. Schyns, F. Bureau, and T. Marichal, ‘Lung Interstitial Macrophages: Past, Present, and Future’, *J Immunol Res*, vol. 2018, p. 5160794, 2018, doi: 10.1155/2018/5160794.

[89] N. A-Gonzalez *et al.*, ‘Phagocytosis imprints heterogeneity in tissue-resident macrophages’, *J Exp Med*, vol. 214, no. 5, pp. 1281–1296, May 2017, doi: 10.1084/jem.20161375.

[90] S. L. Gibbings *et al.*, ‘Three Unique Interstitial Macrophages in the Murine Lung at Steady State’, *Am J Respir Cell Mol Biol*, vol. 57, no. 1, pp. 66–76, Jul. 2017, doi: 10.1165/rcmb.2016-0361OC.

[91] J. Hoppstädter *et al.*, ‘Differential cell reaction upon Toll-like receptor 4 and 9 activation in human alveolar and lung interstitial macrophages’, *Respir Res*, vol. 11, no. 1, p. 124, Sep. 2010, doi: 10.1186/1465-9921-11-124.

[92] D. Bedoret *et al.*, ‘Lung interstitial macrophages alter dendritic cell functions to prevent airway allergy in mice’, *J Clin Invest*, vol. 119, no. 12, pp. 3723–3738, Dec. 2009, doi: 10.1172/JCI39717.

[93] C. Sabatel *et al.*, ‘Exposure to Bacterial CpG DNA Protects from Airway Allergic Inflammation by Expanding Regulatory Lung Interstitial Macrophages’, *Immunity*, vol. 46, no. 3, pp. 457–473, Mar. 2017, doi: 10.1016/j.immuni.2017.02.016.

[94] P. K. Moore *et al.*, ‘Single-cell RNA sequencing reveals unique monocyte-derived interstitial macrophage subsets during lipopolysaccharide-induced acute lung inflammation’, *Am J Physiol Lung Cell Mol Physiol*, vol. 324, no. 4, pp. L536–L549, Apr. 2023, doi: 10.1152/ajplung.00223.2022.

[95] K. Ogawa, M. Tsurutani, A. Hashimoto, and M. Soeda, ‘Simple propagation method for resident macrophages by co-culture and subculture, and their isolation from various organs’, *BMC Immunol*, vol. 20, p. 34, Sep. 2019, doi: 10.1186/s12865-019-0314-z.

[96] M. Tsurutani, H. Horie, and K. Ogawa, ‘Cell Properties of Lung Tissue-Resident Macrophages Propagated by Co-Culture with Lung Fibroblastic Cells from C57BL/6 and BALB/c Mice’, *Biomedicines*, vol. 9, no. 9, p. 1241, Sep. 2021, doi: 10.3390/biomedicines9091241.

Acknowledgements

I am deeply grateful to Alexander for his unwavering support and mentorship throughout my academic journey. His guidance has been indispensable in shaping me into an independent researcher. I am also thankful to Prof. Gudermann for the opportunity at the Walter-Straub Institute and to my TAC members, Prof. Nicke and Dr. Staab-Weijnitz.

My gratitude to Larissa, Jonas, and Susanne for instilling in me the fundamentals of cell culture and isolations, which laid the foundation for my laboratory skills. Bettina's thoughtful gifts have brought warmth and joy to my lab days, and I appreciate her kindness. I am also grateful to my lab mates Christian, Philipp, Isabel, Martina, and Fabienne for their ideas and engaging conversations during our lab meetings.

I would also like to express my appreciation to Lena for her unwavering support, inspiration, and positivity. Her encouragement to think outside the box has been instrumental in my growth as a researcher. Thanks, Rachel and Gonxhe for being my work besties.

Luisa's introduction to programming has transformed my research approach, and I am forever grateful for her guidance and mentorship. Ananya, thank you for letting me be your mentor and for providing a second home in Munich. Ms. Schreier’s, Ms. Kuno’s, and Steffi's assistance with official matters has been invaluable.

I am deeply thankful to my dear friend Madhura for inspiring me to pursue research and for her constant motivation. My former supervisor Prof. Seneviratne for inspiring me to continue with research and training me to think like a scientist. My mom, Pushpa, has been my biggest role model, and my dad, Rajan’s belief in me during tough times has been a source of strength. My brother Venkatesa Kumar's encouragement to push the boundaries as he has showcased, has been instrumental in my journey. I am grateful to my father- and mother-in-law for their unconditional support.

Finally, to my sweet partners in crime, Vinod and Aazhi kutty, thank you for your immense support and for keeping me grounded during challenging times. I could not have done it without you guys!

I dedicate my PhD to Pushpa, Rajan, and Vinod.